Cell

Cytomegalovirus subverts macrophage identity

Graphical abstract

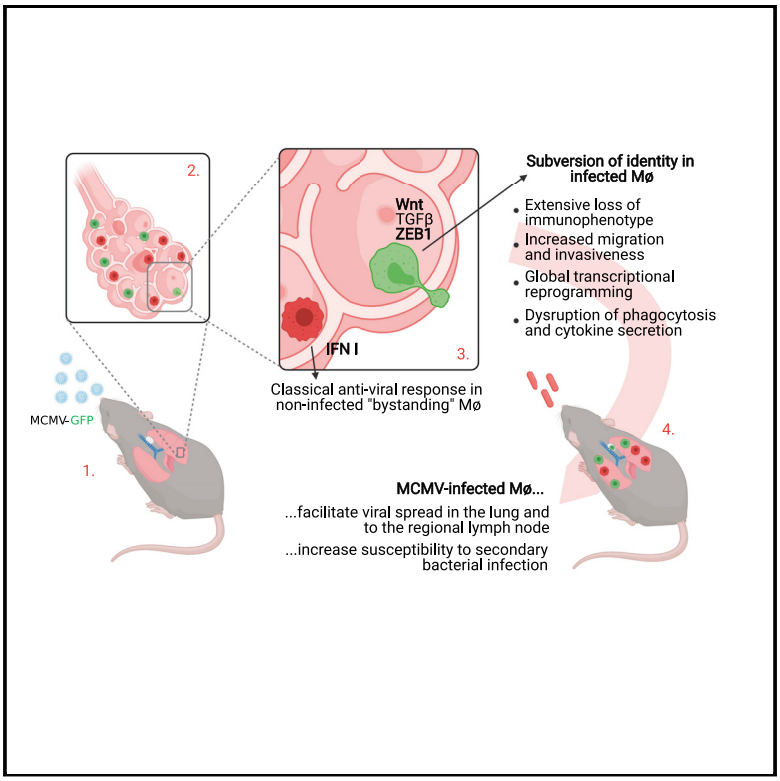

Highlights

- Two distinct subtypes of infected and non-infected macrophages arise in MCMV infection
- Infected macrophages acquire stem cell-like properties to serve MCMV replication
- Infected macrophages become invasive and spread MCMV locally in the lung
- Infected macrophages lose cell-specific traits and increase susceptibility to infections

Authors

Sebastian Baasch, Piero Giansanti, Julia Kolter, ..., Manfred Kopf, Zsolt Ruzsics, Philipp Henneke

Correspondence

philipp.henneke@uniklinik-freiburg.de

In brief

Co-evolution of CMVs and their hosts has led to exploitation of the first line of defense and conserved signaling pathways. Upon infection, macrophages are targeted primarily by MCMV and reprogrammed via activation of Wnt and TGF-β. This cell state serves viral replication and dissemination at the expense of cell-intrinsic traits.

Baasch et al., 2021, Cell *184*, 1–20
July 8, 2021
https://doi.org/10.1016/j.cell.2021.05.009

Please cite this article in press as: Baasch et al., Cytomegalovirus subverts macrophage identity, Cell (2021), https://doi.org/10.1016/j.cell.2021.05.009

Cell

CellPress

Article

Cytomegalovirus subverts macrophage identity

Sebastian Baasch,[1] Piero Giansanti,[3,14] Julia Kolter,[1,14] André Riedl,[4,5] Aaron James Forde,[1,5] Solveig Runge,[1,5] Simon Zenke,[1,5] Roland Elling,[1,2] Anne Halenius,[4] Simone Brabletz,[6] Hartmut Hengel,[4] Bernhard Kuster,[3,7] Thomas Brabletz,[6] Luka Cicin-Sain,[8,13] Ramon Arens,[9] Andreas Vlachos,[10,11] Jan Christopher Rohr,[1,2] Marc Philippe Stemmler,[6] Manfred Kopf,[12] Zsolt Ruzsics,[4] and Philipp Henneke[1,2,15,*]

[1]Institute for Immunodeficiency, Center for Chronic Immunodeficiency (CCI), University Medical Center, Faculty of Medicine, University of Freiburg, 79106 Freiburg, Germany
[2]Center for Pediatrics and Adolescent Medicine, University Medical Center, 79106 Freiburg, Germany
[3]Chair of Proteomics and Bioanalytics, Technical University of Munich, 85354 Freising, Germany
[4]Institute of Virology, University Medical Center, Faculty of Medicine, University of Freiburg, 79104 Freiburg, Germany
[5]Faculty of Biology, University of Freiburg, 79104 Freiburg, Germany
[6]Department of Experimental Medicine I, Nikolaus-Fiebiger Center for Molecular Medicine, Friedrich Alexander University of Erlangen-Nürnberg, 91054 Erlangen, Germany
[7]Bavarian Center for Biomolecular Mass Spectrometry (BayBioMS), Technical University Munich, 85354 Freising, Germany
[8]Immune Aging and Chronic Infections Group, Helmholtz Centre for Infection Research, 38124 Braunschweig, Germany
[9]Department of Immunology, Leiden University Medical Center, 2333 ZA Leiden, the Netherlands
[10]Department of Neuroanatomy, Institute of Anatomy and Cell Biology, Faculty of Medicine, University of Freiburg, 79104 Freiburg, Germany
[11]Center for Basics in Neuromodulation (NeuroModulBasics), Faculty of Medicine, University of Freiburg, 79106 Freiburg, Germany
[12]Institute of Molecular Health Sciences, ETH Zürich, 8093 Zürich, Switzerland
[13]Cluster of Excellence RESIST (EXC 2155), Hanover Medical School (MHH), 30625 Hanover, Germany
[14]These authors contributed equally
[15]Lead contact
*Correspondence: philipp.henneke@uniklinik-freiburg.de
https://doi.org/10.1016/j.cell.2021.05.009

SUMMARY

Cytomegaloviruses (CMVs) have co-evolved with their mammalian hosts for millions of years, leading to remarkable host specificity and high infection prevalence. Macrophages, which already populate barrier tissues in the embryo, are the predominant immune cells at potential CMV entry sites. Here we show that, upon CMV infection, macrophages undergo a morphological, immunophenotypic, and metabolic transformation process with features of stemness, altered migration, enhanced invasiveness, and provision of the cell cycle machinery for viral proliferation. This complex process depends on Wnt signaling and the transcription factor ZEB1. In pulmonary infection, mouse CMV primarily targets and reprograms alveolar macrophages, which alters lung physiology and facilitates primary CMV and secondary bacterial infection by attenuating the inflammatory response. Thus, CMV profoundly perturbs macrophage identity beyond established limits of plasticity and rewires specific differentiation processes, allowing viral spread and impairing innate tissue immunity.

INTRODUCTION

Host specificity of pathogens requires regulatory mechanisms between species to allow formation and preservation of ecological niches (Elinav et al., 2011). In the case of the bacterial and fungal microbiome, regulation may occur on the population level (Muegge et al., 2011). In contrast, viruses with an intracellular lifestyle may rely on adaptations in the single infected host cell (Pfeffer et al., 2004).

Cytomegalovirus (CMV), a β-herpesvirus, exhibits strict host specificity originating in co-evolution with mammals since ancient times (McGeoch et al., 2006). Human CMV (HCMV) frequently infects humans in the first months of life. It enters the host via the intestinal or respiratory tract and establishes life-long persistence with alternating phases of latency and productive infection. CMV encodes for a plethora of gene products that serve to evade the immune system by intercepting, e.g., nuclear factor κB (NF-κB)-, interferon-regulatory factor (IRF)-, and signal transducer and activator of transcription (STAT)-dependent signaling (Le et al., 2008; Abate et al., 2004; Browne and Shenk, 2003; Paulus et al., 2006). It remains largely elusive how immune cells respond to the presence of CMV at the earliest stages of infection, when host immunity adapts to the permanent presence of the virus. Mouse CMV (MCMV) exhibits a remarkably similar pathogenic potential as HCMV. Thus, MCMV is commonly used to study CMV biology.

Macrophages are the most frequent immune cell type in barrier tissues. They rely on tissue-specific transcriptional and

Please cite this article in press as: Baasch et al., Cytomegalovirus subverts macrophage identity, Cell (2021), https://doi.org/10.1016/j.cell.2021.05.009

environmental cues (e.g., peroxisome proliferator-activated receptor-γ [PPAR-γ] and granulocyte-macrophage colony-stimulating factor [GM-CSF] in the lungs) and show varying renewal patterns (Gosselin et al., 2014; Guilliams et al., 2013). Within the tissue, macrophages are adapted to microanatomical structures, such as nerves and vessels (De Schepper et al., 2018; Kolter et al., 2019). Although differentiation of resident macrophages is largely unidirectional, plasticity needs to be retained to respond to challenges inherent to interfaces between host and environment. However, this plasticity is generally restricted to homeostatic or inflammatory polarization states within the limits of site-adapted macrophage identity (Ginhoux et al., 2016; Piccolo et al., 2017). Under homeostatic conditions, macrophages take up apoptotic cells and form immunomodulating cytokines (e.g., interleukin-10 [IL-10]) to maintain tolerogenic conditions. Simultaneously, macrophages are also first responders to intruding microbes. They ingest pathogens and promote recruitment of neutrophils, monocytes, and other immune cells.

Here we uncover that CMV induces dynamic immunophenotypic and functional changes in fully differentiated macrophages from distinct tissue; e.g., lung and colon. CMV-infected, bone marrow (BM)-derived macrophages show transcriptional and proteomic features of stemness and increased motility and invasiveness. Moreover, CMV exploits the BM-derived macrophage cell cycle machinery at the expense of host cell proliferation. Overall, this process shares similarities with the epithelial-mesenchymal transition (EMT), including upregulation of the transcription factors ZEB1 and SNAI2. Importantly, CMV primarily infects alveolar macrophages *in vivo*. Respiratory infection with CMV leads to a dichotomy of transformed infected and activated bystander alveolar macrophages. Rewiring of alveolar macrophage identity-defining signaling processes facilitates viral spread and increases susceptibility of mice to bacterial infection.

RESULTS

CMV-infected macrophages are phenotypically distinct from bystander macrophages

To discriminate infected from uninfected cells, we engineered a MCMV strain that expressed GFP under control of viral *M36* upon active replication (MCMV-GFP; Figure S1A). Mouse embryonic fibroblasts (MEFs) infected with this construct showed GFP expression, indicating ongoing viral replication (Figure S1B). Upon intraperitoneal infection, MCMV-GFP reached high titers in the salivary gland 14 days post infection (dpi), indicating that reporter gene insertion did not alter the virulence and ability to disseminate (Figure S1C).

Next we analyzed MCMV-infected BM-derived macrophages by flow cytometry (Figure 1A) and fluorescence microscopy (Figure 1B) and identified two distinct populations. Infected, GFP^+ macrophages exhibited a decreased surface area (Figure 1C) and increased circularity (Figure 1D) compared with non-infected bystander BM-derived macrophages. Importantly, BM-derived macrophage cultures were initially homogeneous after differentiation with M-CSF; i.e., residual monocytes were not present (Figure S1D). Moreover, MCMV-GFP infected macrophages isolated from distinct tissues, including intestinal macrophages, which are largely derived from definitive hematopoiesis, and yolk sac-derived microglia (Figure S1E).

Employing low infectious dosages, the number of GFP^+ BM-derived macrophages plateaued in the first 48 h of infection, in line with the slow replication of β-herpesviruses. Within 10 days, almost all BM-derived macrophages were infected (Figures 1E and S1F). Foscarnet, a pyrophosphate analog viral DNA polymerase inhibitor, prevented CMV spread in BM-derived macrophages (Figure S1G). Notably, the emergence of infected BM-derived macrophages was dose dependent; i.e., a high multiplicity of infection (MOI) resulted in a homogeneous GFP^+ BM-derived macrophage population (Figure 1F). Because type I interferons (IFNs) have been shown previously to mediate resistance to CMV infection (Gil et al., 2001), we analyzed type I IFN receptor-deficient ($Ifnar^{-/-}$) mice. Although $Ifnar^{-/-}$ and wild-type (WT) BM-derived macrophages did not differ in initial infection rate (Figure 1F), bystander $Ifnar^{-/-}$ BM-derived macrophages were more prone to viral spread than WT cells (Figure 1E). This indicated that initial infection is a stochastic process in which bystander BM-derived macrophages are temporarily protected from viral spread via type I IFN. To verify that lack of GFP expression reflected an uninfected state rather than impaired MCMV replication, bystander macrophages were sorted 1 dpi and cultured further. A GFP signal was not detectable in bystander BM-derived macrophages up to 6 dpi, confirming that these cells were not infected productively by MCMV (Figure 1G).

CMV infection changes the phenotype and function of macrophages

CMV-infected BM-derived macrophages showed a substantially altered morphology (i.e., loss of their typical spread shape; Figures 1B–1D), suggesting alterations in surface molecule expression. Immunophenotypic analysis showed that CD45, F4/80, CD11b, and CD64 were downregulated as early as 1 dpi (Figures 2A and 2B), following different kinetics (Figures 2C and S2A). Moreover, total loss of cellular CD11b protein was observed (Figures 2C and S2B). At 3 dpi, BM-derived macrophages were no longer identifiable as such, based on immunological markers (Figure 2D). These changes were independent of myeloid differentiation primary response (MyD88)- and stimulator of interferon genes (STING)-mediated activation (Figure S2C) and independent of viral GFP expression (Figure S2D). To verify that the emerging cells indeed were macrophages, we constitutively labeled BM-derived macrophages of Cx_3cr1^{creER} ROSA26-$Tomato^{flox}$ mice by administration of hydroxytamoxifen (OH-TAM) before infection. Because of the incomplete recombination, we were able to distinguish GFP^- $Tomato^-$, GFP^+, $Tomato^+$ and GFP^+ $Tomato^+$ BM-derived macrophages (Figures S2E and S2F). We found that both infected (GFP^+) populations changed their morphology and downregulated their surface markers to the same extent (Figures S2E and S2F). Moreover, MCMV substantially affected the characteristic immunophenotype of tissue-resident macrophages (Figure S2G). In intestinal and peritoneal macrophages, CD11b, F4/80, and CD45 were downregulated; alveolar macrophages lost CD11c and SiglecF expression; and microglia downregulated CD11b, MerTK, and

Please cite this article in press as: Baasch et al., Cytomegalovirus subverts macrophage identity, Cell (2021), https://doi.org/10.1016/j.cell.2021.05.009

CellPress

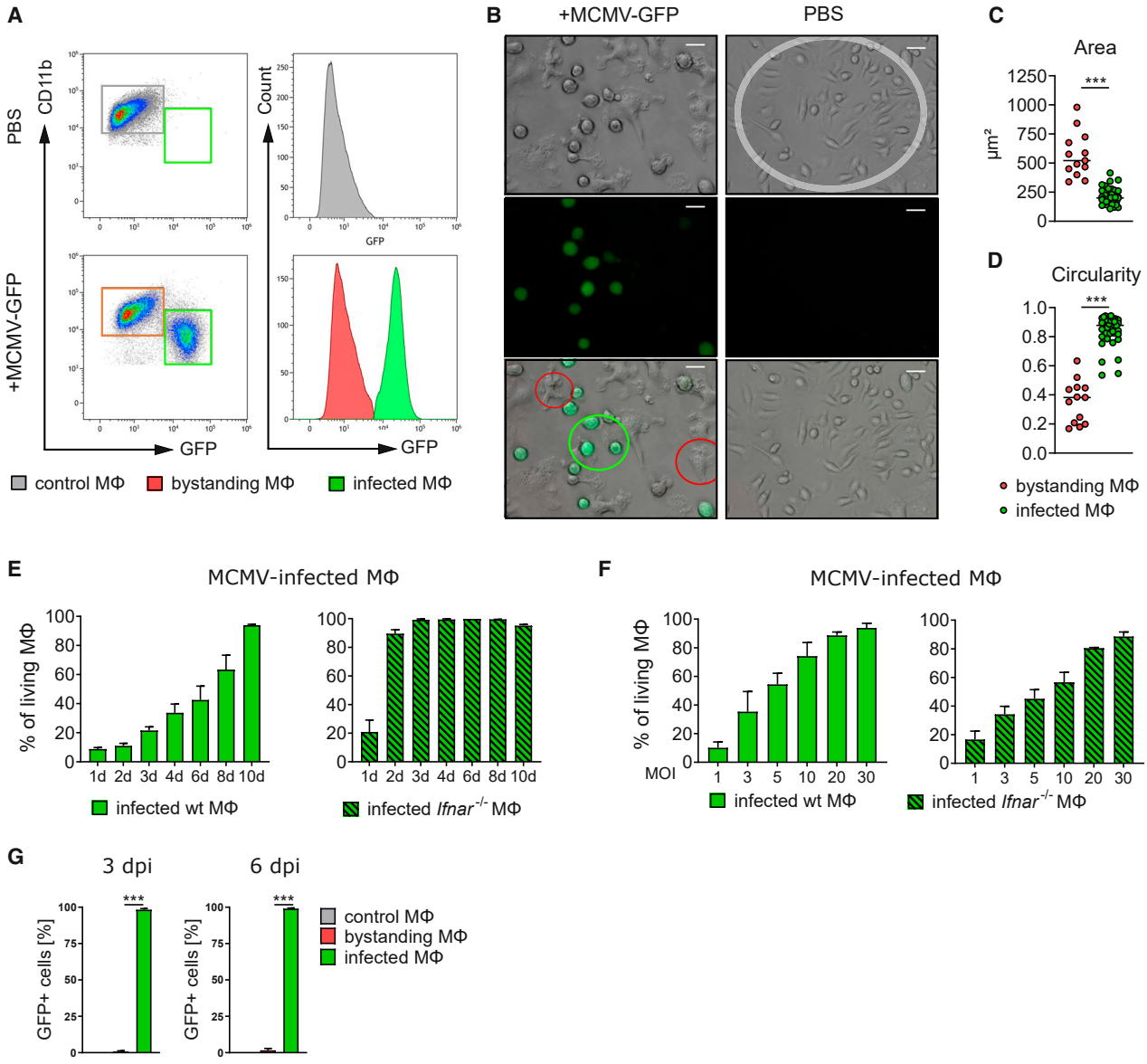

Figure 1. CMV-infected macrophages are phenotypically distinct from bystander macrophages

(A) Flow cytometry of GFP expression in BM-derived macrophages (MΦ) 1 dpi (mock, gray; bystander, red; MCMV-GFP infected, green). representative of n = 6/6.

(B) Fluorescence microscopy 2 dpi. Scale bars, 20 μm; n = 3/3.

(C and D) Analysis of cell area (C) and circularity (D) of infected and bystander BM-derived macrophages 2 dpi via ImageJ. n = 5/5, two-tailed unpaired t test.

(E) Flow cytometry of GFP$^+$ WT and *Ifnar*$^{-/-}$ macrophages at the indicated time points. n = 5–7/2 (*Ifnar*$^{-/-}$) and 5–7/3 (WT) independent experiments.

(F) Dose dependency of MCMV infection determined via flow cytometry of GFP$^+$ WT and *Ifnar*$^{-/-}$ macrophages 1 dpi. n = 3/2 (*Ifnar*$^{-/-}$) and 3/3 (WT).

(G) GFP expression of sorted BM-derived macrophages (1 dpi/mock) was analyzed at 3 and 6 dpi. n = 5/3 per time point; one-way ANOVA followed by Tukey's multiple comparisons test.

Data are mean ± SEM. *p < 0.05, **p < 0.01, ***p < 0.001.

CD64 after infection (Figure S2H). Transmission electron microscopy demonstrated, next to viral particles (Figure S2I), a lack of membrane protrusions and filopodia (Figure 2E), increased cellular circularity (Figure 2F), and an elevated number of mitochondria (Figure 2G). In line with the latter, the maximal respiration rate was increased in infected BM-derived macrophages (Figure 2H). The loss of macrophage identity-defining parameters and the marked morphological changes suggested that CMV infection may affect key macrophage functions. Since their discovery over 130 years ago, macrophages have been defined by their ability to take up particles; i.e., phagocytosis (Metchnikoff, 1883). Remarkably, MCMV-infected BM-derived

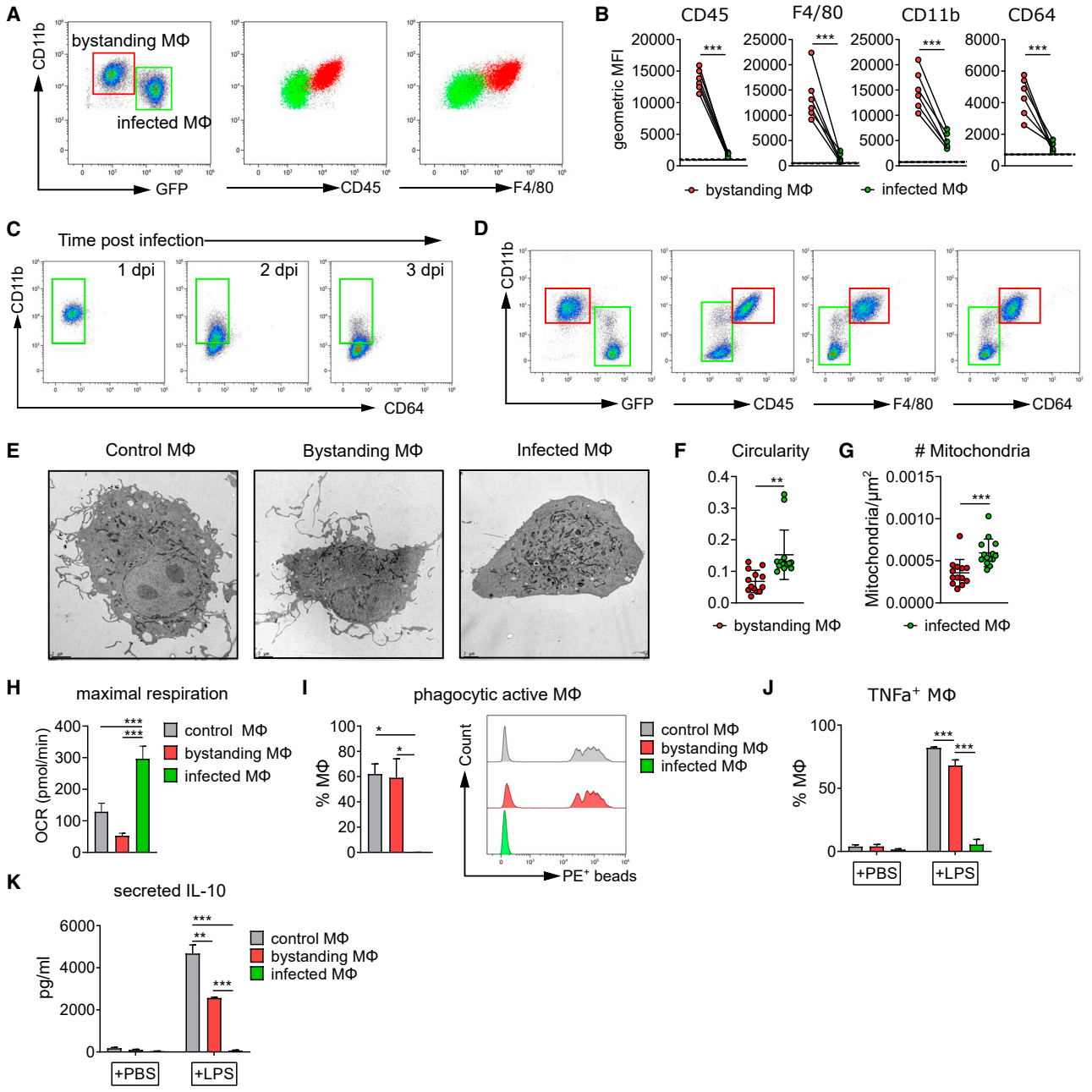

Figure 2. CMV infection changes macrophage phenotype and functionality

(A) Flow cytometry of bystander (red) and infected (green) macrophages 1 dpi. Representative of n = 6/6.

(B) Expression level of surface markers on BM-derived macrophages 1 dpi, obtained by flow cytometry. Dashed lines indicate Fluorescence Minus One (FMO) controls. n = 6/6; two-tailed unpaired t test.

(C) Flow cytometry of BM-derived macrophages sorted 1 dpi and analyzed at the indicated time points. Gate was defined via FMO controls. Representative of n = 3/3.

(D) Flow cytometry of BM-derived macrophage subsets 3 dpi. Expression of CD11b, CD45, F4/80, and CD64 by bystander (red squares) and infected (green squares) macrophages. Representative of at least 8 independent experiments.

(E) Transmission electron microscopy (TEM) images of sorted BM-derived macrophage subsets 3 dpi. Scale bars, 2 μm. Representative of 13 images per subset from 4 mice in 2 independent experiments.

(F) Quantification of circularity of TEM images 3 dpi. Two-tailed unpaired t test.

(G) Quantification of number of mitochondria/cell area of TEM images 3 dpi. Two-tailed unpaired t test.

(H) Maximal respiration rate of sorted BM-derived macrophage subsets 3 dpi. n = 8/4; one-way ANOVA followed by Tukey's multiple comparisons test.

(legend continued on next page)

Please cite this article in press as: Baasch et al., Cytomegalovirus subverts macrophage identity, Cell (2021), https://doi.org/10.1016/j.cell.2021.05.009

macrophages completely lost the ability to phagocytose particles (Figure 2I) despite intact endocytosis (Figure S2J). Furthermore, lipopolysaccharide (LPS)-induced cytokine formation was abrogated with respect to the inflammatory tumor necrosis factor (TNF) (Figures 2J and S2K) and the regulatory IL-10 (Figure 2K). Together, CMV infection was associated with profound loss of macrophage identity.

CMV elicits stem cell-like features in macrophages

To further dissect this transformation process, we performed RNA sequencing (RNA-seq) of BM-derived macrophages 3 days after infection, when surface marker downregulation was at its maximum. Importantly, viral gene transcripts were not detectable in bystander cells at this time point (Figure S3A). This allowed us to compare cells cultivated in the same microenvironment, only differing in the intracellular CMV. Principal-component analysis (PCA) pointed to highly distinct transcriptomes in control, bystander, and infected BM-derived macrophages (Figure 3A). In CMV-infected BM-derived macrophages, over 3,600 and 3,900 genes were upregulated significantly compared with control and bystander BM-derived macrophages, respectively (Figure 3B). Genes associated with Gene Ontology (GO) terms, including the keyword "macrophage," were downregulated in CMV-infected BM-derived macrophages (Figure 3C). Furthermore, the expression of core transcription factors in macrophage lineage commitment and differentiation, such as *Spi1*, *Cebpa*, *Cebpb*, and *Irf8* (Cain et al., 2013; Heath et al., 2004; Heinz et al., 2010; McKercher et al., 1996; Tamura et al., 2000), was significantly lower (Figure 3D), which supported the loss of macrophage identity. While bystander BM-derived macrophages displayed a signature related to type I IFN activation and viral defense response, GO terms enriched in CMV-infected macrophages were associated with tissue development and morphogenesis (Figure 3E). Moreover, the majority of genes defining the GO term "stem cell population maintenance" was upregulated in infected compared with bystander macrophages (Figure 3F). In tissue macrophages, self-renewal is driven by upregulation of the stemness-inducing factors *Klf4* and *Myc* and repression of the differentiation factors *Mafb* and *Maf* (Aziz et al., 2009). Interestingly, CMV decreased expression of *Maf* and *Mafb* and increased that of *Klf4* (Figure 3G). In addition, *Kit*, *Flt3*, and *Bmi1*, which are typically expressed in hematopoietic progenitors (Boyer et al., 2011; Lyman and Jacobsen, 1998; Park et al., 2003), were upregulated in CMV-infected BM-derived macrophages, indicating a stem cell-like phenotype (Figure S3B). In contrast, bystander BM-derived macrophages highly expressed *Myc* (Figure 3G).

Other Herpesviridae members have been found to modulate host protein expression via post-transcriptional mechanisms (Rutkowski et al., 2015). Thus, we performed time-resolved proteome analysis by mass spectrometry (Table S1). We found increasing divergence of the proteomes from CMV-infected and bystander BM-derived macrophages with time (Figure 3H) and confirmed broad loss of macrophage-defining surface markers (Figure S3C). Moreover, the GO terms "regulation of IFN I" and "response to virus" were overrepresented in bystander macrophages, whereas infected macrophages showed enrichment of genes involved in the mitotic cell cycle, embryo development, stem cell population maintenance, and telomere maintenance (Figure 3I). The latter, again, corresponded to an increase in gene expression of telomere subunits at 3 dpi (Figure S3D). Overall, the proteome showed a strong correlation with the transcriptome data at 3 dpi (Figure S3E). This in-depth analysis suggested that CMV infection steered macrophages transcriptionally and translationally away from their identity-specifying characteristics to features of stemness.

CMV-infected macrophages lose antigen-presenting capacity and provide their cell cycle machinery for viral replication

Next to dendritic cells (DC), macrophages can also serve as antigen-presenting cells in tissues and lymph nodes and express co-stimulatory proteins to activate lymphocytes in viral infection. In line with upregulation of IFN-stimulated proteins, such as RSAD2, OASL1, and ISG15, bystander BM-derived macrophages expressed the co-stimulatory receptor CD40 and proteins involved in lymphoid cell interaction and major histocompatibility complex (MHC) class I loading (Figures S4A and S4B). In contrast, infected BM-derived macrophages did not process Ovalbumin (OVA) protein to stimulate T cell proliferation (Figures 4A). Notably, the capacity to present the OVA-derived peptide epitope SIINFEKL to $CD8^+$ T cells was preserved in infected BM-derived macrophages (Figure S4C). Thus, CMV-infected BM-derived macrophages lose the ability to process proteins via the immunoproteasome while retaining MHC class I expression. In agreement with this, infected BM-derived macrophages showed broad loss of transcripts and proteins associated with the antigen-presenting machinery (Figures S4D and S4E), which may contribute to interference with MHC class I trafficking via viral gene products (LoPiccolo et al., 2003). In contrast, proteins essential for peptide loading (i.e., TAP1, TAP2, TAPBP, and TAPBPL) were upregulated in bystander BM-derived macrophages, suggesting a role in antigen presentation (Figure S4E).

Next we performed time-resolved proteome profiling of MCMV-infected BM-derived macrophages. At early time points, proteins associated with macrophage activation, receptor internalization, and actin cytoskeleton reorganization were overrepresented, indicating an acute cellular stress response (Figure 4B). A second cluster with peak expression at 2 and 3 dpi comprised proteins involved in mitochondrial processes and redox signaling, supporting metabolic changes in CMV-infected macrophages (Figure 2H). In addition, proteins associated with

(I) Quantification of phagocytosis of BM-derived macrophage subsets (left) and representative histogram (right). n = 3/3; one-way ANOVA followed by Tukey's multiple comparisons test.

(J and K) Cytokine production of sorted BM-derived macrophage subsets (3 dpi) was determined via flow cytometry (J) or ELISA (K) after LPS stimulation. n = 3/3; two-way ANOVA followed by Tukey's multiple comparisons test.

Data are mean ± SEM. *$p < 0.05$, **$p < 0.01$, ***$p < 0.001$.

Please cite this article in press as: Baasch et al., Cytomegalovirus subverts macrophage identity, Cell (2021), https://doi.org/10.1016/j.cell.2021.05.009

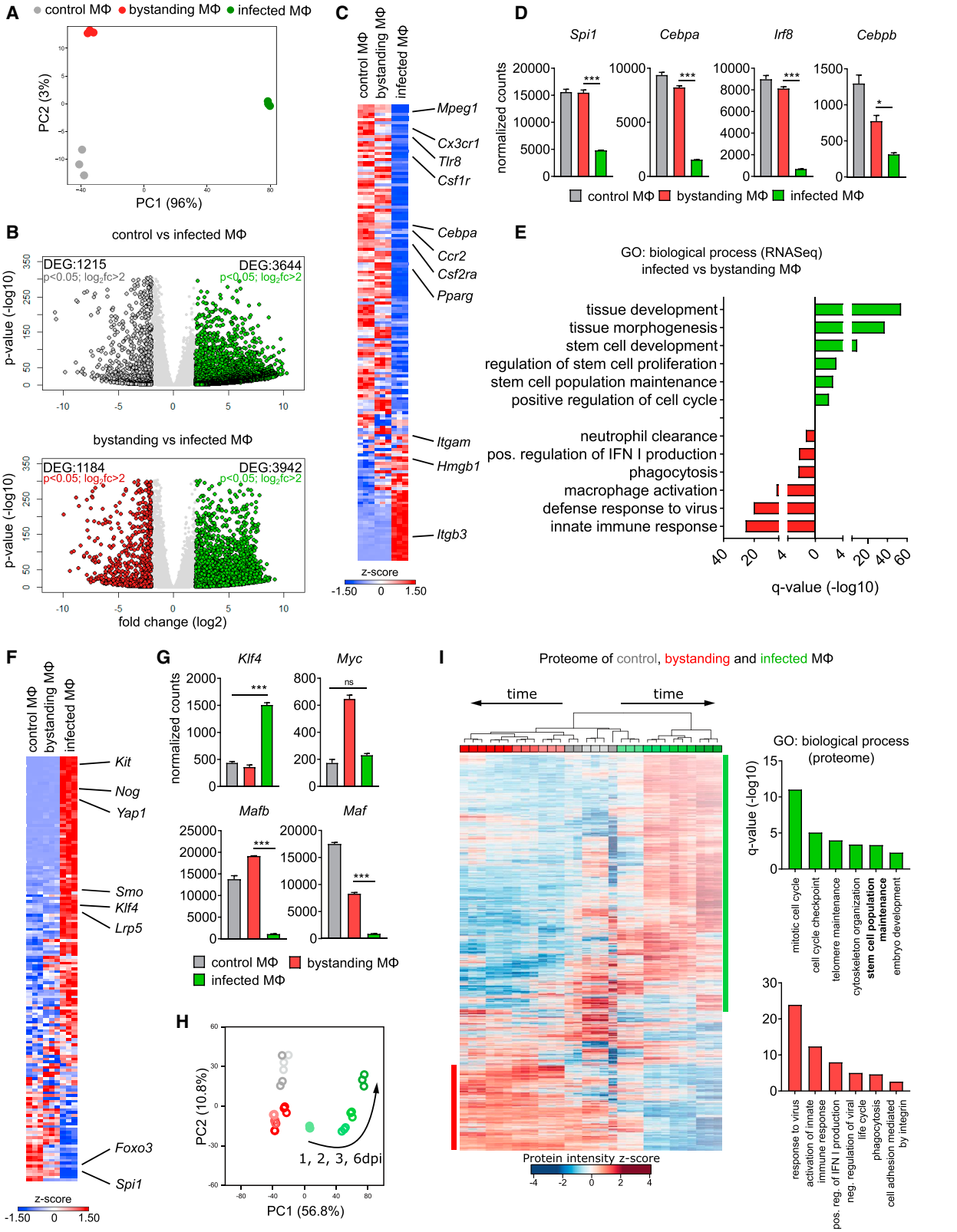

(legend on next page)

Please cite this article in press as: Baasch et al., Cytomegalovirus subverts macrophage identity, Cell (2021), https://doi.org/10.1016/j.cell.2021.05.009

chromatin processing, DNA-dependent transcription regulation, mitosis, and cell cycle were upregulated from 2–6 dpi (Figure 4B). Because stemness is closely connected to proliferation and differentiation potential (Park et al., 2004), we wondered whether progenitor properties were acquired as well. However, no colonies were formed by infected BM-derived macrophages in colony-forming unit (CFU) assays, even under most permissive conditions (Figure S4F). This was in contrast to a steady increase in cell cycling proteins from 1–6 dpi (Figure 4C). CMV and other herpesviruses perturb cell cycle progression in fibroblasts, leading to G1/S phase arrest (Lu and Shenk, 1996; Wiebusch et al., 2008), but macrophages have not been studied in this context. Therefore, we dissected the cell cycle of control, bystander, and infected BM-derived macrophages (Figure 4D). Significantly more infected macrophages showed Ki67 accessibility, indicating active cell cycling (Figure 4E). The tumor suppressor retinoblastoma protein (RB1) and its family members retinoblastoma-like proteins 1/2 (RBL1/2) are potent regulators of cell cycle progression. Their phosphorylation allows dissociation of the transcription factor E2F, leading to S phase progression (Weinberg, 1995). In line with phosphorylation of RB proteins in infected macrophages (Figure S4G; Table S2), RNA-seq analysis showed increased transcription of E2F target genes at 3 dpi (Figure S4H). This suggests that infected macrophages overcome G1/S phase arrest and initiate cellular DNA synthesis in early S phase via induction of polymerases and DNA replication-licensing proteins (Figure S4H). Alternatively, they may provide these proteins to MCMV for replication. To resolve this, we pulsed uninfected and infected BM-derived macrophages with bromodeoxyuridine (BrdU) and found a high BrdU signal in bystander BM-derived macrophages (gate B) and a predominantly intermediate BrdU signal (gate A) in infected BM-derived macrophages (Figures 4F and 4G). To determine whether the DNA in $BrdU^+$ cells was of eukaryotic or viral origin, we analyzed cellular and viral proliferation. We found bystander BM-derived macrophages to increase and infected BM-derived macrophages to decrease slightly over time (Figure 4H), whereas extracellular and intracellular CMV DNA increased progressively (Figures 4I and 4J). Thus, BrdU intermediate events indeed represent MCMV particles, comprising less DNA. This observation was in line with the viral proteome data indicating a complete viral replication cycle of CMV in infected macrophages (Figure 4K). Furthermore, protein expression kinetics demonstrated a lytic cycle of MCMV infection because viral gene products clustered in immediate-early (cluster 3; e.g., ie1 and ie3), early (cluster 4; e.g., m152), early-late (cluster 1; e.g., m36, m37, and m45), and late (cluster 2; e.g., m94, m48, m47, and m50) groups (Figure 4K; Table S3). Finally, A- and B-type lamins were expressed and phosphorylated (Figure S4I; Table S2) in infected macrophages, implying remodeling of the nuclear envelope and chromatin structures, which is associated with viral nuclear egress (Muranyi et al., 2002). In summary, CMV induced a stem cell-like state in infected macrophages to exploit and redirect the cellular equipment for DNA replication toward virus production.

Induction of the Wnt pathway causes transformation of CMV-infected macrophages with increased mobility and invasiveness

Pathway analysis on RNA-seq and proteome/phosphoproteome data revealed signaling pathways associated with adhesion (cadherin, integrin, and focal adhesion signaling pathway), Wnt, transforming growth factor β (TGF-β) and Notch signaling were overrepresented in the transcriptome and phosphoproteome of infected BM-derived macrophages (Table S4). Modulation of these pathways induces EMT in epithelial cells (Fodde and Brabletz, 2007; Lee et al., 2006; Miettinen et al., 1994). EMT occurs during embryogenesis and in cancer metastasis. GO terms directly linked to mesenchymal transition and its regulation as well as GO terms related to EMT (Gröger et al., 2012) were overrepresented in the RNA-seq dataset (Figures 5A and S5A). Moreover, the transcription factors Twist-related protein 1 (*Twist1*), Zinc finger protein SNAI2 (*Snai2*), and zinc-finger E-box-binding homeobox 1 (*Zeb1*) and their targets N-cadherin (*Cdh2*) and Fibronectin (*Fn1*) were upregulated in infected macrophages (Figures 5B and 5C). Importantly, this was not due to contaminating multipotent mesenchymal stromal cells, as BM-derived macrophages expressed similar levels of transcripts when they were sorted before infection (Figure S5B). SNAI2, TWIST1, and ZEB1 orchestrate cellular reprogramming in embryogenesis and tumor progression, are associated with stemness, morphological, and functional changes (Nieto et al., 2016), and have been linked to increased mobility and invasion (Peinado et al., 2007). To explore these features, we performed time-lapse microscopy. CMV-infected macrophages migrated longer distances and with higher velocity compared with control macrophages (Figures 5D and S5C). Furthermore, they interacted with other cells and exhibited an altered, ameboid mode of

Figure 3. CMV elicits stem cell-like features in macrophages

(A) Transcriptomic principal-component analysis (PCA) of sorted BM-derived macrophage subsets 3 dpi.

(B) Volcano plot of differentially expressed genes (DEGs; ≥ 2 $\log_2$-fold change, $p \leq 0.05$) of infected (green) versus control (dark gray) or infected (green) versus bystander (red) BM-derived macrophages.

(C) Heatmap of murine genes associated with GO terms containing the keyword "macrophage."

(D) Normalized read counts of genes determining macrophage differentiation.

(E) Overrepresented GO terms of infected (green) compared with bystander (red) BM-derived macrophages.

(F) Heatmap of genes associated with the GO term "stem cell population maintenance."

(G) Normalized read counts of genes promoting (*Klf4* and *Myc*) or preventing (*Mafb* and *Maf*) self-renewal in tissue macrophages.

(H) Proteomics PCA. Control BM-derived macrophages 1 day and 3 days after mock infection (gray) and bystander (red) and infected BM-derived macrophages (green) 1, 2, 3, and 6 dpi. Consecutive time points are displayed in increasing color intensity (e.g., light green, 1 dpi; dark green, 6 dpi).

(I) Heatmap and GO term analysis of differentially regulated proteins in macrophage subsets. Each column represents one biological replicate. A full list of proteins is provided in Table S1.

Data are mean ± SEM. *$p < 0.05$, **$p < 0.01$, ***$p < 0.001$. One-way ANOVA followed by Tukey's multiple comparisons test, unless stated otherwise.

Please cite this article in press as: Baasch et al., Cytomegalovirus subverts macrophage identity, Cell (2021), https://doi.org/10.1016/j.cell.2021.05.009

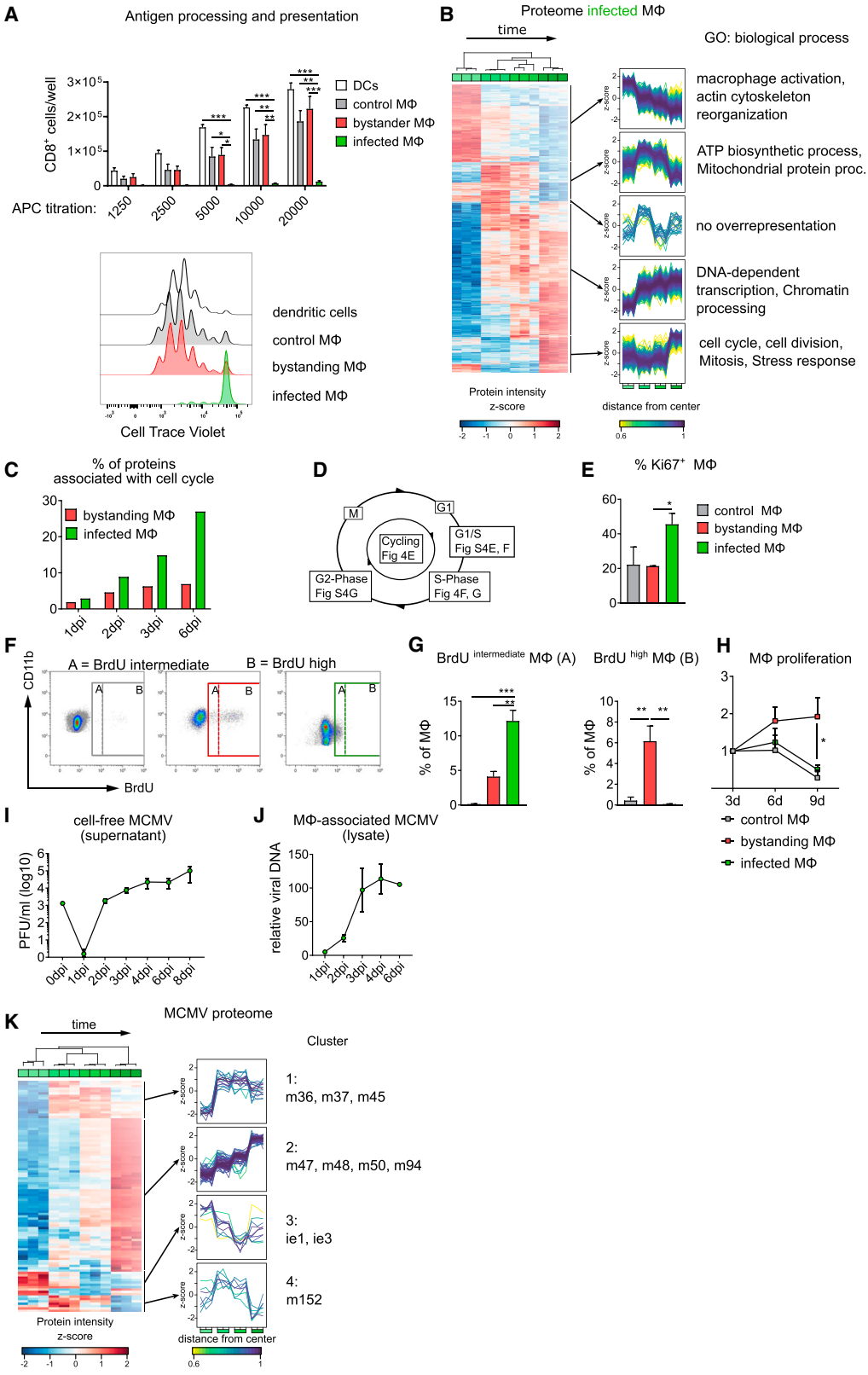

(legend on next page)

Please cite this article in press as: Baasch et al., Cytomegalovirus subverts macrophage identity, Cell (2021), https://doi.org/10.1016/j.cell.2021.05.009

migration with bleb formation (Figure S5D; Videos S1 and S2). In addition, only infected, but not bystander or control macrophages, migrated through the extracellular matrix in a transwell invasion assay with Matrigel-coated inserts (Figures 5E and S5E). To test, whether the altered mobility promoted viral spread, we analyzed whether CMV dissemination occurred via cell-free virus released into the supernatant or via direct physical contact (Figure S5F). We found that CMV transmission by direct contact of infected macrophages to uninfected fibroblasts was substantially more efficient than via cell-free supernatant (Figure 5F). Additionally, CMV-neutralizing antibodies did not prevent intercellular viral spread (Figure 5F and S5G), indicating that CMV disseminated via immediate contact of infected with uninfected cells.

To further specify the pathways contributing to macrophage transformation, we compared the proteome data with a database on mesenchymal transition, dbEMT, and constructed an interactive network with proteins present in CMV-infected BM-derived macrophages (Figures 5G and S5H). This analysis supported the particular involvement of the TGF-β and Wnt signaling pathways (Figure 5H). Moreover, Wnt target genes and proteins were upregulated in infected compared with control and bystander macrophages (Figures 5I, S5I, and S5J). In particular, we found integrin β3 (*Itgb3*/CD61) to be highly expressed in infected compared with bystander macrophages (Figure S5H), which was confirmed by flow cytometry (Figure 5J). This identified CD61 as an endogenous reporter of the transformation process.

Wnt may signal via canonical and non-canonical activation. The non-canonical planar cell polarity pathway regulates the cytoskeleton and, therefore, cell shape via downstream Rho/Rho kinase (ROCK) signaling (Wallingford and Habas, 2005). ROCK, on the other hand, has been linked to cellular contractility and bleb formation (Coleman et al., 2001). Accordingly, we found that infected macrophages were more spread out and lost their circularity in the presence of the ROCK inhibitor Y27632 (Figures 5K and S5K). Further analysis of the protein network identified β-catenin, p300, and CBP of the canonical Wnt pathway as central hubs that interacted intensely with other proteins (Figure 5L). To explore these putative signaling knots, we inhibited the p300-β-catenin interaction with IQ-1 and the CBP-β-catenin interaction with ICG001 (Kahn, 2011). Blocking the Wnt pathway (Figure S5L) partially rescued CD11b expression and prevented CD61 upregulation on infected macrophages (Figures 5M and 5N) without affecting cell viability or numbers (Figures S5M and S5N). In contrast, interfering with TGF-β signaling did not reverse CMV-induced BM-derived macrophage transformation (Figure S5O). β-Catenin activates the *Zeb1* promotor via the lymphoid enhancer factor/T cell factor (LEF/TCF) transcription factors (Sánchez-Tilló et al., 2015), subsequently, inducing invasion (Burk et al., 2008; Sánchez-Tilló et al., 2011). Analysis of BM-derived macrophages from *LysM*$^{cre/+}$:*Zeb1*$^{flox/flox}$ mice, in which exon 6 of *Zeb1* is deleted in myeloid cells (Brabletz et al., 2017), revealed that fewer Zeb1-deficient than WT macrophages invaded Matrigel upon CMV infection (Figure 5O). Notably, mesenchymal markers and matrix metalloprotease 2 (*Mmp2*) were expressed at slightly but not significantly lower levels in infected macrophages lacking Zeb1 compared with controls (Figure S5P). Moreover, *Zeb1* deletion did not influence the low expression of the related *Zeb2* in infected BM-derived macrophages (Figure S5P). Finally, human monocyte-derived macrophages similarly upregulated *AXIN2*, *SOX9*, *ZEB1*, *SNAI2*, and *CDH2* transcription after infection with the HCMV strain TB40-SE-GFP (Figure 5P). Our data suggest that CMV-induced Wnt signaling leads to increased mobility and invasiveness of BM-derived macrophages, which is in part mediated by Zeb1.

Infected alveolar macrophages are reprogrammed *in vivo*

Finally, we explored whether CMV reprograms alveolar macrophages *in vivo* after intranasal infection (Figure 6A). At 1 dpi, most of the infected cells in the lungs were CD11b^{int}, CD11c^{+} (Figures 6B and 6C), representing alveolar macrophages or dendritic cells. To elucidate the role of CD11c^{+} cells in this model, we infected *Itgax*$^{cre/+}$ mice with MCMV-floxGFP. Thus, infected cells expressed GFP only when CMV passed through CD11c^{+} cells (Figure S6A). 93% (±0.88%) of all GFP^{+} cells showed CD11c, SiglecF, and CD64 but not CD103 expression 12 hpi (Figures 6D and S6B). Therefore, alveolar macrophages were the predominant target cells early after respiratory infection with CMV. In agreement with the *in vitro* and *ex vivo* data (Figures 2A–2D and S2H), MCMV-infected alveolar macrophages downregulated CD11c, SiglecF, and CD64

Figure 4. CMV-infected macrophages lose antigen-presenting capacity and provide their cell cycle machinery for viral replication

(A) Absolute numbers of CD8^{+} T cells (top) and representative proliferation profile of CD8^{+} T cells (bottom) assessed via flow cytometry. n = 4/2.

(B) Unsupervised hierarchical clustering and profile plots of mouse proteins regulated significantly in infected BM-derived macrophages at 1, 2, 3, and 6 dpi. Enrichment analysis (GO) highlights cluster-specific annotations.

(C) Percentage of proteins associated with the "cell cycle" (UniProtKB) and upregulated significantly in bystander (red) versus infected (green) BM-derived macrophages.

(D) Schematic of the cell cycle and corresponding subfigures.

(E) Ki67 accessibility, determined 6 dpi via flow cytometry. n = 3/3.

(F) Representative flow cytometry plots of sorted BM-derived macrophage subsets 6 dpi. Representative of n = 3/3.

(G) BrdU^{+} BM-derived macrophage subsets were subdivided in BrdU^{intermediate} (A) and BrdU^{high} (B) and quantified 6 dpi via flow cytometry. n = 3/3.

(H) Cell counts of sorted BM-derived macrophage subsets 3, 6, and 9 dpi. Cell counts were normalized to 3 dpi. n = 3/3.

(I) Cell-free viral particles in supernatant of infected BM-derived macrophages were quantified via plaque assay. n = 4/2.

(J) Cell-associated virus counts were determined via qPCR of viral m45 (DNA) in infected BM-derived macrophage lysates. n = 5/3.

(K) Unsupervised hierarchical clustering as in Figure 4B for viral gene products. Profile plot clusters are annotated with representative viral gene products; a full list is provided in Table S3.

Data are mean ± SEM. *p < 0.05, **p < 0.01, ***p < 0.001. One-way ANOVA followed by Tukey's multiple comparisons test unless stated otherwise.

Please cite this article in press as: Baasch et al., Cytomegalovirus subverts macrophage identity, Cell (2021), https://doi.org/10.1016/j.cell.2021.05.009

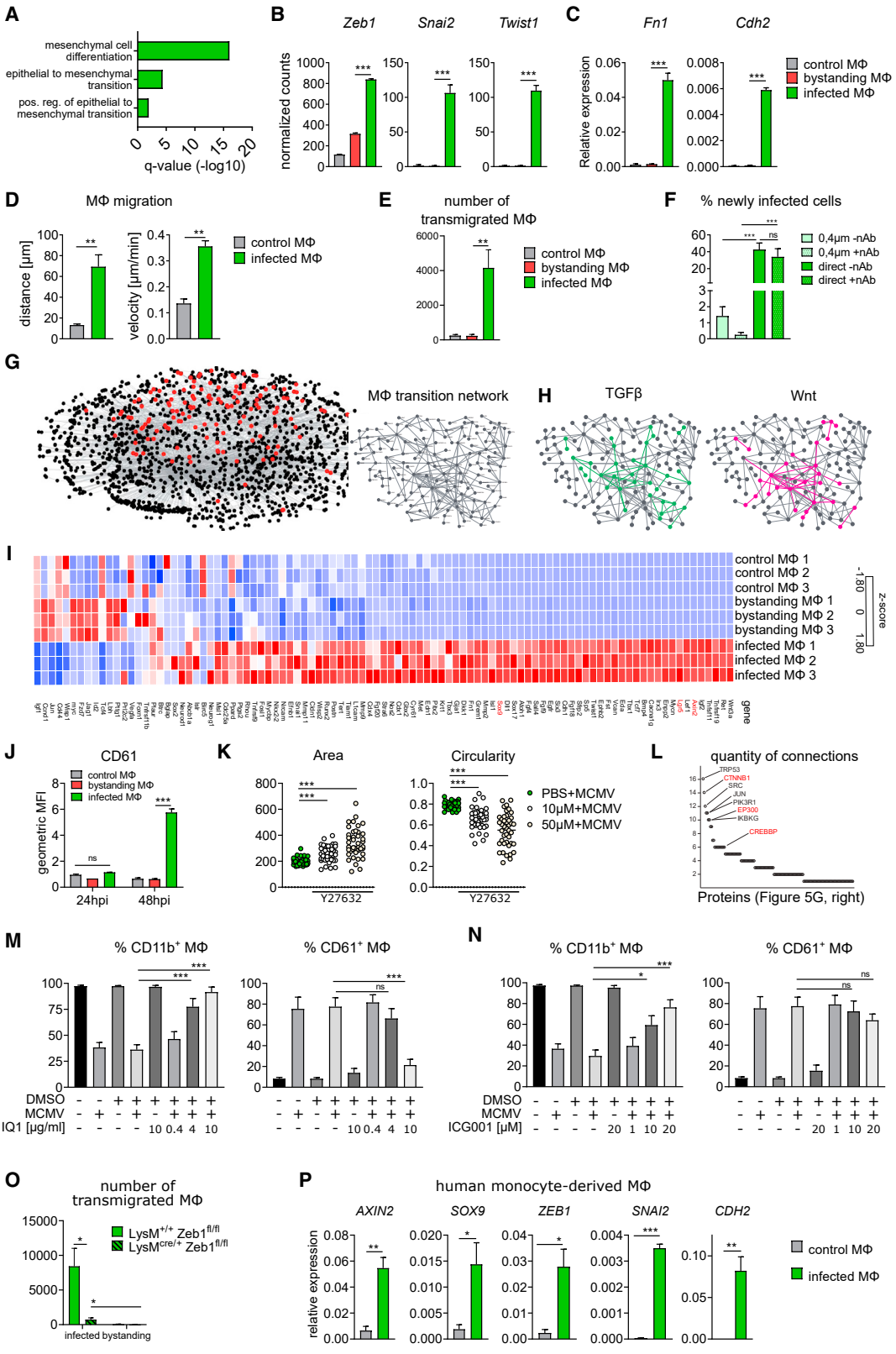

(legend on next page)

Please cite this article in press as: Baasch et al., Cytomegalovirus subverts macrophage identity, Cell (2021), https://doi.org/10.1016/j.cell.2021.05.009

(Figures 6E, 6F and S6C). We next performed RNA-seq of *in-vivo*-infected alveolar macrophages 3 dpi. To assure that GFP$^+$ cells were indeed alveolar macrophages, despite the loss of surface markers after infection, we infected *Itgax*$^{cre/+}$ ROSA26-Tomato^{flox} mice with MCMV-floxGFP. Thus, CD11c$^+$ alveolar macrophages were labeled endogenously (Tomato$^+$), and infected alveolar macrophages harbored both fluorescent proteins (GFP$^+$ Tomato$^+$) (Figures 6G and S6D). PCA revealed a distinct transcriptome of infected macrophages (Figure 6H) because key transcription factors for alveolar macrophage fate determination (e.g., *Pparg*; Schneider et al., 2014) and tissue maintenance (e.g., *Zeb2*; Scott et al., 2018) as well as typical markers were strongly downregulated (Figures 6I, 6J and S6E). Similarly, expression of characteristic gene sets in alveolar macrophages (Gautier et al., 2012) was no longer detectable in infected alveolar macrophages (Figure 6K). Overall, the transcriptional profile of infected alveolar macrophages showed a strong correlation with infected BM-derived macrophages, whereas control and bystander macrophages correlated weakly with their *in vitro* counterparts, again indicating that infection with CMV overrides the inherent profile of tissue macrophages (Figure S6F). Next we analyzed key effector molecules, which we had identified previously *in vitro*. We found Wnt target genes, N-cadherin, as well as *Snai2* and *Zeb1* to be upregulated in infected alveolar macrophages *in vivo* (Figure 6L). Gene set enrichment analysis confirmed involvement of Wnt signaling and genes associated with EMT in infected alveolar macrophages, whereas bystander alveolar macrophages showed an IFN signature and NF-κB activation (Figures 6M and S6G). Finally, CMV-infected alveolar macrophages could be identified by *Itgb3*/CD61 expression as an immunophenotypic hallmark (Figures 6F, 6N, 6O, and S6H).

In respiratory infection, MCMV primarily targeted and perturbed alveolar macrophage lineage identity via downregulation of signature surface markers and increased expression of mesenchymal markers and activation of the transcription factors *Snai2* and *Zeb1*.

Alveolar macrophages promote intercellular viral spread and invade the lung interstitium

Tissue macrophages and their environment interact reciprocally; i.e., macrophages perform essential and niche-specific functions to shape and maintain tissue integrity. On the other hand, the immediate environment affects macrophage phenotype and function, especially after infection (Guilliams and Svedberg, 2021; Guilliams et al., 2020). Thus, we assessed alveolar macrophage population dynamics by infecting *Itgax*$^{cre/+}$ ROSA26-Tomato^{flox} mice with MCMV-floxGFP and analyzed bystander (Tomato$^+$) and infected (GFP$^+$ Tomato$^+$) alveolar macrophages (Figure 7A). Interestingly, GFP$^+$ Tomato$^-$ cells, which represented cells newly infected by virus originating from cre-expressing cells, increased steadily in number from 3 dpi onward, indicating secondary viral spread from alveolar macrophages to other cells (Figure 7A). To analyze the fate of infected alveolar macrophages, we sorted alveolar macrophages from MCMV-infected *Itgax*$^{cre/+}$ ROSA26-Tomato^{flox} mice and transferred them intratracheally into WT mice (Figure S7A). Notably, the number of transferred infected alveolar macrophages remained stable for up to 6 days (Figure S7B).

To test whether MCMV infection increases the invasiveness of alveolar macrophages *in vivo*, similar to the situation *in vitro*, we intratracheally administered SiglecF and CD61 antibodies to label bystander (SiglecF) and infected (CD61) alveolar macrophages in the airways (Figure 7B). We found less efficient labeling of infected compared with bystander alveolar macrophages (Figure 7C). Thus, a fraction of infected alveolar macrophages appeared to invade the lung tissue. To confirm the interstitial translocation of alveolar macrophages, we transferred sorted alveolar macrophages from *Itgax*$^{cre/+}$ ROSA26-Tomato^{flox} mice into *Csf2rb*$^{-/-}$ mice, which are devoid of endogenous alveolar macrophages. 8 weeks after the transfer, when the lungs were repopulated with Tomato$^+$ alveolar macrophages, mice were infected with MCMV (Figure S7C). Importantly, in the reconstituted *Csf2rb*$^{-/-}$ mice, exclusively alveolar macrophages express the Cre recombinase; i.e., they are Tomato$^+$ and recombine

Figure 5. Induction of the Wnt pathway causes CMV-induced transformation of macrophages with increased mobility and invasiveness

(A) GO term analysis of infected macrophages versus bystander macrophages (3 dpi). The plot shows the q value of overrepresented GO terms associated with EMT.

(B) Normalized reads of EMT-inducing transcription factors.

(C) qRT-PCR of *Cdh2*and *Fn1* 3 dpi. n = 3/3.

(D) Quantification of time-lapse microscopy of control and infected BM-derived macrophages. Data represent the mean of 12 BM-derived macrophages/condition in 3 independent experiments; unpaired t test.

(E) Total number of invasive BM-derived macrophages. n = 5/3.

(F) Quantification of cells newly infected via cell-free virus (light green) or cell-to-cell spread (dark green). n = 3/3.

(G) Protein interaction network (STRING) in which the red proteins are found in the dbEMT database (left) and a labeled diagram of the EMT-associated protein subnetwork (right).

(H) TGF-β (left) and Wnt (right) pathway-associated proteins in the macrophage transition network in (G).

(I) Heatmap of Wnt target genes (RNA-seq). Highlighted (red) genes are quantified via qRT-PCR in Figure S5I.

(J) Expression intensity of CD61 (*Itgb3*) on the BM-derived macrophage subsets, measured via flow cytometry. n = 3/3; two-way ANOVA followed by Tukey's multiple comparisons test.

(K) Cell area (left) and circularity (right) of infected BM-derived macrophages with vehicle (PBS) or increasing dosages of the ROCK inhibitor Y27632. n = 4/2.

(L) Number of protein network connections in (G) (right panel). β-Catenin and its co-activating histone acetyltransferases are highlighted (red).

(M and N) Quantification of CD11b$^+$ (left) and CD61$^+$ (right) BM-derived macrophages cultured with medium including vehicle (DMSO) or IQ1 (M)/ICG001 (N) with and without MCMV-GFP infection, measured via flow cytometry 2 dpi. n = 5–12/3.

(O) Invasion assay of sorted bystander and infected BM-derived macrophages of *LysM*$^{cre/+}$:*Zeb1*$^{fl/fl}$ or *LysM*$^{+/+}$:*Zeb1*$^{fl/fl}$ controls. n = 4/2; unpaired t test.

(P) qRT-PCR of human monocyte-derived macrophage transcripts after infection with HCMV-GFP 3 dpi. 4 donors in 3 independent experiments; unpaired t test.

Data are mean ± SEM. *p < 0.05, **p < 0.01, ***p < 0.001. One-way ANOVA followed by Tukey's multiple comparisons test unless stated otherwise.

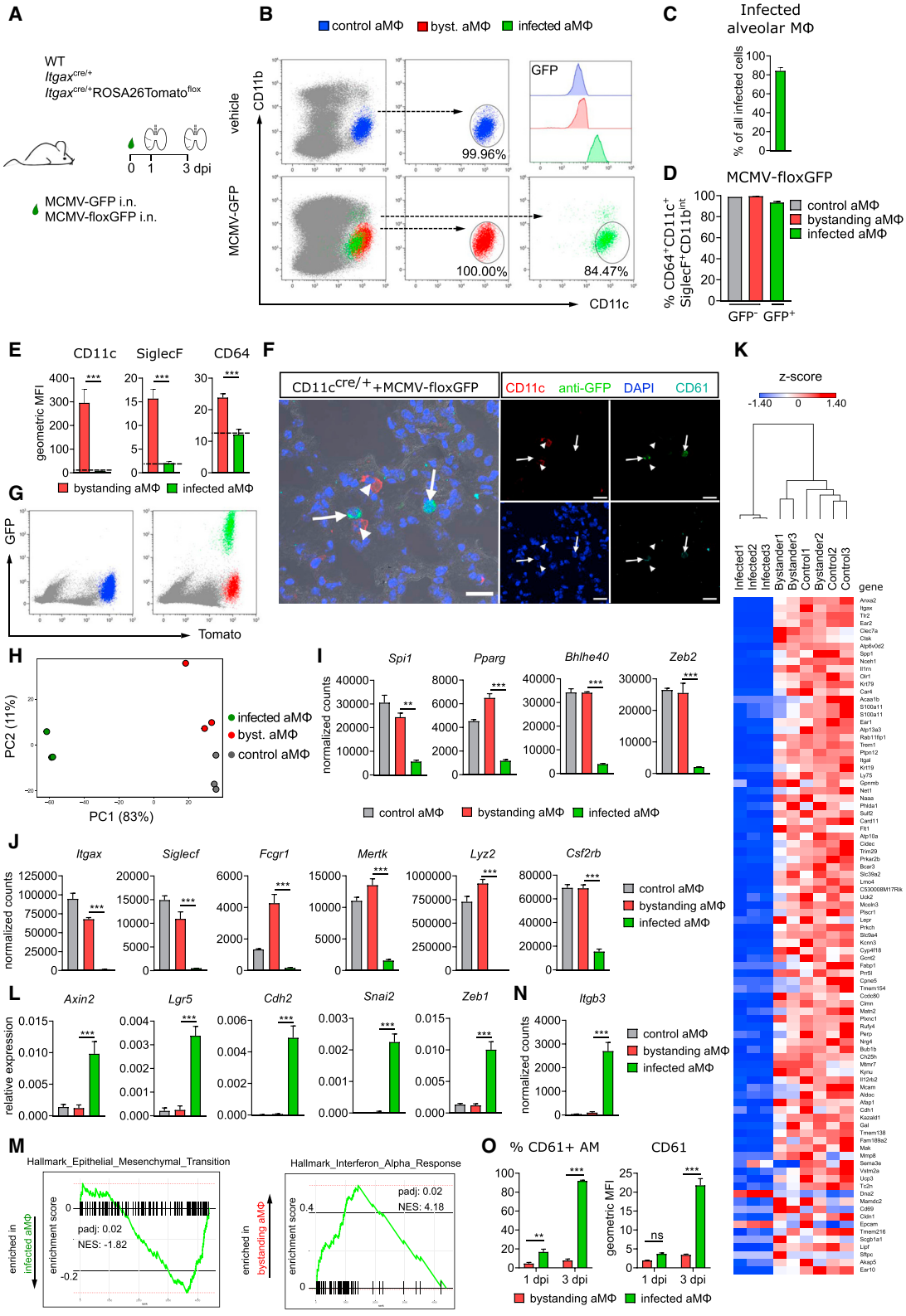

(legend on next page)

Please cite this article in press as: Baasch et al., Cytomegalovirus subverts macrophage identity, Cell (2021), https://doi.org/10.1016/j.cell.2021.05.009

MCMV-floxGFP. Lung histology revealed that infected GFP$^+$ Tomato$^+$ alveolar macrophages can be found in the interstitium already at 1 dpi (Figures 7D and S7D).

Notably, we found some GFP$^+$ cells in the draining mediastinal lymph nodes in *Itgax*$^{cre/+}$ mice infected with MCMV-floxGFP at 1 dpi (Figure 7E), and the majority of these cells were labeled endogenously with Tomato after infection of *Itgax*$^{cre/+}$ ROSA26-Tomato^{flox} mice (Figure 7F). To analyze the origin of these cells, we employed *Csf2rb*$^{-/-}$ mice reconstituted with Tomato$^+$ alveolar macrophages (Figure S7C) and found GFP$^+$ Tomato$^+$ alveolar macrophages in the draining lymph nodes (Figures S7E and S7F). Accordingly, a small number of CMV-infected alveolar macrophages translocate to relatively distant sites.

Because we identified ZEB1 to be essential for MCMV-induced BM-derived macrophage invasion *in vitro*, we next explored its role in alveolar macrophage migration during MCMV infection *in vivo*. In full support of the *in vitro* data, we found a reduced number of GFP$^+$ cells in the lymph nodes of intranasally MCMV-infected *LysM*$^{cre/+}$:*Zeb1*$^{flox/flox}$ mice compared with infected control mice (Figure 7G). Of note, ZEB1 deficiency did not substantially alter the number of infected cells (Figure S7G). Similarly to *Itgax*$^{cre/+}$ mice (Figures 6D and S6B), only alveolar macrophages and not CD103$^+$ DCs were initially infected in *LysM*$^{cre/+}$ mice (Figure S7H). Moreover, neutrophils and especially monocytes, which also express *LysM*, were not targeted by CMV at early stages (Figure S7I).

Finally, RNA-seq of MCMV-infected alveolar macrophages (3 dpi) revealed differentially expressed genes in infected *LysM*$^{cre/+}$ compared with infected alveolar macrophages from *LysM*$^{cre/+}$:Zeb1$^{flox/flox}$ mice with overrepresentation in GO terms associated with regulation of cell migration (GO0030334), immune response (GO0006955), response to oxygen compound (GO1901700), and cellular response to IFN beta (GO0035458) (Figure S7J).

Thus, MCMV-infected alveolar macrophages promote viral spread in the lungs and potentially other tissues via invasion of the lung interstitium and, in some cases, the draining lymph nodes in a ZEB1-dependent fashion.

CMV infection of alveolar macrophages impairs their function and confers susceptibility to secondary infection

One of the hallmark functions of alveolar macrophages is phagocytic clearance of constantly produced surfactant. To analyze the phagocytic capacity of infected alveolar macrophages, we applied the fluorescent dye PKH26 intranasally 2 dpi (Neupane et al., 2020; Figure 7H). We found markedly reduced uptake of PKH26 in infected alveolar macrophages from bronchoalveolar lavage (BAL) and lung homogenates compared with bystander and uninfected alveolar macrophages (Figures 7I). Moreover, components of surfactant (i.e., cholesterol and phospholipids) accumulated in the BAL fluid (Figure 7J).

In the postnatal period, when CMV infection is usually established, the immune system encounters numerous microorganisms and other viruses for the first time and needs to establish an appropriate immune response. Therefore, we further explored the functional consequences of CMV-induced alveolar macrophage transformation and analyzed the response to secondary challenges. First, we administered poly(I:C), an RNA analog to mimic infection with RNA viruses, intranasally 3 days after CMV infection and analyzed sorted macrophage subsets 8 h later (Figure 7K). In contrast to bystander alveolar macrophages, infected alveolar macrophages did not form NF-κB- and IFN-mediated cytokines (Figures 7L, 7M, and S7K). Next we infected mice with *Legionella pneumophila* (*Lp*), a frequent environmental inhabitant and cause of severe pneumonia in humans that has been shown to target alveolar macrophages (Chandler et al., 1977; Fraser et al., 1977; Ziltener et al., 2016; Figure 7N). In full accordance with the notion that CMV profoundly remodels the first-line macrophage response, we found mice in which approximately half of the alveolar macrophage population was infected with CMV (Figure S7L) to be severely impaired in their antibacterial response because they failed to reduce the bacterial load in the lungs (Figure 7O) and lost weight continuously (Figure 7P). In contrast, mice only infected with *Lp* recovered after 3 dpi. Strikingly, the lungs of CMV-*Lp*-infected mice showed decreased numbers of neutrophils, which are important for bacterial clearance and alveolar macrophage activation in bacterial infection

Figure 6. Infected alveolar macrophages are reprogrammed *in vivo*

(A) Schematic of mice and MCMVs used in *in vivo* experiments.
(B) Representative flow cytometry plots of the lungs of MCMV-GFP-infected or vehicle-administered WT mice 1 dpi and GFP expression (histogram) of CD11b^{int} CD11c$^+$ alveolar macrophages (aMΦ; top right). Representative of n = 6/3.
(C) Quantification of infected GFP$^+$ CD11b^{int} CD11c$^+$ alveolar macrophages 1 dpi. n = 6/3.
(D) Quantification of non-infected (GFP$^-$) control and bystander alveolar macrophages and infected (GFP$^+$) alveolar macrophages of *Itgax*$^{cre/+}$ mice infected with MCMV-floxGFP 12 hpi. n = 7/3.
(E) Expression intensity of CD11c, SiglecF, and CD64 on bystander and infected alveolar macrophages of *Itgax*$^{cre/+}$ mice infected with MCMV-floxGFP 3 dpi.
(F) Bystander (arrow head) and infected (arrow) alveolar macrophages in the lungs of *Itgax*$^{cre/+}$ mice infected with MCMV-floxGFP 3 dpi. Scale bars, 20 μm. Representative of n = 3/2.
(G) Representative flow cytometry plot of vehicle- (left) and MCMV-floxGFP-infected *Itgax*$^{cre/+}$ ROSA26-Tomato^{flox} mice 3 dpi.
(H) PCA of control (gray), bystander (red), and infected (green) alveolar macrophages transcriptomes.
(I) Normalized counts of transcription factors determining alveolar macrophage fate and maintenance.
(J) Normalized counts of surface marker and *Lyz2* gene expression characteristic for alveolar macrophages.
(K) Heatmap of the alveolar macrophage gene profile 3 dpi.
(L) qRT-PCR of Wnt target genes, mesenchymal genes, and genes of EMT-driving transcription factors in alveolar macrophages.
(M) Gene set enrichment analysis comparing infected and bystander alveolar macrophages.
(N) Normalized counts of *Itgb3* (alveolar macrophage RNA-seq).
(O) CD61$^+$ bystander and infected alveolar macrophages (left) and expression intensity of CD61 (right) 1 and 3 dpi.
Data are mean ± SEM. *p < 0.05, **p < 0.01, ***p < 0.001. One-way ANOVA followed by Tukey's multiple comparison test unless stated otherwise.

Please cite this article in press as: Baasch et al., Cytomegalovirus subverts macrophage identity, Cell (2021), https://doi.org/10.1016/j.cell.2021.05.009

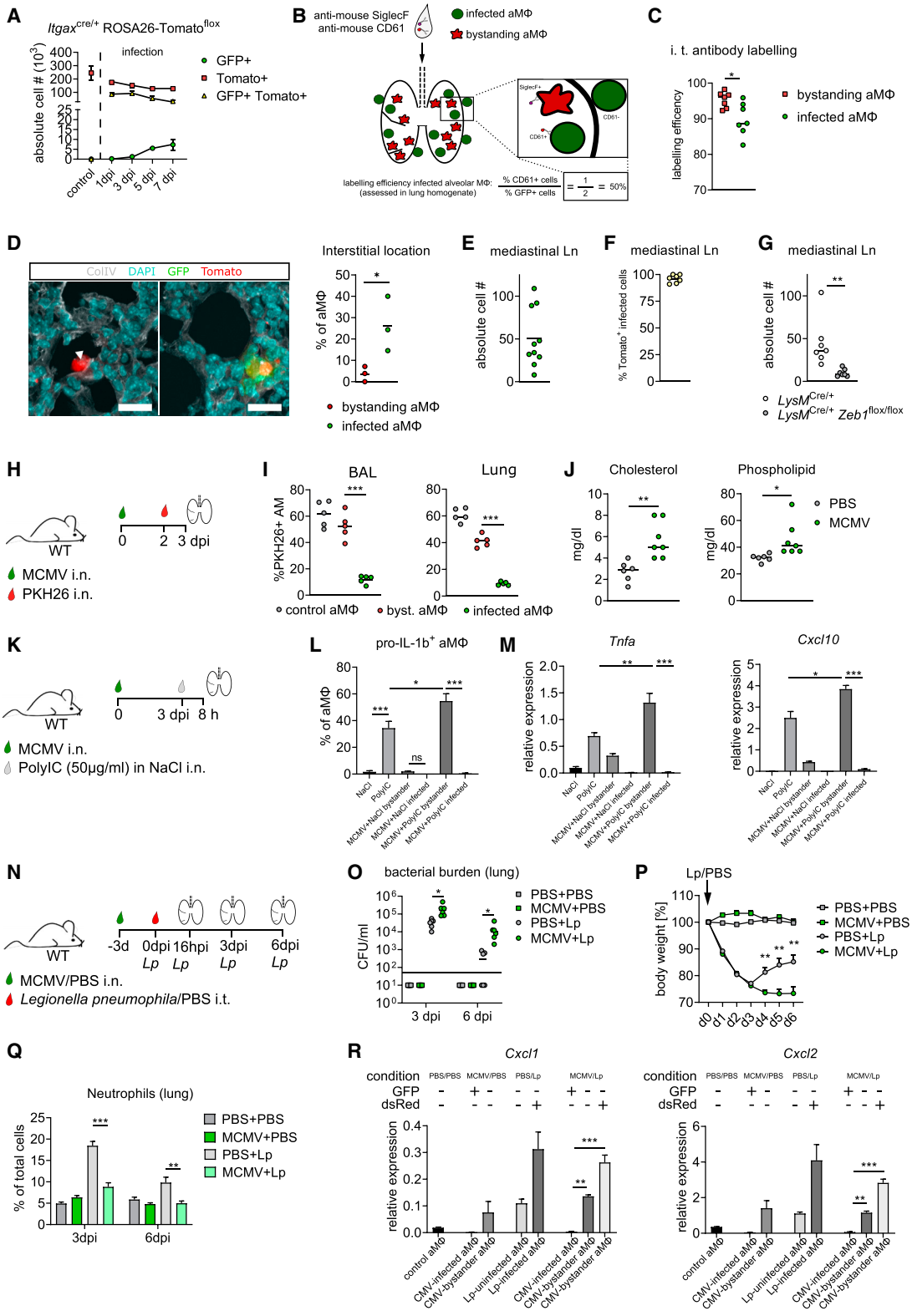

Figure 7. CMV infection of alveolar macrophages impairs their function and renders them susceptible to secondary infection

(A) Number of alveolar macrophage subsets and newly infected cells in *Itgax*$^{cre/+}$ ROSA26-Tomato^{flox} mice after treatment with PBS (control) or infection with MCMV-floxGFP via flow cytometry. n = 3–9/2–3.

(legend continued on next page)

Please cite this article in press as: Baasch et al., Cytomegalovirus subverts macrophage identity, Cell (2021), https://doi.org/10.1016/j.cell.2021.05.009

(Tateda et al., 2001; Figure 7Q). In contrast to the lungs, neutrophil numbers in the peripheral blood were elevated early after secondary bacterial infection (Figure S7M). This suggested impaired chemokine production by CMV-infected alveolar macrophages. Therefore, we sorted alveolar macrophage populations after infection with a dsRed-expressing reporter *Lp* strain, which allowed us to distinguish CMV-infected (GFP^+) and uninfected (GFP^-) as well as *Lp*-infected ($dsRed^+$) and uninfected ($dsRed^-$) alveolar macrophages. Notably, CMV-infected alveolar macrophages did not take up *Lp*, in line with the phagocytic impairment of infected alveolar macrophages (Figure 7I). Moreover, cytokines and the neutrophil chemoattractants *Cxcl1* and *Cxcl2* were strongly reduced in acute CMV-infected alveolar macrophages after bacterial infection (Figures 7R and S7N). Altogether, CMV specifically targets alveolar macrophages, alters their physiological functions, and affects the outcome of secondary infections.

DISCUSSION

Early postnatal infection links CMV to development of the individual immune system in most humans worldwide. In this study, analysis of a virulent GFP reporter MCMV enabled us to resolve the effect of CMV infection on macrophage-autonomous immunity *in vitro* and *in vivo*. Previously, downregulation of individual surface proteins (e.g., natural killer [NK] cell ligands) has been reported upon CMV infection, mainly in fibroblasts, but also in macrophages (Lenac et al., 2006; Lodoen et al., 2003; Thiel et al., 2016; Zarama et al., 2014; Ziegler et al., 1997). Furthermore, macrophages show dysfunctional behavior after CMV infection (Pesanti and Shanley, 1984; Shanley and Pesanti, 1980). However, the underlying mechanism and the extent of these changes had not been resolved. Based on large-scale and kinetic transcriptome and proteome analyses, we uncovered that surface protein downregulation is not only mere avoidance of receptor-ligand interaction but part of a complete rewiring process in infected macrophages. The transcriptional and translational changes in infected macrophages differ from previously described changes of the polarization state in differentiated macrophages and represent a novel, ambiguous cell state. Notably, CMV-transformed macrophages do not suffer from host shutoff, as reported for other herpesviruses (Kwong and Frenkel, 1987; Rowe et al., 2007). Mechanistically, Wnt signaling is at the heart of macrophage transformation by CMV. Inhibition of the interaction of p300- and CBP/β-catenin as well as ROCK partially rescued macrophage reprogramming, suggesting involvement of the canonical and non-canonical Wnt pathways. Wnt pathway engagement induces ZEB1 (Kahlert et al., 2012; Yang et al., 2015), which, in turn, enhances cellular transformation and Wnt target gene expression by interaction with p300 (Sánchez-Tilló et al., 2015), suggesting a positive feedback loop. Moreover, it induces stemness and invasion (Burk et al., 2008; Wellner et al., 2009). Because conditional disruption of *Zeb1* prevented CMV-induced macrophage invasiveness without affecting other phenotypical changes, conserved pathways such as Notch and TGF-β might also be involved. This is supported by our pathway analysis because TGF-β signaling might be activated downstream of TGF-β receptor I in CMV infection. Wnt pathway-related soluble factors have been identified previously as biomarkers in CMV reactivation after solid organ transplantation (Ueland et al., 2014). Together with our finding that human monocyte-derived macrophages upregulate Wnt-target genes, *ZEB1* and *SNAI2*, upon HCMV infection, this points toward a conserved role of the Wnt pathway in CMV infection. Importantly, our *in vivo* results uncover a central role of alveolar macrophages in CMV infection. A portion of infected alveolar macrophages invade the lung tissue and may initiate formation of nodular inflammatory foci with delayed viral clearance (Stahl et al., 2013). Moreover, infected alveolar macrophages may seed CMV to distal sites (i.e., the draining lymph nodes), which has also been described for dendritic cells (Farrell et al., 2017). However, here we establish that alveolar macrophages and not dendritic cells are initially infected in pulmonary MCMV infection.

(B) Schematic of *in vivo* labeling of infected and bystander alveolar macrophages in the alveolar space.
(C) *In vivo* labeling efficiency of bystander and infected alveolar macrophages via flow cytometry. n = 7/2.
(D) Representative immunofluorescence image (left) and quantification (right) of alveolar macrophage subsets 1 dpi with MCMV-floxGFP; bystander alveolar macrophages in the alveolus (arrowhead), infected alveolar macrophages in the interstitium (asterisk). Scale bars, 20 μm. For quantification, a minimum of 15 fields of view/mouse were analyzed. n = 3/2.
(E) Number of GFP^+ cells in the mediastinal lymph nodes 1 dpi with MCMV-floxGFP. n = 10/3.
(F) Relative number of $Tomato^+$ infected cells in the mediastinal lymph node 1 dpi. n = 7/2.
(G) Number of GFP^+ cells in the mediastinal lymph nodes of $LysM^{cre/+}$ and $LysM^{cre/+}$:$Zeb1^{flox/flox}$ mice 1 dpi with MCMV-floxGFP. n = 7/2.
(H) Scheme of the phagocytosis assay *in vivo*.
(I) Phagocytic alveolar macrophages in BAL or lung homogenates 3 dpi. n = 5/2.
(J) Cholesterol and phospholipid concentrations in the BAL fluid of mice 5 dpi with PBS or MCMV-GFP. n = 6/3 (PBS) or n = 7/3 (MCMV-GFP). Two-tailed unpaired t test.
(K) Schematic of intranasal poly(I:C) (re)challenge.
(L) Quantification of pro-IL-1beta$^+$ alveolar macrophages via flow cytometry. n = 6/2.
(M) qRT-PCR of *Tnfa* and IFN-stimulated genes of sorted alveolar macrophages after (re) stimulation with poly(I:C). n = 3/2.
(N) Scheme of secondary intratracheal infection with *Lp*.
(O) Quantification of *Lp* (CFU/mL) in the lungs. A line indicates the detection limit. n = 6/2.
(P) Weight curve of mice after infection with *Lp* or PBS administration. Mice were infected previously with MCMV-GFP or treated with PBS. n = 5–10/3 (without *Lp* infection) or n = 9–18/3 (with *Lp* infection). Two-tailed unpaired t test.
(Q) Relative neutrophil numbers in the lungs, determined via flow cytometry. n = 5/3 (without *Lp* infection) or n = 9/3 (with *Lp* infection).
(R) qRT-PCR of cytokines and chemokines expressed by sorted alveolar macrophage subsets 16 hpi with *Lp*. n = 3/1.
Data are mean ± SEM. *p < 0.05, **p < 0.01, ***p < 0.001. One-way ANOVA followed by Tukey's multiple comparisons test unless stated otherwise.

Moreover, analysis of BM-derived macrophage number after infection *in vitro* and transfer of infected alveolar macrophages did not provide any evidence for early cell death, which could provide viral antigen (and GFP) for cross-presentation by dendritic cells. This is probably due to MCMV-encoding proteins, which inhibit early necroptosis and apoptosis specifically in macrophages (Daley-Bauer et al., 2017). Additionally, transplantation of alveolar macrophages revealed that MCMV-infected alveolar macrophages can reach the mediastinal lymph nodes as early as 1 dpi.

Downregulation of macrophage lineage markers may have led to underestimation of macrophages in CMV infection in previous work. Moreover, CMV latency has been reported in precursor cells of the myeloid lineage bearing unorthodox phenotypes (Hahn et al., 1998). Our data imply that these cells may actually be reprogrammed mature cells rather than *bona fide* precursors. Inclusion of non-conventional surface markers such as CD61 should be helpful in future work regarding this issue.

Our findings have important implications for understanding macrophage biology, CMV pathogenesis, and CMV-related diseases. The diversity of tissue-resident macrophages has recently become more evident, with identification of distinct immunophenotypes and gene signatures shaped by individual microenvironmental niches (Blériot et al., 2020). The changes observed in CMV-infected macrophages, however, exceed the established limits of macrophage plasticity and niche adaptation. Moreover, macrophages reprogrammed by CMV could be implicated in breast cancer, where tumor tissue often bears CMV (Taher et al., 2013). Secretion of bioactive molecules by macrophages, which induce the Wnt signaling pathway, may promote tumor growth and de-differentiation (Luga et al., 2012; Yook et al., 2006). CMV-induced reprogramming of macrophages may also be of significance in coinfections (e.g., in congenital HIV infection; Gartner et al., 1986), where CMV-driven invasion may facilitate maternal-fetal transmission. Furthermore, we provide evidence that, through modulation of the macrophage phenotype, CMV affects site-specific immunity against bacteria and, thus, the course and outcome of secondary infection. Whether a prior CMV infection is beneficial or detrimental may then depend on the ratio of emerging "non-functional" infected macrophages to pre-activated bystander macrophages and the time point of secondary infection.

This work substantially expands the known immune-modulating properties of CMV leading to identity loss of specialized and highly differentiated tissue macrophages. Co-evolution appears to have led to interference with conserved signaling pathways and, ultimately, to subversion of macrophage properties. Thus, previously established limits of macrophage plasticity are exceeded, and a novel cell state evolves, which serves the needs of the virus for proliferation and propagation.

Limitations of the study

Our study describes the parallel emergence of two macrophage populations after respiratory infection with CMV. Although the transformation process of infected macrophages was explored in detail, bystander macrophages were characterized less well beyond the IFN I signature.

Several lines of evidence are provided, showing that CMV-infected alveolar macrophages migrate to the regional lymph nodes. However, this concerns only a small number of "pioneering" cells. Cellular characteristics beyond *Zeb1* expression that allow this behavior in CMV infection need to be resolved, as well as the role of these translocated cells in immunity to CMV.

Finally, whether CMV induces similar transformation events in other myeloid cells, in particular dendritic cells, and how these contribute to specific infection pathogenesis awaits clarification.

STAR★METHODS

Detailed methods are provided in the online version of this paper and include the following:

- KEY RESOURCES TABLE
- RESOURCE AVAILABILITY
  - Lead contact
  - Materials availability
  - Data and code availability
- EXPERIMENTAL MODEL AND SUBJECT DETAILS
  - Mice
  - Human samples
- METHOD DETAILS
  - Viruses and bacteria
  - In vitro
  - Animal procedures
  - Molecular analyses
  - Flow cytometry
  - Image techniques and analysis
  - RNA-seq and transcriptomic data analysis
  - Mass spectrometry
- QUANTIFICATION AND STATISTICAL ANALYSIS

SUPPLEMENTAL INFORMATION

Supplemental information can be found online at https://doi.org/10.1016/j.cell.2021.05.009.

ACKNOWLEDGMENTS

The authors thank A. Imm, D. Gütle and B. Joch, J. Bodinek-Wersing, and the Lighthouse facility (University Medical Center Freiburg) for excellent technical support. We further thank A. Ablasser (Lausanne) for *Tmem173*$^{-/-}$ mice and B. Adler (Munich) for Rep3.3 MCMV as well as F. Piattini (Zurich) and F. Li (Zurich) for advice and help with *Lp* infections. The authors acknowledge support from B. Grüning and R. Backofen (University of Freiburg, European Galaxy Project). Funding was provided by the Else-Kröner-Fresenius Foundation (to P.H.), the German Ministry of Education and Research (BMBF; grants 01EO0803, 01GL1746A, and 01EK1602A to P.H. and grant 031L0090 to H.H.), and the German Research Council (DFG; grants HE3127/9, HE3127/12, HE3127/16, and SFB/TRR167 to P.H.; HE2526/9-1 to H.H.; 406922110 to Z.R.; and SFB/TRR305 to T.B.). R.E. received support from the Berta Ottenstein Program (Faculty of Medicine, University of Freiburg) and J.K. was funded by EQUIP (Faculty of Medicine, University of Freiburg). The graphical abstract has been created with BioRender.com.

AUTHOR CONTRIBUTIONS

Conceptualization, S. Baasch and P.H.; methodology and study design, S. Baasch, Z.R., and P.H.; investigation, S. Baasch, J.K., A.R., S.R., A.J.F., and S.Z.; (phospho)proteome analysis, P.G. and B.K.; transmission electron microscopy, A.V.; funding acquisition, P.H. and H.H.; resources, R.E., A.H., S. Brabletz, T.B., J.R., L.C.-S., R.A., M.P.S., M.K., and Z.R.; supervision, P.H.; writing of draft, S.B. and P.H.

DECLARATION OF INTERESTS

The authors declare no competing interests.

Received: October 26, 2020
Revised: February 26, 2021
Accepted: May 7, 2021
Published: June 10, 2021

REFERENCES

Abate, D.A., Watanabe, S., and Mocarski, E.S. (2004). Major human cytomegalovirus structural protein pp65 (ppUL83) prevents interferon response factor 3 activation in the interferon response. J. Virol. *78*, 10995–11006.

Adachi, O., Kawai, T., Takeda, K., Matsumoto, M., Tsutsui, H., Sakagami, M., Nakanishi, K., and Akira, S. (1998). Targeted Disruption of the MyD88 Gene Results in Loss of IL-1- and IL-18-Mediated Function. Immunity *9*, 143–150. https://doi.org/10.1016/S1074-7613(00)80596-8.

Afgan, E., Baker, D., Batut, B., van den Beek, M., Bouvier, D., Čech, M., Chilton, J., Clements, D., Coraor, N., Grüning, B.A., et al. (2018). The Galaxy platform for accessible, reproducible and collaborative biomedical analyses: 2018 update. Nucleic Acids Res. *46* (W1), W537–W544.

Aziz, A., Soucie, E., Sarrazin, S., and Sieweke, M.H. (2009). MafB/c-Maf deficiency enables self-renewal of differentiated functional macrophages. Science *326*, 867–871.

Blériot, C., Chakarov, S., and Ginhoux, F. (2020). Determinants of Resident Tissue Macrophage Identity and Function. Immunity *52*, 957–970.

Boyer, S.W., Schroeder, A.V., Smith-Berdan, S., and Forsberg, E.C. (2011). All hematopoietic cells develop from hematopoietic stem cells through Flk2/Flt3-positive progenitor cells. Cell Stem Cell *9*, 64–73.

Brabletz, S., Lasierra Losada, M., Schmalhofer, O., Mitschke, J., Krebs, A., Brabletz, T., and Stemmler, M.P. (2017). Generation and characterization of mice for conditional inactivation of Zeb1. Genesis *55*.

Browne, E.P., and Shenk, T. (2003). Human cytomegalovirus UL83-coded pp65 virion protein inhibits antiviral gene expression in infected cells. Proc. Natl. Acad. Sci. USA *100*, 11439–11444.

Burk, U., Schubert, J., Wellner, U., Schmalhofer, O., Vincan, E., Spaderna, S., and Brabletz, T. (2008). A reciprocal repression between ZEB1 and members of the miR-200 family promotes EMT and invasion in cancer cells. EMBO Rep. *9*, 582–589.

Cain, D.W., O'Koren, E.G., Kan, M.J., Womble, M., Sempowski, G.D., Hopper, K., Gunn, M.D., and Kelsoe, G. (2013). Identification of a tissue-specific, C/EBPβ-dependent pathway of differentiation for murine peritoneal macrophages. J. Immunol. *191*, 4665–4675.

Chandler, F.W., Hicklin, M.D., and Blackmon, J.A. (1977). Demonstration of the agent of Legionnaires' disease in tissue. N. Engl. J. Med. *297*, 1218–1220.

Coleman, M.L., Sahai, E.A., Yeo, M., Bosch, M., Dewar, A., and Olson, M.F. (2001). Membrane blebbing during apoptosis results from caspase-mediated activation of ROCK I. Nat. Cell Biol. *3*, 339–345.

Cox, J., and Mann, M. (2008). MaxQuant enables high peptide identification rates, individualized p.p.b.-range mass accuracies and proteome-wide protein quantification. Nat. Biotechnol. *26*, 1367–1372.

Cox, J., and Mann, M. (2012). 1D and 2D annotation enrichment: a statistical method integrating quantitative proteomics with complementary high-throughput data. BMC Bioinformatics *13* (*Suppl 16*), S12.

Daley-Bauer, L.P., Roback, L., Crosby, L.N., McCormick, A.L., Feng, Y., Kaiser, W.J., and Mocarski, E.S. (2017). Mouse cytomegalovirus M36 and M45 death suppressors cooperate to prevent inflammation resulting from antiviral programmed cell death pathways. Proc. Natl. Acad. Sci. USA *114*, E2786–E2795.

De Schepper, S., Verheijden, S., Aguilera-Lizarraga, J., Viola, M.F., Boesmans, W., Stakenborg, N., Voytyuk, I., Schmidt, I., Boeckx, B., Dierckx de Casterlé, I., et al. (2018). Self-Maintaining Gut Macrophages Are Essential for Intestinal Homeostasis. Cell *175*, 400–415.e13.

Dobin, A., Davis, C.A., Schlesinger, F., Drenkow, J., Zaleski, C., Jha, S., Batut, P., Chaisson, M., and Gingeras, T.R. (2013). STAR: ultrafast universal RNA-seq aligner. Bioinformatics *29*, 15–21.

Edgar, R., Domrachev, M., and Lash, A.E. (2002). Gene Expression Omnibus: NCBI gene expression and hybridization array data repository. Nucleic Acids Res. *30*, 207–210.

El-Gebali, S., Mistry, J., Bateman, A., Eddy, S.R., Luciani, A., Potter, S.C., Qureshi, M., Richardson, L.J., Salazar, G.A., Smart, A., et al. (2019). The Pfam protein families database in 2019. Nucleic Acids Res. *47* (D1), D427–D432.

Elinav, E., Strowig, T., Kau, A.L., Henao-Mejia, J., Thaiss, C.A., Booth, C.J., Peaper, D.R., Bertin, J., Eisenbarth, S.C., Gordon, J.I., and Flavell, R.A. (2011). NLRP6 inflammasome regulates colonic microbial ecology and risk for colitis. Cell *145*, 745–757.

Farrell, H.E., Bruce, K., Lawler, C., Oliveira, M., Cardin, R., Davis-Poynter, N., and Stevenson, P.G. (2017). Murine Cytomegalovirus Spreads by Dendritic Cell Recirculation. mBio *8*, e01264–17.

Feuerstein, R., Gres, V., Elias Perdigó, N., Baasch, S., Freudenhammer, M., Elling, R., and Henneke, P. (2019). Macrophages Are a Potent Source of *Streptococcus*-Induced IFN-β. J. Immunol. *203*, 3416–3426.

Fodde, R., and Brabletz, T. (2007). Wnt/beta-catenin signaling in cancer stemness and malignant behavior. Curr. Opin. Cell Biol. *19*, 150–158.

Fraser, D.W., Tsai, T.R., Orenstein, W., Parkin, W.E., Beecham, H.J., Sharrar, R.G., Harris, J., Mallison, G.F., Martin, S.M., McDade, J.E., et al. (1977). Legionnaires' disease: description of an epidemic of pneumonia. N. Engl. J. Med. *297*, 1189–1197.

Gartner, S., Markovits, P., Markovitz, D.M., Kaplan, M.H., Gallo, R.C., and Popovic, M. (1986). The role of mononuclear phagocytes in HTLV-III/LAV infection. Science *233*, 215–219.

Gautier, E.L., Shay, T., Miller, J., Greter, M., Jakubzick, C., Ivanov, S., Helft, J., Chow, A., Elpek, K.G., Gordonov, S., et al.; Immunological Genome Consortium (2012). Gene-expression profiles and transcriptional regulatory pathways that underlie the identity and diversity of mouse tissue macrophages. Nat. Immunol. *13*, 1118–1128.

Gil, M.P., Bohn, E., O'Guin, A.K., Ramana, C.V., Levine, B., Stark, G.R., Virgin, H.W., and Schreiber, R.D. (2001). Biologic consequences of Stat1-independent IFN signaling. Proc. Natl. Acad. Sci. USA *98*, 6680–6685.

Ginhoux, F., Schultze, J.L., Murray, P.J., Ochando, J., and Biswas, S.K. (2016). New insights into the multidimensional concept of macrophage ontogeny, activation and function. Nat. Immunol. *17*, 34–40.

Gosselin, D., Link, V.M., Romanoski, C.E., Fonseca, G.J., Eichenfield, D.Z., Spann, N.J., Stender, J.D., Chun, H.B., Garner, H., Geissmann, F., and Glass, C.K. (2014). Environment drives selection and function of enhancers controlling tissue-specific macrophage identities. Cell *159*, 1327–1340.

Gröger, C.J., Grubinger, M., Waldhör, T., Vierlinger, K., and Mikulits, W. (2012). Meta-analysis of gene expression signatures defining the epithelial to mesenchymal transition during cancer progression. PLoS ONE *7*, e51136.

Guilliams, M., and Svedberg, F.R. (2021). Does tissue imprinting restrict macrophage plasticity? Nat. Immunol. *22*, 118–127.

Guilliams, M., De Kleer, I., Henri, S., Post, S., Vanhoutte, L., De Prijck, S., Deswarte, K., Malissen, B., Hammad, H., and Lambrecht, B.N. (2013).

Alveolar macrophages develop from fetal monocytes that differentiate into long-lived cells in the first week of life via GM-CSF. J. Exp. Med. *210*, 1977–1992.

Guilliams, M., Thierry, G.R., Bonnardel, J., and Bajenoff, M. (2020). Establishment and Maintenance of the Macrophage Niche. Immunity *52*, 434–451.

Hahn, G., Jores, R., and Mocarski, E.S. (1998). Cytomegalovirus remains latent in a common precursor of dendritic and myeloid cells. Proc. Natl. Acad. Sci. USA *95*, 3937–3942.

Heath, V., Suh, H.C., Holman, M., Renn, K., Gooya, J.M., Parkin, S., Klarmann, K.D., Ortiz, M., Johnson, P., and Keller, J. (2004). C/EBPalpha deficiency results in hyperproliferation of hematopoietic progenitor cells and disrupts macrophage development in vitro and in vivo. Blood *104*, 1639–1647.

Heinz, S., Benner, C., Spann, N., Bertolino, E., Lin, Y.C., Laslo, P., Cheng, J.X., Murre, C., Singh, H., and Glass, C.K. (2010). Simple combinations of lineage-determining transcription factors prime cis-regulatory elements required for macrophage and B cell identities. Mol. Cell *38*, 576–589.

Hornbeck, P.V., Zhang, B., Murray, B., Kornhauser, J.M., Latham, V., and Skrzypek, E. (2015). PhosphoSitePlus, 2014: mutations, PTMs and recalibrations. Nucleic Acids Res. *43*, D512–D520.

Jiang, H., Lei, R., Ding, S.W., and Zhu, S. (2014). Skewer: a fast and accurate adapter trimmer for next-generation sequencing paired-end reads. BMC Bioinformatics *15*, 182.

Jordan, S., Krause, J., Prager, A., Mitrovic, M., Jonjic, S., Koszinowski, U.H., and Adler, B. (2011). Virus progeny of murine cytomegalovirus bacterial artificial chromosome pSM3fr show reduced growth in salivary Glands due to a fixed mutation of MCK-2. J. Virol. *85*, 10346–10353.

Kahlert, U.D., Maciaczyk, D., Doostkam, S., Orr, B.A., Simons, B., Bogiel, T., Reithmeier, T., Prinz, M., Schubert, J., Niedermann, G., et al. (2012). Activation of canonical WNT/β-catenin signaling enhances in vitro motility of glioblastoma cells by activation of ZEB1 and other activators of epithelial-to-mesenchymal transition. Cancer Lett. *325*, 42–53.

Kahn, M. (2011). Symmetric division versus asymmetric division: a tale of two coactivators. Future Med. Chem. *3*, 1745–1763.

Kolter, J., Feuerstein, R., Spoeri, E., Gharun, K., Elling, R., Trieu-Cuot, P., Goldmann, T., Waskow, C., Chen, Z.J., Kirschning, C.J., et al. (2016). Streptococci Engage TLR13 on Myeloid Cells in a Site-Specific Fashion. J. Immunol. *196*, 2733–2741.

Kolter, J., Feuerstein, R., Zeis, P., Hagemeyer, N., Paterson, N., d'Errico, P., Baasch, S., Amann, L., Masuda, T., Lösslein, A., et al. (2019). A Subset of Skin Macrophages Contributes to the Surveillance and Regeneration of Local Nerves. Immunity *50*, 1482–1497.e7.

Kwong, A.D., and Frenkel, N. (1987). Herpes simplex virus-infected cells contain a function(s) that destabilizes both host and viral mRNAs. Proc. Natl. Acad. Sci. USA *84*, 1926–1930.

Le, V.T.K., Trilling, M., Zimmermann, A., and Hengel, H. (2008). Mouse cytomegalovirus inhibits beta interferon (IFN-beta) gene expression and controls activation pathways of the IFN-beta enhanceosome. Journal of general virology *89*. https://doi.org/10.1099/vir.0.83538-0.

Lee, J.M., Dedhar, S., Kalluri, R., and Thompson, E.W. (2006). The epithelial-mesenchymal transition: new insights in signaling, development, and disease. J. Cell Biol. *172*, 973–981.

Lenac, T., Budt, M., Arapovic, J., Hasan, M., Zimmermann, A., Simic, H., Krmpotic, A., Messerle, M., Ruzsics, Z., Koszinowski, U.H., et al. (2006). The herpesviral Fc receptor fcr-1 down-regulates the NKG2D ligands MULT-1 and H60. J. Exp. Med. *203*, 1843–1850.

Liao, Y., Smyth, G.K., and Shi, W. (2014). featureCounts: an efficient general purpose program for assigning sequence reads to genomic features. Bioinformatics *30*, 923–930.

Lodoen, M., Ogasawara, K., Hamerman, J.A., Arase, H., Houchins, J.P., Mocarski, E.S., and Lanier, L.L. (2003). NKG2D-mediated natural killer cell protection against cytomegalovirus is impaired by viral gp40 modulation of retinoic acid early inducible 1 gene molecules. J. Exp. Med. *197*, 1245–1253.

LoPiccolo, D.M., Gold, M.C., Kavanagh, D.G., Wagner, M., Koszinowski, U.H., and Hill, A.B. (2003). Effective inhibition of K(b)- and D(b)-restricted antigen presentation in primary macrophages by murine cytomegalovirus. J. Virol. *77*, 301–308.

Love, M.I., Huber, W., and Anders, S. (2014). Moderated estimation of fold change and dispersion for RNA-seq data with DESeq2. Genome Biol. *15*, 550.

Lu, M., and Shenk, T. (1996). Human cytomegalovirus infection inhibits cell cycle progression at multiple points, including the transition from G1 to S. J. Virol. *70*, 8850–8857.

Luga, V., Zhang, L., Viloria-Petit, A.M., Ogunjimi, A.A., Inanlou, M.R., Chiu, E., Buchanan, M., Hosein, A.N., Basik, M., and Wrana, J.L. (2012). Exosomes mediate stromal mobilization of autocrine Wnt-PCP signaling in breast cancer cell migration. Cell *151*, 1542–1556.

Lyman, S.D., and Jacobsen, S.E. (1998). c-kit ligand and Flt3 ligand: stem/progenitor cell factors with overlapping yet distinct activities. Blood *91*, 1101–1134.

Mampel, J., Spirig, T., Weber, S.S., Haagensen, J.A., Molin, S., and Hilbi, H. (2006). Planktonic replication is essential for biofilm formation by Legionella pneumophila in a complex medium under static and dynamic flow conditions. Appl. Environ. Microbiol. *72*, 2885–2895.

Martin, M. (2011). Cutadapt removes adapter sequences from high-throughput sequencing reads. EMBnet. J. *17*, 10–12.

McGeoch, D.J., Rixon, F.J., and Davison, A.J. (2006). Topics in herpesvirus genomics and evolution. Virus Res. *117*, 90–104.

McKercher, S.R., Torbett, B.E., Anderson, K.L., Henkel, G.W., Vestal, D.J., Baribault, H., Klemsz, M., Feeney, A.J., Wu, G.E., Paige, C.J., and Maki, R.A. (1996). Targeted disruption of the PU.1 gene results in multiple hematopoietic abnormalities. EMBO J. *15*, 5647–5658.

Metchnikoff, E. (1883). Untersuchungen über die mesodermalen Phagocyten einiger Wirbeltiere. Biol. Zent. Bl. *3*, 560–565.

Mi, H., Muruganujan, A., Ebert, D., Huang, X., and Thomas, P.D. (2019). PANTHER version 14: more genomes, a new PANTHER GO-slim and improvements in enrichment analysis tools. Nucleic Acids Res. *47* (D1), D419–D426.

Miettinen, P.J., Ebner, R., Lopez, A.R., and Derynck, R. (1994). TGF-beta induced transdifferentiation of mammary epithelial cells to mesenchymal cells: involvement of type I receptors. J. Cell Biol. *127*, 2021–2036.

Muegge, B.D., Kuczynski, J., Knights, D., Clemente, J.C., González, A., Fontana, L., Henrissat, B., Knight, R., and Gordon, J.I. (2011). Diet drives convergence in gut microbiome functions across mammalian phylogeny and within humans. Science *332*, 970–974.

Muranyi, W., Haas, J., Wagner, M., Krohne, G., and Koszinowski, U.H. (2002). Cytomegalovirus recruitment of cellular kinases to dissolve the nuclear lamina. Science *297*, 854–857.

Neupane, A.S., Willson, M., Chojnacki, A.K., Vargas E Silva Castanheira, F., Morehouse, C., Carestia, A., Keller, A.E., Peiseler, M., DiGiandomenico, A., Kelly, M.M., et al. (2020). Patrolling Alveolar Macrophages Conceal Bacteria from the Immune System to Maintain Homeostasis. Cell *183*, 110–125.e11.

Nieto, M.A., Huang, R.Y., Jackson, R.A., and Thiery, J.P. (2016). EMT: 2016. Cell *166*, 21–45.

Park, I.K., Qian, D., Kiel, M., Becker, M.W., Pihalja, M., Weissman, I.L., Morrison, S.J., and Clarke, M.F. (2003). Bmi-1 is required for maintenance of adult self-renewing haematopoietic stem cells. Nature *423*, 302–305.

Park, I.K., Morrison, S.J., and Clarke, M.F. (2004). Bmi1, stem cells, and senescence regulation. J. Clin. Invest. *113*, 175–179.

Paulus, C., Krauss, S., and Nevels, M. (2006). A human cytomegalovirus antagonist of type I IFN-dependent signal transducer and activator of transcription signaling. Proc. Natl. Acad. Sci. USA *103*, 3840–3845.

Peinado, H., Olmeda, D., and Cano, A. (2007). Snail, Zeb and bHLH factors in tumour progression: an alliance against the epithelial phenotype? Nat. Rev. Cancer *7*, 415–428.

Pesanti, E.L., and Shanley, J.D. (1984). Murine cytomegalovirus-induced macrophage dysfunction. J. Leukoc. Biol. *36*, 133–141.

Pfeffer, S., Zavolan, M., Grässer, F.A., Chien, M., Russo, J.J., Ju, J., John, B., Enright, A.J., Marks, D., Sander, C., and Tuschl, T. (2004). Identification of virus-encoded microRNAs. Science *304*, 734–736.

Piccolo, V., Curina, A., Genua, M., Ghisletti, S., Simonatto, M., Sabò, A., Amati, B., Ostuni, R., and Natoli, G. (2017). Opposing macrophage polarization programs show extensive epigenomic and transcriptional cross-talk. Nat. Immunol. *18*, 530–540.

Raaijmakers, L.M., Giansanti, P., Possik, P.A., Mueller, J., Peeper, D.S., Heck, A.J., and Altelaar, A.F. (2015). PhosphoPath: Visualization of Phosphosite-centric Dynamics in Temporal Molecular Networks. J. Proteome Res. *14*, 4332–4341.

Rawlinson, W.D., Farrell, H.E., and Barrell, B.G. (1996). Analysis of the complete DNA sequence of murine cytomegalovirus. J. Virol. *70*, 8833–8849.

R Core Team. (2013). R: A language and environment for statistical computing.

Reddehase, M.J., Weiland, F., Münch, K., Jonjic, S., Lüske, A., and Koszinowski, U.H. (1985). Interstitial murine cytomegalovirus pneumonia after irradiation: characterization of cells that limit viral replication during established infection of the lungs. J. Virol. *55*, 264–273.

Ren, J., Wen, L., Gao, X., Jin, C., Xue, Y., and Yao, X. (2009). DOG 1.0: illustrator of protein domain structures. Cell Res. *19*, 271–273.

Ritchie, M.E., Phipson, B., Wu, D., Hu, Y., Law, C.W., Shi, W., and Smyth, G.K. (2015). limma powers differential expression analyses for RNA-sequencing and microarray studies. Nucleic Acids Res. *43*, e47.

Rowe, M., Glaunsinger, B., van Leeuwen, D., Zuo, J., Sweetman, D., Ganem, D., Middeldorp, J., Wiertz, E.J., and Ressing, M.E. (2007). Host shutoff during productive Epstein-Barr virus infection is mediated by BGLF5 and may contribute to immune evasion. Proc. Natl. Acad. Sci. USA *104*, 3366–3371.

Ruprecht, B., Koch, H., Medard, G., Mundt, M., Kuster, B., and Lemeer, S. (2015). Comprehensive and reproducible phosphopeptide enrichment using iron immobilized metal ion affinity chromatography (Fe-IMAC) columns. Mol. Cell. Proteomics *14*, 205–215.

Ruprecht, B., Wang, D., Chiozzi, R.Z., Li, L.H., Hahne, H., and Kuster, B. (2017a). Hydrophilic Strong Anion Exchange (hSAX) Chromatography Enables Deep Fractionation of Tissue Proteomes. Methods Mol. Biol. *1550*, 69–82.

Ruprecht, B., Zecha, J., Zolg, D.P., and Kuster, B. (2017b). High pH Reversed-Phase Micro-Columns for Simple, Sensitive, and Efficient Fractionation of Proteome and (TMT labeled) Phosphoproteome Digests. Methods Mol. Biol. *1550*, 83–98.

Rutkowski, A.J., Erhard, F., L'Hernault, A., Bonfert, T., Schilhabel, M., Crump, C., Rosenstiel, P., Efstathiou, S., Zimmer, R., Friedel, C.C., and Dölken, L. (2015). Widespread disruption of host transcription termination in HSV-1 infection. Nat. Commun. *6*, 7126.

Sampaio, K.L., Weyell, A., Subramanian, N., Wu, Z., and Sinzger, C. (2017). A TB40/E-derived human cytomegalovirus genome with an intact US-gene region and a self-excisable BAC cassette for immunological research. Biotechniques *63*, 205–214.

Sánchez-Tilló, E., de Barrios, O., Siles, L., Cuatrecasas, M., Castells, A., and Postigo, A. (2011). β-catenin/TCF4 complex induces the epithelial-to-mesenchymal transition (EMT)-activator ZEB1 to regulate tumor invasiveness. Proc. Natl. Acad. Sci. USA *108*, 19204–19209.

Sánchez-Tilló, E., de Barrios, O., Valls, E., Darling, D.S., Castells, A., and Postigo, A. (2015). ZEB1 and TCF4 reciprocally modulate their transcriptional activities to regulate Wnt target gene expression. Oncogene *34*, 5760–5770.

Schindelin, J., Arganda-Carreras, I., Frise, E., Kaynig, V., Longair, M., Pietzsch, T., Preibisch, S., Rueden, C., Saalfeld, S., Schmid, B., et al. (2012). Fiji: an open-source platform for biological-image analysis. Nat. Methods *9*, 676–682.

Schlake, T., and Bode, J. (1994). Use of mutated FLP recognition target (FRT) sites for the exchange of expression cassettes at defined chromosomal loci. Biochemistry *33*, 12746–12751.

Schneider, C., Nobs, S.P., Kurrer, M., Rehrauer, H., Thiele, C., and Kopf, M. (2014). Induction of the nuclear receptor PPAR-γ by the cytokine GM-CSF is critical for the differentiation of fetal monocytes into alveolar macrophages. Nat. Immunol. *15*, 1026–1037.

Scott, C.L., T'Jonck, W., Martens, L., Todorov, H., Sichien, D., Soen, B., Bonnardel, J., De Prijck, S., Vandamme, N., Cannoodt, R., et al. (2018). The Transcription Factor ZEB2 Is Required to Maintain the Tissue-Specific Identities of Macrophages. Immunity *49*, 312–325.e5.

Shanley, J.D., and Pesanti, E.L. (1980). Replication of murine cytomegalovirus in lung macrophages: effect of phagocytosis of bacteria. Infect. Immun. *29*, 1152–1159.

Shannon, P., Markiel, A., Ozier, O., Baliga, N.S., Wang, J.T., Ramage, D., Amin, N., Schwikowski, B., and Ideker, T. (2003). Cytoscape: a software environment for integrated models of biomolecular interaction networks. Genome Res. *13*, 2498–2504.

Slenter, D.N., Kutmon, M., Hanspers, K., Riutta, A., Windsor, J., Nunes, N., Mélius, J., Cirillo, E., Coort, S.L., Digles, D., et al. (2018). WikiPathways: a multifaceted pathway database bridging metabolomics to other omics research. Nucleic Acids Res. *46* (D1), D661–D667.

Stahl, F.R., Heller, K., Halle, S., Keyser, K.A., Busche, A., Marquardt, A., Wagner, K., Boelter, J., Bischoff, Y., Kremmer, E., et al. (2013). Nodular inflammatory foci are sites of T cell priming and control of murine cytomegalovirus infection in the neonatal lung. PLoS Pathog. *9*, e1003828.

Szklarczyk, D., Gable, A.L., Lyon, D., Junge, A., Wyder, S., Huerta-Cepas, J., Simonovic, M., Doncheva, N.T., Morris, J.H., Bork, P., et al. (2019). STRING v11: protein-protein association networks with increased coverage, supporting functional discovery in genome-wide experimental datasets. Nucleic Acids Res. *47* (D1), D607–D613.

Taher, C., de Boniface, J., Mohammad, A.A., Religa, P., Hartman, J., Yaiw, K.C., Frisell, J., Rahbar, A., and Söderberg-Naucler, C. (2013). High prevalence of human cytomegalovirus proteins and nucleic acids in primary breast cancer and metastatic sentinel lymph nodes. PLoS ONE *8*, e56795.

Tamura, T., Nagamura-Inoue, T., Shmeltzer, Z., Kuwata, T., and Ozato, K. (2000). ICSBP directs bipotential myeloid progenitor cells to differentiate into mature macrophages. Immunity *13*, 155–165.

Tateda, K., Moore, T.A., Deng, J.C., Newstead, M.W., Zeng, X., Matsukawa, A., Swanson, M.S., Yamaguchi, K., and Standiford, T.J. (2001). Early recruitment of neutrophils determines subsequent T1/T2 host responses in a murine model of Legionella pneumophila pneumonia. J. Immunol. *166*, 3355–3361.

Tegtmeyer, P.K., Spanier, J., Borst, K., Becker, J., Riedl, A., Hirche, C., Ghita, L., Skerra, J., Baumann, K., Lienenklaus, S., et al. (2019). STING induces early IFN-β in the liver and constrains myeloid cell-mediated dissemination of murine cytomegalovirus. Nat. Commun. *10*, 2830.

Thiel, N., Keyser, K.A., and Lemmermann, N.A. (2016). The Mouse Cytomegalovirus Gene m42 Targets Surface Expression of the Protein Tyrosine Phosphatase CD45 in Infected Macrophages. PLoS Pathog. *12*, e1006057.

Tyanova, S., Temu, T., and Sinitcyn, P. (2016). The Perseus computational platform for comprehensive analysis of (prote)omics data. Nat. Methods *13*, 731–740.

Ueland, T., Rollag, H., Hartmann, A., Jardine, A.G., Humar, A., Michelsen, A.E., Bignamini, A.A., Åsberg, A., and Aukrust, P. (2014). Secreted Wnt antagonists during eradication of cytomegalovirus infection in solid organ transplant recipients. Am. J. Transplant. *14*, 210–215.

Vizcaíno, J.A., Côté, R.G., Csordas, A., Dianes, J.A., Fabregat, A., Foster, J.M., Griss, J., Alpi, E., Birim, M., Contell, J., et al. (2013). The PRoteomics IDEntifications (PRIDE) database and associated tools: status in 2013. Nucleic Acids Res. *41*, D1063–D1069.

Wagner, M., Jonjic, S., Koszinowski, U.H., and Messerle, M. (1999). Systematic excision of vector sequences from the BAC-cloned herpesvirus genome during virus reconstitution. J. Virol. *73*, 7056–7060.

Wallingford, J.B., and Habas, R. (2005). The developmental biology of Dishevelled: an enigmatic protein governing cell fate and cell polarity. Development *132*, 4421–4436.

Weinberg, R.A. (1995). The retinoblastoma protein and cell cycle control. Cell *81*, 323–330.

Wellner, U., Schubert, J., Burk, U.C., Schmalhofer, O., Zhu, F., Sonntag, A., Waldvogel, B., Vannier, C., Darling, D., zur Hausen, A., et al. (2009). The EMT-activator ZEB1 promotes tumorigenicity by repressing stemness-inhibiting microRNAs. Nat. Cell Biol. *11*, 1487–1495.

Wiebusch, L., Neuwirth, A., Grabenhenrich, L., Voigt, S., and Hagemeier, C. (2008). Cell cycle-independent expression of immediate-early gene 3 results in G1 and G2 arrest in murine cytomegalovirus-infected cells. J. Virol. *82*, 10188–10198.

Yang, X., Li, L., Huang, Q., Xu, W., Cai, X., Zhang, J., Yan, W., Song, D., Liu, T., Zhou, W., et al. (2015). Wnt signaling through Snail1 and Zeb1 regulates bone metastasis in lung cancer. Am. J. Cancer Res. *5*, 748–755.

Yona, S., Kim, K.W., Wolf, Y., Mildner, A., Varol, D., Breker, M., Strauss-Ayali, D., Viukov, S., Guilliams, M., Misharin, A., et al. (2013). Fate mapping reveals origins and dynamics of monocytes and tissue macrophages under homeostasis. Immunity *38*, 79–91.

Yook, J.I., Li, X.Y., Ota, I., Hu, C., Kim, H.S., Kim, N.H., Cha, S.Y., Ryu, J.K., Choi, Y.J., Kim, J., et al. (2006). A Wnt-Axin2-GSK3beta cascade regulates Snail1 activity in breast cancer cells. Nat. Cell Biol. *8*, 1398–1406.

Yu, P., Petzoldt, S., Wilhelm, M., Zolg, D.P., Zheng, R., Sun, X., Liu, X., Schneider, G., Huhmer, A., and Kuster, B. (2017). Trimodal Mixed Mode Chromatography That Enables Efficient Offline Two-Dimensional Peptide Fractionation for Proteome Analysis. Anal. Chem. *89*, 8884–8891.

Zarama, A., Pérez-Carmona, N., Farré, D., Tomic, A., Borst, E.M., Messerle, M., Jonjic, S., Engel, P., and Angulo, A. (2014). Cytomegalovirus m154 hinders CD48 cell-surface expression and promotes viral escape from host natural killer cell control. PLoS Pathog. *10*, e1004000.

Zhao, M., Kong, L., Liu, Y., and Qu, H. (2015). dbEMT: an epithelial-mesenchymal transition associated gene resource. Sci. Rep. *5*, 11459.

Ziegler, H., Thale, R., Lucin, P., Muranyi, W., Flohr, T., Hengel, H., Farrell, H., Rawlinson, W., and Koszinowski, U.H. (1997). A mouse cytomegalovirus glycoprotein retains MHC class I complexes in the ERGIC/cis-Golgi compartments. Immunity *6*, 57–66.

Ziltener, P., Reinheckel, T., and Oxenius, A. (2016). Neutrophil and Alveolar Macrophage-Mediated Innate Immune Control of Legionella pneumophila Lung Infection via TNF and ROS. PLoS Pathog. *12*, e1005591.

Please cite this article in press as: Baasch et al., Cytomegalovirus subverts macrophage identity, Cell (2021), https://doi.org/10.1016/j.cell.2021.05.009

STAR★METHODS

KEY RESOURCES TABLE

REAGENT or RESOURCE	SOURCE	IDENTIFIER
Antibodies		
Flow cytometry: anti-mouse CD8a (clone 53-6.7)	eBioscience	Cat#46-0081-80, RRID: AB_1834434
Flow cytometry: anti-mouse CD11b (clone M1/70)	eBioscience	Cat# 25-0112-82; RRID: AB_469588
Flow cytometry: anti-mouse CD11c (clone HL3)	BD Biosciences	Cat# 550261; RRID: AB_398460
Flow cytometry: anti-mouse CD16/32 (clone 93)	BioLegend	Cat# 101302; RRID: AB_312801
Flow cytometry: anti-mouse CD45.1 (clone A20)	BioLegend	Cat#110723, RRID: AB_493732
Flow cytometry: anti-mouse CD45 (clone 30-F11)	eBioscience	Cat# 48-0451-82; RRID: AB_1518806
Flow cytometry: anti-mouse CD61 (clone 2C9.G2)	BioLegend	Cat# 104314; RRID: AB_2234024
Flow cytometry: anti-mouse CD64 (clone X54-5/7.1)	BioLegend	Cat# 139308; RRID: AB_2561963
Flow cytometry: anti-mouse CD103 (clone M290)	BD Biosciences	Cat# 561043; RRID: AB_10565963
Flow cytometry: anti-mouse F4/80 (clone: CI:A3-1)	BioRad	Cat# MCA497APC; RRID: AB_324435
Flow cytometry: anti-mouse H-2K^{b} bound to SIINFEKL (clone 25-D1.16)	BioLegend	Cat#141608, RRID: AB_11218593
Flow cytometry: anti-mouse Ki67 (clone: SolA15)	eBioscience	Cat# 25-5698-82; RRID: AB_11220070
Flow cytometry: anti-mouse Ly6C (clone: HK1.4)	eBioscience	Cat# 45-5932-82; RRID: AB_2723343
Flow cytometry: anti-mouse Ly6G (clone: 1A8)	BD Biosciences	Cat# 551461; RRID: AB_394208
Flow cytometry: anti-mouse MerTK (clone: DS5MMER)	eBioscience	Cat# 12-5751-80; RRID: AB_2572622
Flow cytometry: anti-mouse MHCII (clone:M5/114.15.2)	BioLegend	Cat# 107635; RRID: AB_2561397
Flow cytometry: anti-mouse (pro)-IL1 beta (clone: NJTEN3)	eBioscience	Cat# 17-7114-80; RRID: AB_10670739
Flow cytometry: anti-mouse SiglecF (clone: S17007L)	BioLegend	Cat# 155505; RRID: AB_2750234
Flow cytometry: anti-mouse SiglecF (clone: E50-2440)	BD Biosciences	Cat# 562681; RRID: AB_2722581
Flow cytometry: anti-mouse TNFa (clone: MP6-XT22)	BD Biosciences	Cat# 554420; RRID: AB_398553
IF-microscopy: anti-mouse CD68 (FA-11)	BioLegend	Cat# 137004; RRID: AB_2044002
IF-microscopy: anti-GFP (polyclonal)	Rockland	Cat# 600-101-215; RRID: AB_218182
IF-microscopy: anti-mouse Podoplanin (clone 8.1.1)	BioLegend	Cat# 127407; RRID: AB_2161929
IF-microscopy: anti-mouse CD11c (clone HL3)	BD Biosciences	Cat# 550261; RRID: AB_398460
IF-microscopy: anti-mouse CD61 (clone 2C9.G2)	BioLegend	Cat# 104314; RRID: AB_2234024
IF-microscopy: anti-mouse SiglecF (clone: E50-2440)	BD Biosciences	Cat# 562681; RRID: AB_2722581
IF-microscopy: anti-mouse CollagenIV (polyclonal)	Abcam	Cat# ab19808; RRID: AB_445160
Western blot: CD11b, anti-mouse, polyclonal unconjugated	Biotechne	Cat# NB110-89474; RRID: AB_1216361
Western blot: beta-Actin, anti-mouse, monoclonal, unconjugated	Sigma Aldrich	Cat# A1978; RRID: AB_476692
Bacterial and virus strains		
MCMV-Mck2^{def} (C3X/MW97.01)	Wagner et al., 1999	N/A
MCMV-Mck^{rep} (Rep3.3)	Barbara Adler (Jordan et al., 2011)	N/A
MCMV-GFP	This study	N/A
MCMV-floxGFP	Zsolt Ruzsics {Tegtmeyer, 2019 #437}	N/A
Legionella pneumophila JR32 (dsRed)	Manfred Kopf (Mampel et al., 2006)	N/A
Biological samples		
Fetal bovine serum (FCS)	PAN Biotech	Cat# P30-1502
Normal goat serum	abcam	Cat# ab7481

(*Continued on next page*)

Please cite this article in press as: Baasch et al., Cytomegalovirus subverts macrophage identity, Cell (2021), https://doi.org/10.1016/j.cell.2021.05.009

Continued

REAGENT or RESOURCE	SOURCE	IDENTIFIER
Chemicals, peptides, and recombinant proteins		
Accutase solution	Sigma Aldrich	Cat# A6964
Antimycin A	Sigma-Aldrich	Cat# A8674-25MG
Fluospheres (beads), PE-labeled, 1μm	Thermo Fisher	Cat# F13083
CellTrace violet cell proliferation kit	Thermo Fisher	Cat# C34557
Ciprofloxacin	Fresenius Kabi	N/A
Collagenase IV	Worthington	Cat# LS004188
cOmplete mini, EDTA-free protease inhibitor cocktail	Sigma Aldrich	Cat# 11836170001
4′,6-diamidino-2-phenylindole (DAPI)	Thermo Fisher	Cat# D9542
Dextran AF647 (MW 10 000 Da)	Thermo Fisher	Cat# D22914
Dimethyl sulfoxide anhydrous (MS)	Sigma Aldrich	Cat# 276855
DNase I from bovine pancreas	Sigma Aldrich	Cat# DN25-1G
Durcupan	Sigma-Aldrich	Cat# 44611
Ethylenediamine tetraacetic acid (EDTA)	Sigma-Aldrich	Cat# E5134
Carbonyl cyanide 4-(trifluoromethoxy) phenylhydrazone (FCCP)	Sigma-Aldrich	Cat# C2920-10MG
Ficoll-Paque plus	Cytiva	Cat# GE17-1440-02
Fixable viability dye	Invitrogen	Cat# 65-0863-14
Galunisertib, LY2157299	Cayman Chemical	Cat# 15312
Glucose	Agilent	Cat# 103577-100
Glutaraldehyd EM Grade	Roth	Cat# 4157.2
GM-CSF, recombinant, murine	PeproTech	Cat# 315-03
Hydroxytamoxifen	Sigma Aldrich	Cat# T7904
IC fixation buffer	Thermo Fisher	Cat# 00-8222-49
ICG001	Cayman Chemical	Cat# 16257
IQ1	Cayman Chemical	Cat# 16153
Legionella BCYE + antibiotics	Oxoid	Cat# PO5325A
L-Glutamine	Agilent	Cat# 103579-100
LIVE/DEAD fixable near-IR dead cell stain kit	Thermo Fisher	Cat# L10119
Matrigel	Corning	Cat# 356230
M-CSF, recombinant, human	PeproTech	Cat# 300-25
M-CSF, recombinant, murine	PeproTech	Cat# 315-02
MethoCult M3434	StemCell	Cat# 03434
Oligomycin A	Sigma Aldrich	Cat# 75351-5MG
Osmium tetroxide 4%	Roth	Cat# 8088.1
Ovalbumin (protein)	Sigma-Aldrich	Cat# A5503
Ovalbumin peptide SIINFEKL	IBA GmbH	Cat# 6-7015-901
Paraformaldehyde for TEM	Polysciences	Cat# 18814-10
Percoll	Sigma-Aldrich	Cat# P1644
Permeabilization buffer 10x	Thermo Fisher	Cat# 00-8333-56
Phosphatase inhibitor cocktail 1	Sigma-Aldrich	Cat# P2850
Phosphatase inhibitor cocktail 2	Sigma-Aldrich	Cat# P5726
Polyinosinic-polycytidylic acid (Poly(I:C))	Invivogen	Cat# tlrl-pic
Precision count beads	BioLegend	Cat# 424902
ProLong Diamond antifade mountant	Thermo Fisher	Cat# P36965
Propylenoxid	Sigma-Aldrich	Cat# 82320
Pyruvate	Agilent	Cat# 103578-100
RBC lysis buffer (1x)	GIBCO	Cat# 21875-034
Rotenone	Sigma-Aldrich	Cat# R8875-1G

(*Continued on next page*)

Please cite this article in press as: Baasch et al., Cytomegalovirus subverts macrophage identity, Cell (2021), https://doi.org/10.1016/j.cell.2021.05.009

Continued

REAGENT or RESOURCE	SOURCE	IDENTIFIER
Seahorse XF DMEM (base) media	Agilent	Cat# 103575-100
TMT 10-plex	Thermo Fisher	Cat# 90110
Tris	VWR Chemicals	103156X
Triton X-100	Sigma-Aldrich	Cat# 93418
Trypsin	Promega	V5117
Uranylacetat	Merck	Cat# 8473
Urea	Sigma-Aldrich	Cat# u5378
Y27632 (ROCK inhibitor)	Tocris (BioTechne)	Cat# 1254
2-chloroacetamide	Sigma-Aldrich	Cat# 8.02412
5-Brom-2′-deoxyuridin	Sigma-Aldrich	Cat# B5002
Critical commercial assays		
Absolute qPCR SYBR green	Thermo Fisher	Cat# AB1159A
BrdU flow kit	BD PharMingen	Cat# 552598
DuoSet Mouse IL-10 (ELISA)	R&D	Cat# DY417
Easy sep human monocyte enrichment kit without CD16 depletion	StemCell	Cat# 19058
FoxP3 transcription factor staining buffer kit	Thermo Fisher	Cat# 00-5523-00
iScript cDNA synthesis kit	BioRad	Cat# 1708891
Mouse CD8 T lymphocyte enrichment set - DM	BD Bioscience	Cat# 558471
Pierce Coomassie Plus (Bradford) assay kit	Thermo Fisher	Cat# 23236
PKH26 red fluorescent cell linker kit for phagocytic cell labeling	Sigma-Aldrich	Cat# PKH26PCL-1KT
RNeasy micro kit	QIAGEN	Cat# 74004
Superscript IV VILO Mastermix	Thermo Fisher	Cat# 11756050
Deposited data		
RNA sequencing datasets	This paper	GSE159389 (NCBI GEO)
(Phospho-)proteomics datasets	This paper	PXD015923 (PRIDE)
Experimental models: Organisms/strains		
Mouse: C57BL/6J	The Jackson Laboratory	JAX 000664; RRID: IMSR_JAX:000664
Mouse: C57BL/6JRj	Janvier Labs	N/A
Mouse: Balb/cJ	The Jackson Laboratory	JAX 000651; RRID: IMSR_JAX:000651
Mouse: B6.Cg-Tg(Itgax-cre)1-1Reiz/J, (*Itgax*$^{cre/+}$)	The Jackson Laboratory	JAX 008068; RRID: IMSR_JAX:008068
Mouse: B6.Cg-Gt(ROSA)26Sortm9(CAG-tdTomato) Hze/J, (ROSA26-Tomato^{flox})	The Jackson Laboratory	JAX 007909; RRID: IMSR_JAX:007909
Mouse B6.129P2-Lyz2tm1(cre)Ifo/J, (LysM$^{cre/+}$)	The Jackson Laboratory	JAX 004781; RRID: IMSR_JAX:004781
Mouse: Zeb1$^{flox/flox}$	Thomas Brabletz, Simone Brabletz and Marc P. Stemmler (Brabletz et al., 2017)	N/A
Mouse: B6.129P2(C)-Cx3cr1tm2.1(cre/ERT2)Jung/J, (CX3CR1^{creER}ROSA-Tomato^{flox})	Steffen Jung (Yona et al., 2013)	N/A
Mouse: B6.129P2-Myd88tm1Aki/Ob (Myd88$^{-/-}$)	Shizuo Akira (Adachi et al., 1998)	N/A
Mouse: B6(Cg)-*Sting1*$^{tm1.2Camb}$/J (Tmem173$^{-/-}$)	Andrea Ablasser	JAX 025805; RRID: IMSR_JAX:025805
Mouse: C57BL/6-Tg(TcraTcrb)1100Mjb/J (OT-I TCR transgenic mice)	The Jackson Laboratory	JAX 003831 RRID:IMSR_JAX:003831
Mouse: B6.129S1-*Csf2rb2*^{tm1Cgb} *Csf2rb*^{tm1Clsc}/J (*Csf2rb*$^{-/-}$)	The Jackson Laboratory	JAX: 005963; RRID: IMSR_JAX:005963
Oligonucleotides		
See Table S5	This paper	N/A

(*Continued on next page*)

Continued

REAGENT or RESOURCE	SOURCE	IDENTIFIER
Software and algorithms		
Cytoscape v.3.6.1 or v.3.7.2	Shannon et al., 2003; #903	https://cytoscape.org
DOG v2.0	Ren et al., 2009	http://dog.biocuckoo.org/
Galaxy	Afgan et al., 2018	https://galaxyproject.eu/
ImageJ/FiJi	Schindelin et al., 2012	https://fiji.sc/
Kaluza v.13	Beckman Coulter	https://www.beckman.de/flow-cytometry/software/kaluza
MaxQuant v.1.3.0.13	Cox and Mann, 2008	https://www.maxquant.org/
Microsoft Excel 2016	Microsoft	https://www.microsoft.com/en-us/
Panther	Paul Thomas	http://pantherdb.org/
Perseus v.1.6.1.1	Tyanova et al., 2016	https://maxquant.net/perseus/
PhosphoPath v3.2	Raaijmakers et al., 2015	http://apps.cytoscape.org/apps/phosphopath
Prism 8.4.2	GraphPad Software	https://www.graphpad.com/scientific-software/prism/
R v.3.5.1 or v.3.6.2	R Core Team, 2013	https://www.r-project.org/
Zen	Zeiss	https://www.zeiss.de/mikroskopie/produkte/mikroskopsoftware/zen.html

RESOURCE AVAILABILITY

Lead contact

Further information and requests for resources and reagents should be directed to and will be fulfilled by the Lead Contact, Philipp Henneke (philipp.henneke@uniklinik-freiburg.de).

Materials availability

The BAC-sequence of the BACmid-derived MCMV-GFP generated in this study has not been deposited to a publicly available repository. However, requests for the MCMV strains used in this study can be directed and will be fulfilled by the Lead Contact, Philipp Henneke (philipp.henneke@uniklinik-freiburg.de).

Data and code availability

The RNA-seq datasets of BM-derived macrophages and alveolar macrophages generated in this study have been deposited in NCBI's Gene Expression Omnibus (GEO) (Edgar et al., 2002) under the accession number GSE159389.

The mass spectrometry proteomics datasets generated in this study have been deposited in the ProteomeXchange Consortium via the PRIDE partner repository (Vizcaíno et al., 2013) under the accession number PXD015923.

EXPERIMENTAL MODEL AND SUBJECT DETAILS

Mice

BALB/c and C57BL/6J mice were purchased from Jackson Laboratories (USA) or Janvier Laboratories (France). Mice were bred under specific pathogen-free conditions in the animal facilities of the University of Freiburg and housed in groups of up to five mice. Mice were kept in 12h light/dark cycles and food and water was provided *ad libitum*. If not mentioned specifically, adult mice were between 6 and 18-week of age. Male and female mice were used for experiments; no differences were observed within the parameters analyzed. Littermates were randomly assigned to experimental groups. All animal experiments were approved by the Federal Ministry for Nature, Environment and Consumer's protection of the state of Baden-Wuerttemberg.

Human samples

Healthy donors included in this study were two male and two female individuals between the ages of 20 and 35 years. To obtain **human monocyte-derived MΦ** blood was drawn from healthy donors in agreement with institutional ethics regulations. Subsequently, peripheral blood mononuclear cells (PBMC) were enriched by Ficoll (Cytiva) density gradient centrifugation and $CD14^+$ monocytes

were magnetically purified from PBMC via negative selection (Human monocyte enrichment kit, StemCell). Monocytes were then cultured in supplemented RPMI with recombinant human macrophage colony-stimulating factor (M-CSF) (40ng/ml, PeproTech) with medium exchange every other day.

METHOD DETAILS

Viruses and bacteria

Cytomegaloviruses

MCMV-Mck2^{rep}, MCMV-GFP and MCMV-floxGFP were rescued from the bacterial artificial chromosomes (BACs) pSM3fr-MCK-2fl (Jordan et al., 2011), pSM3fr-MCK-2fl-M36GFP (described below) and pSM3fr-MCK-2fl-Dm157-flox-eGFP (Tegtmeyer et al., 2019), respectively, by transfection of MEFs. All rescued viruses were further propagated on mouse embryonic fibroblasts (MEF) and purified using a sucrose cushion. A total of five MCMV-GFP batches were used during the project. HCMV TB40-SE-GFP was generated as described before (Sampaio et al., 2017) and propagated on human MRC-5 cells.

Construction of the recombinant MCMV BAC pSM3fr-MCK-2fl-M36GFP

In order to generate MCMV-GFP, we inserted the GFP ORF into the viral m36 transcription unit after the M36 ORF linked by an internal ribosomal entry site (IRES) using BAC technology.

First of all, we constructed an IRES-GFP cassette containing template plasmid which also carried a mFRT-site flanked kanamycin resistance cassette. The pGPS-IRES-GFP-Kan-mFRT was constructed as follows: the PCR amplified IRES-GFP cassette from pIRES2-EGFP (Clontech) using the primers GFPSACfor (5′- GTGTGCGGCCGCGACGAGCTCTCATAATCAGCCATACCACATT – 3′) and GFPSACrev (5′- ACGCCTTAAGATACATTGATGAGTTTGGAC-3′) were assembled with a PCR fragment containing a kanamycin cassette flanked with mFRT-sites amplified from pGPS1.1 (NEB) using the primers KnmFRTfor (5′- AAATAGATCT GAAGTTCCTATTCTTCAAAAGGTATAGGAACTTCCACGTTGTGTCTCAAAATCTCTGA-3′) and KnmFRT (5′- ACAGGGTACCTGT GGGCGGACAAAATAGTTGGGAAGTTCCTATACCTTTTGAAGAATAGGAACTTCATTAAGCCAGTGTTACAACC-3′), and both were inserted into pGPS2 (NEB) digested with SacI and KpnI.

To insert the IRES-GFP cassette at the viral m36 locus, we used BAC recombineering. In brief, a linear DNA fragment consisting of the IRES and GFP expression cassette as well as a kanamycin (Kan) marker gene flanked by m-FRT-sites (Schlake and Bode, 1994) was generated by PCR using the primers H3-M36iGFPfor (5′- TCGAGAGGAGGAGGGTCAAGCTCTTTAAGATGACACGGGGA TATCGATAGGCCCCTCTCCCTCCCCCCCCCCTAA-3′), H5-M36iGFPrev (5′-TTTTTTTTTCTCCCCTCACCCTCTCCGTCCCTTTCT TATCCGTTTTCCCTTGTGGGCGGACAAAATAGTTGG-3′) on the template plasmid pIRES-GFP-Kan-mFRT . This fragment was then inserted in pSM3fr-MCK-2fl (between nt position 47.568 - 47.668 according to Rawlinson (Rawlinson et al., 1996)) by homologous recombination in *E.coli*. Subsequently, the marker gene was excised by Flp recombinase via the m-FRT sites.

Quantification of infectious MCMV particles by plaque assay

Plaque assay was performed as described earlier (Reddehase et al., 1985). In brief, cell culture supernatant or homogenized tissue of infected MΦ or mice, respectively, was added to a monolayer of MEF, centrifuged (2x 15 minutes at 400 g; centrifugal enhancement) and incubated for one hour. Next, the supernatant was removed and MEFs were covered with supplemented DMEM containing methylcellulose to locally restrain viral spread. At day three to five, the virus infection induced plaques were counted under the microscope.

Serum neutralization of MCMV by plaque reduction assay

Pooled sera of uninfected and infected (42-72dpi) mice were diluted into two-fold dilution series. 40 PFU of MCMV-Mck2^{rep} was incubated in the presence of the serum dilutions in triplicates for one hour at 37°C. MEFs seeded on a 48-well-plate were infected with the serum treated inoculums for 90 min without centrifugal enhancement. Next, the supernatants were removed and monolayers were covered with supplemented DMEM containing methylcellulose. At day three to five the plaques were counted under the microscope. The reduction of plaque number was plotted and the IC90 was calculated by Graphpad Prism.

Legionella pneumophila

Legionella pneumophila strain JR32 was used. Bacteria were plated on buffered charcoal yeast extract (BCYE) agar (Thermo Fisher). The optical density (OD600) of one and more single colonies was measured using an optical spectrophotometer. Subsequently, the suspension was plated on BCYE agar plates to create a standard curve. For infection, single colonies were picked, suspended in sterile PBS and the OD600 was measured to determine the infectious dose.

Quantification of colony forming units (Legionella pneumophila)

Mice were sacrificed and the left lung was removed. The lung was cut, homogenized in PBS using a TissueLyser (QIAGEN) and filtered through 70μm strainer. Colony forming units in the lung were determined by serial dilutions of the flow through on BYCE agar plates (Thermo Fisher) and quantified 3 days later.

In vitro

Cell culture

To generate **BM-derived macrophages,** adult mice were sacrificed and femur and tibia removed. The bones were first rinsed with 60% isopropanol and sterile phosphate buffered saline (PBS). Subsequently, the bone marrow was flushed with RPMI containing 10% fetal calf serum (FCS; Invitrogen) and 10 mg/ml ciprofloxacin (Fresenius Kabi) (supplemented RPMI) and passed through a

70 μm cell strainer. After centrifugation (300 g for 7 minutes), cells were resuspended in supplemented RPMI plus recombinant M-CSF (20 ng/ml, PeproTech) and cultured in Petri dishes. Medium was exchanged at day 4. At day 6 BM-derived macrophages were detached enzymatically (Accutase; Thermo Fisher) and re-seeded with supplemented RPMI.

For bone marrow-derived dendritic cells (**BMDC**) isolated bone marrow was cultured in supplemented RPMI plus recombinant GM-CSF (20ng/ml, PeproTech). Half of the medium was removed at day 2 and replaced with fresh supplemented RPMI plus 40ng/ml GM-CSF. At day 3 and 6 the medium was fully exchanged and BMDC were separated from MΦ according to their high expression of MHCII and the lack of CD115 ($MHCII^+$ $CD115^-$) (Feuerstein et al., 2019) at day 8.

To harvest **peritoneal macrophages**, adult mice were sacrificed and the skin covering the abdomen removed to visualize the peritoneum. The abdominal cavity was flushed with ice-cold PBS containing ethylenediaminetetraacetic acid (EDTA, 2 mM). The collected cell suspension was centrifuged and seeded into cell culture dishes with fully supplemented RPMI. After 2 h non-adherent cells were removed by thorough washing, and adherent cells were infected.

Alveolar macrophages were obtained via broncho-alveolar-lavage (BAL). Briefly, adult mice were sacrificed, the thorax opened and the trachea uncovered. Next a vein catheter (27G) was installed into the trachea through a small incision. PBS with EDTA (2 mM) was administered until lungs unfolded, then the cell suspension was retrieved. Cells were centrifuged and seeded into cell culture dishes with supplemented RPMI plus 20 ng/ml GM-CSF (PeproTech). After 2 h non-adherent cells were removed by thorough washing, and adherent cells were infected.

Intestinal macrophages were extracted as described before (Kolter et al., 2016). Briefly, the colon was opened longitudinally and rinsed. Epithelial cells were dissociated by shaking twice for 15 min at 37°C in 2 mM EDTA and 10 mM HEPES in HBSS. Remaining tissue was washed, minced, and digested three times for 15 min at 37°C with 0.3 mg/ml Collagenase IV (Worthington), 5 U/ml Dispase (Corning), and 0.5 mg/ml DNase I (Roche) in HBSS supplemented with 2% FCS. After digestion, the samples were filtered with a 70 μm cell strainer and cultured in supplemented RPMI. After 2 hours non-adherent cells were removed by thorough washing and adherent cells were infected.

Microglia. Two- to four-day old mice were transcardially perfused and the brain extracted. The meninges and the choroid plexus were removed under a stereomicroscope before homogenizing the brain. The homogenate was centrifuged at 300 g 6 min at 4°C, resuspended in DMEM containing 10% FCS (Invitrogen) and 10mg/ml ciprofloxacin (Fresenius Kabi) and plated in cell culture flasks previously coated with poly-L-Lysine for 3 hours. Medium was changed twice a week. After 7 days, the brain culture was stimulated by adding M-CSF (10 ng/ml, PeproTech) for 24 h before harvesting the microglia by shaking on a horizontal shaker for four hours at 37°C. The supernatant was removed, centrifuged (300 g, 6 min, 4°C) and microglia were cultured in supplemented DMEM with M-CSF (10 ng/ml, PeproTech).

In vitro infection

For infection with MCMV, cultured cells were infected with indicated multiplicities of infection (MOI) of MCMV-GFP, centrifuged 2x 15 minutes with 400 g and incubated at 37°C. After 60 minutes, virus containing medium was discarded and the cells were washed thoroughly with sterile PBS before further culture in supplemented RPMI plus M-CSF or GM-CSF (20 ng/ml).

For sorting experiments, BM-derived macrophages were infected and sorted in a GFP^- bystanding subset and a GFP^+ infected subset 1 dpi to obtain homogeneous populations of bystanding and infected cells and to prevent viral spread to bystanding cells at later time points. Subsequently, the subsets were cultured in supplemented RPMI medium for 2 days (3 dpi) with or without M-CSF (20 ng/ml).

Small molecule inhibitors (IQ1, ICG001, Galunitersib, Y27632) and Foscarnet (Clinigen Healthcare Ltd.) were added 1 hour prior to infection or after infection, respectively, at indicated concentrations.

In vitro phagocytosis

For assessment of *in vitro* phagocytosis, PE-labeled beads (1 μm) were added to sorted BM-derived macrophage subsets at 3 dpi. After an incubation period of 30 minutes, the medium was removed and BM-derived macrophages were washed thoroughly three times. The number of PE^+, phagocytic active BM-derived macrophages was determined via flow cytometry.

Endocytosis

To evaluate endocytic capacity of BM-derived macrophage subsets, sorted BM-derived macrophages were starved in FCS-free RPMI for 4 hours before Dextran-AF647 (10 kDa, 0.1 mg/ml) was added. After an incubation period of 1 hour at 37°C or 4°C (negative control), the medium was removed and macrophages were washed thoroughly. The number of $AF647^+$ BM-derived macrophages was analyzed via flow cytometry.

Mitochondrial stress test/Oxygen consumption

Sorted BM-derived macrophage subsets were seeded into a Seahorse XFe96 culture plate (Agilent Technologies) and analyzed 3 dpi on a Seahorse XFe96 Analyzer (Agilent Technologies). For the Mito Stress Test, the culture media was removed carefully from each well and the cells were washed once before addition of 180 μL assay media (Seahorse Base media supplemented with 10 mM Glucose, 2 mM L-Glutamine, 2 mM Sodium Pyruvate, adjusted to pH 7.4). The plate was incubated in a CO_2 free incubator for 45 min. Injection plates were prepared with a final concentration of 1 μM Oligomycin (Port A). 1.5 μM FCCP (Port B) and 0.5 μM of each Rotenone and Antimycin (Port C). The assay protocols were designed using Wave desktop software (Version: 2.4.0.60 Agilent). To assess the maximal respiration rate the difference of oxygen consumption rate-values before and after FCCP injection were calculated.

Please cite this article in press as: Baasch et al., Cytomegalovirus subverts macrophage identity, Cell (2021), https://doi.org/10.1016/j.cell.2021.05.009

Transwell cell culture

Sorted infected BM-derived macrophages were stained with Cell Trace Violet (CTV^+ GFP^+) and cultured in a transwell insert (0.4 μm pore size; Corning) above a monolayer of MEFs or directly together with MEFs (CTV- GFP-). Newly infected (CTV- GFP+) cells were identified via flow cytometry. Serum of infected mice (1:64) was added to either of the conditions to determine cell-free virus contribution to viral spread (dotted bars). The serum's IC90 was priorly determined with a plaque reduction assay (see Serum neutralization of MCMV by plaque reduction assay). After 5 days, the proportion of newly infected cells was assessed via flow cytometry.

Invasion assay

To quantify the capacity of invasion, sorted macrophage subsets were cultured in a transwell insert (8 μm pore size, Corning) coated with Matrigel (1 mg/ml; Corning) in RPMI, Ciprofloxacin (10 mg/ml) and 0.1% FCS. The bottom plate contained RPMI with 10% FCS to build a chemoattractant gradient. Cells which transmigrated through the matrigel layer and pores of the insert were quantified via flow cytometry 4 days later.

Colony forming unit assay

Bone marrow cells and sorted infected BM-derived macrophages were cultured in MethoCult (M3434) at 37°C with 5% CO_2. Colonies were counted and scored after 8 days.

Antigen processing and presentation and T cell proliferation assay

To assess antigen processing and presentation, BM-derived macrophages and BMDCs (see Cell culture) were fed with OVA protein (1mg/ml, Sigma Aldrich) over night. Subsequently, BM-derived macrophages were infected, sorted 1 dpi and subsequently co-cultured. To assess antigen presentation BM-derived macrophages and BMDC were pulsed with ovalbumin peptide SIINFEKL (1 μM, IBA) for 1h at 37°C after infection and sorting . In both experimental setups, $CD8^+$ T cells were magnetically purified from spleens of OTI transgenic mice (Mouse CD8 T lymphocyte enrichment set – DM, BD Biosciences). Enriched $CD8^+$ T cells were labeled with Cell Trace Violet (CTV) proliferation dye (10 μM, Thermo Fisher Scientific). Unless stated otherwise 50 000 $CD8^+$ T cells were co-cultured with 20 000 control, bystanding or infected BM-derived macrophages or BMDCs. Cells were cultured in IMDM L-Glutamin, PenStrep (both from Thermo Fisher Scientific), 10% FCS (PAN Biotech), 5mM β-Mercaptoethanol (Applichem) in 96-well flat-bottom plates (Greiner) at 37°C, 5% CO_2 in a humidified environment for 3 days before analysis.

Animal procedures

In vivo infections and stimulation

For intraperitoneal infection, 8-12 week old BALB/c mice were injected intraperitoneally with $5x10^5$ PFU/ml of MCMV-GFP or MCMV-$Mck2^{rep}$ and MCMV-$Mck2^{def}$ as controls (Jordan et al., 2011).

For intranasal infection, 8-18 week old C57B6/J mice were anesthetized with Ketamin (100 mg/kg body weight) and Xylazin (10 mg/kg body weight). Next, a total of 40 μL MCMV in PBS ($1x10^5$ PFU) was administered intranasally. The same procedure was performed for stimulation with 50μg/ml poly(I:C) (Invivogen) in NaCl (0.9%). The mice were monitored until awakening and analyzed at indicated time points. For intratracheal infection with *Legionella pneumophila* mice were anesthetized via inhalation of isoflurane and inoculated with 45μl bacterial suspension ($5x10^6$ CFU).

In vivo phagocytosis

To measure the capacity of *in vivo* phagocytosis, 2 μM of fluorescent PKH26 phagocyte cell labeling dye, which labels aMΦ *in vivo* (Neupane et al., 2020), was administered intranasally to control mice and to mice, which were infected 2 days before. One day later, mice were sacrificed and aMΦ from BAL and lung homogenate were analyzed for PKH26 uptake via flow cytometry.

Cell transfer

To transfer infected alveolar macrophages, *Itgax*$^{cre/+}$ ROSA26-Tomato^{flox} were infected with MCMV-floxGFP and sacrificed 1 dpi. Subsequently infected aMΦ (GFP^+ $Tomato^+$) were sorted from lung homogenate and immediately transferred into wild-type mice.

To reconstitute lungs of *Csf2rb*$^{-/-}$ mice with alveolar macrophages, adult *Itgax*$^{cre/+}$ ROSA26-Tomato^{flox} mice were sacrificed and alveolar macrophages from lung homogenate were sorted ($CD11b^{int}$ $CD11c^+$/$Tomato^+$ $SiglecF^+$ $MHCII^-$) and immediately transferred into *Csf2rb*$^{-/-}$ mice 48 hours after birth.

Intratracheal airway labeling

To label alveolar macrophages, which reside in the airways, 0.25μg of antibody (SiglecF (clone E50-2440) and CD61) diluted in PBS (total 50μl) were intratracheally administered. 1 hour later, the mice were sacrificed and the lung homogenized. After retrieving a single cell suspension, total bystanding alveolar macrophages were defined as $SiglecF^+$ (clone S17007L) $CD11b^{int}$ and $MHCII^{lo}$ and total infected alveolar macrophages as GFP^+. Labeling efficiency was calculated from *in vivo* labeled and total bystanding or infected alveolar macrophages of lung homogenate.

Measurement of surfactant components

Five days after MCMV-infection or PBS administration, mice were sacrificed and 700μl NaCl were intratracheally installed into the lungs (as described for BAL). The same fluid was retrieved and administered back into the lungs for a total of 5 times before final recovery. Next, the BAL fluid was centrifuged at 300 g for 10 minutes (4°C) and the cell-free supernatant was used to photometrically determine cholesterol and phospholipid concentrations via Beckman AU680 (Beckman Coulter).

Molecular analyses

Western blot

Cells were lysed in RIPA buffer (R0278; Sigma-Aldrich) supplemented with protease inhibitors (539134; Calbiochem) and PMSF (P7626; Sigma-Aldrich) at 1 × 10^6 cells/ml and stored at −80°C. For western blot analysis, cells were incubated at 95°C for 10 min in 2x Laemmli buffer (Bio-Rad) containing 5% β-mercaptoethanol prior to application on a 12% Tris-glycine gel (Anamed). Antibodies for protein detection were anti-CD11b mouse (Biotechne) and β-actin (AC-15; Sigma-Aldrich). Secondary antibodies ECL mouse IgG, HRP-linked (NA931V; Cytiva) and ECL rabbit IgG, HRP-linked (NA934V; Cytiva) were detected using Amersham luminol and peroxide solution (RPN2235; Cytiva).

RNA isolation and qRT-PCR

For RNA extraction, cells were lysed in RLT buffer containing 1% β-mercaptoethanol and RNA was extracted using the RNeasy Micro Kit according to producer's information (QIAGEN). For BM-derived macrophage gene transcript analysis, cells were sorted as described above and cultured in supplemented RPMI plus M-CSF for 2 days (3 dpi) prior to RNA extraction. For BM-derived macrophage stimulation, sorted macrophages were stimulated with lipopolysaccharide (LPS, 50 ng/ml, Invivogen) 3 dpi followed by RNA extraction 6 hours after LPS administration. Alveolar macrophages were sorted from lung homogenates at indicated time points, followed by immediate centrifugation (4°C, 300 g, 6 minutes), washing with PBS and RNA extraction of the cell lysate. RNA was reversely transcribed to cDNA with the iScript™ cDNA synthesis kit (Biorad) for BM-derived macrophages or with the SuperScript IV VILO mix (Thermo Fisher) for sorted alveolar macrophages. QRT-PCR was performed with ABsolute qPCR SYBR Green (Thermo Fisher) at the Realplex Mastercycler (Eppendorf).

Oligonucleotide sequences for qRT-PCR

See Table S5.

Enzyme-linked immunosorbent assay (ELISA)

Infected and uninfected sorted BM-derived macrophages were seeded into 96-well-plates and stimulated with LPS (50 ng/ml) at 3 dpi. After 24 hours, cells were centrifuged (300 g for 2 minutes) and the supernatant collected. IL-10 ELISA was performed according to producer's information (R&D Systems).

Flow cytometry

Surface protein and intracellular staining

Generally, FcγII/III receptors were blocked with anti-CD16/32 antibody (eBioscience) prior to staining the cell surface with respective antibodies (see Key resources table) in PBS containing 2% FCS and 2mM EDTA (FACS buffer).

For *in vitro* assays, cells were enzymatically detached with Accutase and subsequently washed and processed with FACS buffer.

For intracellular staining of TNFα cells were stimulated with 50 ng/ml LPS and the medium was supplemented with GolgiStop to impair cytokine secretion. 6 hpi cells were enzymatically detached, stained for surface markers and washed with PBS. Subsequently, cells were fixed and permeabilized with the Transcription factor staining buffer kit according to manufacturer's instruction. Staining for TNFα was performed in permeabilization buffer.

For intracellular staining of pro-IL-1β, cells were retrieved via BAL 8 hours post intranasal stimulation with poly(I:C). After staining of surface markers, cells were fixed and permeabilized with the Transcription factor staining buffer kit according to manufacturer's instruction. Staining for pro-IL-1β was performed in permeabilization buffer and pro-IL-1β^+ alveolar macrophages identified via surface marker expression.

Cell extraction and tissue preparation

To extract alveolar macrophages, either BAL (see above) or enzymatic digestion of the lung was performed. For digestion, the right lung homogenate was incubated in PBS containing 10% FCS, Collagenase IV (1 mg/ml, Worthington) and DNase I (0.25 mg/ml) for 1.5 hours at 180 rpm at 37°C. The obtained cell suspension was filtered with a 70 μm cell strainer and erythrocytes were lysed with RBC lysis buffer (eBioscience) followed by washing.

To extract cells from the lymph node, adipose tissue surrounding the lymph node was removed under a stereomiscroscope. Next the lymph node was grinded and filtered through a 70 μm cell strainer followed by washing.

Blood was collected retrobulbary and erythrocytes were lysed with RBC lysis buffer. All samples were stained with respective antibodies for flow cytometry analysis.

Cell cycle analysis

For BrdU analysis, sorted cells were cultured in supplemented RPMI and pulsed with BrdU for 2h prior to fixation and permeabilized with the BrdU Flow Kit (BD PharMingen) according to the manufacturer's instructions. The samples were then treated with 0.3 mg/ml DNase I (Roche) for 1h at 37°C and stained for 20 min at room temperature with anti-BrdU antibody (BioLegend). Gates were determined with respective cells stained for BrdU without prior pulsing. For Ki67 staining, cells were sorted, cultured in supplemented RPMI, stained with fixable viability dye (eBioscience) for exclusion of dead cells, fixed and permeabilized using the Transcription factor staining buffer kit (Thermo Fisher) and stained with Ki67.

Flow cytometry analysis

Samples were analyzed with a 3-laser flow cytometer (Gallios, Beckman Coulter) and data were processed with the Kaluza software (v1.3, Beckman Coulter).

Antibodies used for flow cytometry

See Key resources table.

Image techniques and analysis

Fluorescence microscopy

Images of BM-derived macrophages were taken 2 dpi using a fluorescence microscope (ApoTome, Zeiss). Phase contrast and fluorescent (GFP filter) images were acquired with a 40x objective and processed with ZEN software (Zeiss). To assess cellular morphology (circularity and area), random cells of phase contrast images (Figures 1B–1D) or GFP^+ cells of merged images (Figures 5K and S5K) were analyzed blinded via ImageJ/FiJi (1.47v, NIH, USA) (Schindelin et al., 2012). To track cell proliferation (Figure 4H), BM-derived macrophages were sorted as described above, and cultured with 50 ng/ml M-CSF (PeproTech) to stimulate proliferation. At given time points, cells were fixed with 4% paraformaldehyde (PFA) in PBS and nucleostained with 4',6-Diamidin-2-phenylindol (DAPI, 0.1 μg/ml, ThermoFisher). Images were acquired with a 2.5x objective and automated nucleus ($DAPI^+$) counting was performed with ImageJ/FiJi.

Live cell imaging

For time lapse live cell imaging, BM-derived macrophages were seeded into 8-well μ-slide (ibidi, Germany) and infected as described above. After infection, the μ-slide was transferred to the climate chamber (37°C, 5% CO_2) of a Zeiss LSM710 microscope with an epifluorescence live-cell imaging setup. Phase contrast and fluorescent (GFP filter) images were chosen randomly and acquired with a 40x objective every 15 minutes for 48 hours. Single images were then merged and movies recorded with ZEN software (Zeiss). To analyze velocity and migration distance, the chemotaxis and migration tool (ibidi), a plug in for ImageJ/FiJi, was used.

Histology

After transcardial perfusion with PBS, the lungs were refilled with a mixture (1:1) of PBS and Tissue-Tek O.C.T.™ compound (Sakura Finetek Europ B.V. Netherlands) to physiological size. The left lung was then removed and embedded into Tissue TEK O.C.T.™ and shock frozen in liquid nitrogen. Cryosections (10 μm) were fixed in 4% PFA in PBS for 15 minutes, permeabilized for 5 minutes in PBS containing 0.5% Triton X-100 and subsequently blocked with PBS containing 10% normal goat serum (Thermo Fisher) for 3 hours. Antibodies were incubated for 1h at room temperature. Nuclei were counterstained with DAPI (0.1 μg/ml) when necessary. Finally, the sections were mounted with ProLong Diamond Antifade Mountant (ThermoFisher). Confocal microscopy was performed with a LSM 880 confocal microscope. The images were processed with ZEN blue (Carl Zeiss) software.

Transmission electron microscopy

Sorted BM-derived macrophages were seeded on poly-lysine-coated coverslips until 3 dpi at 37°C. Cultures on coverslips were fixed in 4% PFA (w/v) and 2% glutaraldehyde (w/v) containing PBS (0.1 M, pH 7.4) for 30 minutes. After washing with PBS, cultures were incubated with 0.5% Osmiumtetroxide for 30 minutes and washed in graded ethanol (up to 50%) for 5 minutes each, followed by incubation in 1% Uranylacetat for 30 minutes and dehydration of the cultures with graded ethanol solutions (80%, 90%, 98% for 5 minutes, 2 × 100% ethanol for 10 minutes). After incubation in 100% propylenoxide (2 × 10 minutes), cultures were embedded in Durcupan resin (Sigma-Aldrich). Coverslips were removed by liquid nitrogen exposure, and ultrathin sectioning (55 nm) was performed using a Leica UC6 Ultracut. Sections mounted onto coppergrids (Plano) were contrasted using Pb-citrate (3 minutes). Electronmicroscopy was performed at a Philips CM100 microscope equipped with a Gatan Kamera Orius SC600 at 700x (−2950x) magnification. All images were analyzed as TIF-files via ImageJ/FiJi.

RNA-seq and transcriptomic data analysis

BM-derived macrophages

Total RNA of sorted control, bystanding and infected BM-derived macrophages (3 biological replicates each) from wild-type mice was extracted 3 dpi using RNAeasy MicroKit (QIAGEN) according to the manufacturer's instruction. Library preparation was performed with 100ng quality controlled RNA using the Illumina TruSeq Stranded mRNA Library Prep Kit. 100bp paired-end sequencing was carried out with HiSeq4000. Sample processing was done by CeGaT (Center for Genomics and Transciptomics) in Tübingen, Germany (https://www.cegat.de/). Sequencing quality control showed 94.59% of all bases reached a quality score of Q30. Demultiplexing of sequenced reads was performed with Illumina bcl2fastq (version 2.19) and adaptor trimming with Skewer (Version 0.2.2) (Jiang et al., 2014). The raw reads were subsequently mapped to the mm10 murine and the MCMV-GFP reference genome with STAR (Version 2.5.2b) (Dobin et al., 2013). The obtained counts were processed using the DESeq2 package (Love et al., 2014) in R (https://www.R-project.org/). Data were then analyzed with the RStudio software in order to perform principal component analysis between the samples and to visualize expression patterns in volcano plots (limma Bioconductor package; Ritchie et al., 2015). Heatmaps were generated with Morpheus (https://software.broadinstitute.org/morpheus/). For normalization the mean of each gene across macrophage subsets was subtracted from individual values and divided by the standard deviation of that gene (z-score). Gene Ontology (GO) enrichment analysis was performed using the PANTHER classification database (Mi et al., 2019) on regulated (padj: < 0.05 and > 2 $\log_2$ fold change expression) genes. EMT related GO terms were matched to previously reported terms (Gröger et al., 2012).

Alveolar macrophages

Total RNA of sorted control, bystanding and infected alveolar macrophages (3 biological replicates each) from $Itgax^{cre/+}$ $ROSA26\text{-}Tomato^{flox}$ mice or infected $LysM^{cre/+}$:$Zeb1^{+/+}$ and $LysM^{cre/+}$:$Zeb1^{flox/flox}$ was extracted 3 dpi using RNAeasy MicroKit (QIAGEN) according to the manufacturer's instruction. Paired-end sequencing of the quality controlled library was carried out with NovaSeq6000.

Please cite this article in press as: Baasch et al., Cytomegalovirus subverts macrophage identity, Cell (2021), https://doi.org/10.1016/j.cell.2021.05.009

Demultiplexing of sequenced reads was performed with Illumina bcl2fastq (version 2.19) and adaptor trimming with Cutadapt (Martin, 2011) or Skewer (Jiang et al., 2014). The raw reads were subsequently mapped to the mm10 murine reference genome with STAR (Version 2.5.2b) (Dobin et al., 2013) and counted with feature counts (Liao et al., 2014). The obtained counts were processed using the DESeq2 package (Love et al., 2014). Heatmaps were generated with Morpheus (https://software.broadinstitute.org/morpheus/). For normalization the mean of each gene across MΦ subsets was subtracted from individual values and divided by the standard deviation of that gene (z-score). For gene set enrichment analysis (GSEA) fgsea on the Galaxy Freiburg platform (Afgan et al., 2018) and the mouse hallmark gene set were used with significant (padj < 0.05) genes ranked by $\log_2$ fold change of indicated conditions. Gene Ontology (GO) enrichment analysis was performed using the PANTHER classification database (Mi et al., 2019) on regulated (padj: < 0.05 and > 1 $\log_2$ fold change expression) genes.

Mass spectrometry

Cells lysis and proteins digestion for mass spectrometry

BM-derived macrophages were resuspended in 8 M urea, 40 mM Tris-HCl pH 7.6, in the presence of EDTA-free protease inhibitors cocktail (Roche) and phosphatase inhibitors mixture. Lysates were then sonicated and cleared by centrifugation for 10 min at 20,000 *g* and 4°C. Protein lysates (50 μg) were reduced with 10 mM DTT at 37°C for 40 min, and alkylated with 55 mM chloroacetamide at room temperature for 30 min in the dark.

For tryptic digestion, proteins were digested overnight at 37°C with sequencing grade modified trypsin (Promega, 1:50 enzyme-to-substrate ratio) after 4-fold dilution with 40 mM Tris-HCl, pH 7.6. Digests were acidified by addition of formic acid (FA) to 5% (v/v) and desalted using Sep-Pak C18 cartridges, as previously described (Ruprecht et al., 2017a). Peptide solutions were frozen at −80°C and dried *in vacuo*.

TMT labeling, phosphopeptide enrichment and peptide fractionation

TMT 10-plex labeling was performed by reconstituting each digest in 20 μL of 50 mM HEPES (pH 8.5). Five μL of 11.6 mM TMT reagents stock solution (Thermo Fisher) in 100% anhydrous ACN were then added to each sample. Labeling reaction was carried for 1 h at 25°C, and quenched by adding 2 μL of 5% hydroxylamine. Peptide solutions were pooled and acidified using 20 μL of 10% FA. Reaction vessels in which the labeling took place were further rinsed with 20 μL of 10% FA in 10% ACN, and the solvent was then added to the pooled sample. The pools were dried *in vacuo*, desalted and stored dried at −80°C until further use.

Phosphopeptide enrichment was performed by loading the TMT-labeled peptides on a Fe^{3+}-IMAC column (Propac IMAC-10 4 × 50 mm column Thermo Fisher) (Ruprecht et al., 2015). Using a UV-abs signal, the outlet of the column was monitored and two fractions were collected: one containing non-phosphorylated peptides (flow-thought), the other containing phosphorylated peptide (eluate). Both factions were dried in a vacuum centrifuge and stored at −80°C.

For whole proteome analysis, the flow-thought of the IMAC enrichment was re-suspended in 10 mM ammonium acetate, pH 4.7, and subjected to trimodal mixed mode chromatography on an Acclaim Trinity P1 2.1 × 150 mm, 3 μm column (Thermo Fisher) for peptide fractionation (Yu et al., 2017). A total of 32 fractions were collected.

For phosphoproteome analysis, the eluate of the IMAC enrichment was desalted and subjected to high pH RP fractionation (Ruprecht et al., 2017b) using self-packed StageTips, containing 5 disks of C18 material (3M Empore). A total of 6 fractions were collected. All fractions were dried *in vacuo* and stored at −20°C until LC-MS/MS analysis.

LC-MS/MS

Nano flow LC-ESI-MS measurements were performed using a Dionex Ultimate 3000 UHPLC+ system coupled to a Fusion Lumos Tribrid mass spectrometer (Thermo Fisher). Peptides were delivered to a trap column (75 μm × 2 cm, packed in-house with 5 μm Reprosil C18 resin; Dr. Maisch) and washed using 0.1% FA at a flow rate of 5 μL/min for 10 min. Subsequently, peptides were transferred to an analytical column (75 μm × 45 cm, packed in-house with 3 μm Reprosil C18 resin, Dr. Maisch) applying a flow rate of 300 nL/min. Peptides were chromatographically separated using a 50 min linear gradient from 8% to 34% solvent B (0.1% FA, 5% dimethyl sulfoxide (DMSO) in Acetonitrile (ACN)) in solvent A (0.1% FA in 5% DMSO).

The Fusion Lumos was operated in a data-dependent acquisition (DDA) to automatically switch between MS and MS/MS. Briefly, survey full-scan MS spectra were recorded in the orbitrap from 360 to 1300 m/z at a resolution of 60K, using an automatic gain control (AGC) target value of 4e5 charges and maximum injection time (maxIT) of 50 ms.

For the MS3-based TMT method, initial MS2 spectra for peptide identification were recorded in the ion trap in rapid scan mode with a top speed approach using a 2 s duration (isolation window 0.7 m/z, AGC target value of 1e4, maxIT of 35 ms). Fragmentation was set to CID, with a NCE of 35% and activation Q of 0.25. Then, for each peptide precursor, an additional MS3 spectrum for TMT quantification was obtained in the orbitrap at 50K resolution (AGC of 5e4 charges, maxIT of 86 ms). The precursor was fragmented as for the MS2 analysis, followed by synchronous selection of the 10 most intense peptide fragments and further fragmentation via HCD using a NCE of 55%. Dynamic exclusion was set to 90 s.

For the analysis of the phosphopeptide-enriched sample the following modifications were applied: LC gradient from 4% to 32% of solvent B in 100 min, MS2 readout in the Orbitrap, top 10 approach, multistage activation enabled, MS2 AGC target value of 5e4, MS2 maxIT of 60 ms, MS3 AGC of 1.2e5 charges, and MS3 maxIT of 120 ms).

DatapProcessing of LC-MS/MS

Peptide and protein identification and quantification was performed using MaxQuant (version 1.6.0.13) with its built in search engine Andromeda (Cox and Mann, 2008). Spectra were searched against the UniProtKB database (*Mus musculus*, UP000000589, 53,127

entries, and Murid Herpesvirus, UP000122533, 164 entries, downloaded on 04.2018). Enzyme specificity was set to trypsin, and the search included cysteine carbamidomethylation as a fixed modification and Ntem-acetylation of protein, oxidation of methionine, and/or phosphorylation of serine, threonine, tyrosine residue (STY) as variable modifications. TMT10 was specified as label within a reporter ion MS3 experiment type. Up to two missed cleavage sites were allowed. Precursor tolerance was set to 5 ppm, and fragment ion tolerance to 20 ppm. The match between runs feature was enabled. Results were adjusted to 1% false discovery rate at protein, peptide, and site levels.

Bioinformatic analysis of LC-MS/MS

To handle the 30-plex experiment (3 TMT experiments with 10 channels each), bioinformatic analysis was done in Microsoft Excel and Perseus (version 1.6.1.1), which is part of the MaxQuant software suite (Tyanova et al., 2016). To correct for small sample loading, labeling reaction efficiency, and DDA-peptide sampling differences between the 3 TMT experiments, two normalization procedures were applied: total-sum and row-wise normalization. First, the reporter ion intensity for each protein (p) in each TMT channel (c) was divided by the total sum of all protein intensities in the respective channel, obtaining a scaled intensity (SI). Afterward, a row-wise normalization factor (F) was calculated for each protein in each TMT experiment (T), as the ratio between the averaged SI across the 3 experiments to the averaged SI within each experiment. These normalization factors were then applied to respective TMT channels to obtain the final normalized protein reporter intensity (NI):

$$NI(pcT) = SI(pc) \times F(pT)$$

Same normalization procedure was applied to the phosphoproteome dataset.

Both proteome and phosphoproteome datasets were filtered to retain only proteins or sites that have been quantified in all the 3 biological replica in at least one experimental condition, and missing values were imputed in Perseus using default settings.

To identify significantly modulated proteins and sites ANOVA test was used, corrected for multiple hypotheses using a Benjamini-Hochberg false discovery rate of 1%, and followed by Tukey HSD post hoc test in R (https://www.R-project.org/).

A Student t test with a permutation-based FDR of 5% was used to evaluate the temporal dynamics and magnitude of regulations, when comparing bystanding cells versus the control samples at 1 dpi. Here, the S0 parameter was tuned to achieve a minimum 2-fold regulation cut-off, and it was set to 1.

Unsupervised hierarchical clustering was performed on z-scored protein or site intensities, using Euclidian distance and average linkage. Profile plots show the normalized protein abundance (z-scored protein intensity) for each identified cluster. The lines indicate individual proteins and are colored according to the Pearson correlation calculated over the cluster centroid.

Gene ontology (GO) analysis was performed with Perseus software. Categorical annotation was supplied by Gene Ontology biological process, molecular function, and cellular component; and the KEGG pathway database. All annotations were extracted from the UniProt database. The GO terms enrichment was calculated on the basis of a Fisher's exact test with a false discovery rate value of 0.05. One-dimensional (1D) annotation enrichment analysis was performed on the distribution of the measured fold-changes (bystanding versus control BM-derived macrophages) for Reactome pathways with a Benjamini–Hochberg FDR cut-off of 1% (Cox and Mann, 2012).

Schematic diagram of protein domain structures and their phosphorylation sites were generated with DOG (Domain Graph, version 2.0) (Ren et al., 2009). Domain coordinates were obtained from the Pfam (El-Gebali et al., 2019) database and PhosphoStipePlus (Hornbeck et al., 2015).

Signaling networks were created in Cytoscape (Shannon et al., 2003) using the PhosphoPath plugin (Raaijmakers et al., 2015) and default parameters. High confidence protein-protein interaction data (score > 0.7) were downloaded from the STRING database (Szklarczyk et al., 2019) and dbEMT (Zhao et al., 2015), whereas pathways information were retrieved from Wikipathways (Slenter et al., 2018).

QUANTIFICATION AND STATISTICAL ANALYSIS

Statistical analysis was performed with GraphPad Prism (GraphPad software, Version 8). For comparison of two groups, unpaired two-tailed Student's t test was applied unless stated otherwise in the figure legend. For multiple comparisons, one- or two-way ANOVA were performed, followed by Tukey's multiple comparison tests. Differences were considered statistically significant when the p values were ≤ 0.05 (*), ≤ 0.01 (**) and ≤ 0.001 (***). Statistically non-significant data (p value > 0.05) are indicated as n.s.. Data are presented as mean ± SEM if not stated otherwise in the figure legend. The number of mice and the number of independent experiments conducted to generate the data is shown in the figure legend and presented as "n=x/y." "X" represents number of mice and "y" number of independently performed experiments. For example, n = 3-4/3 means 3 to 4 mice (per group) in 3 independent experiments. Sample exclusion was not performed.

Supplemental figures

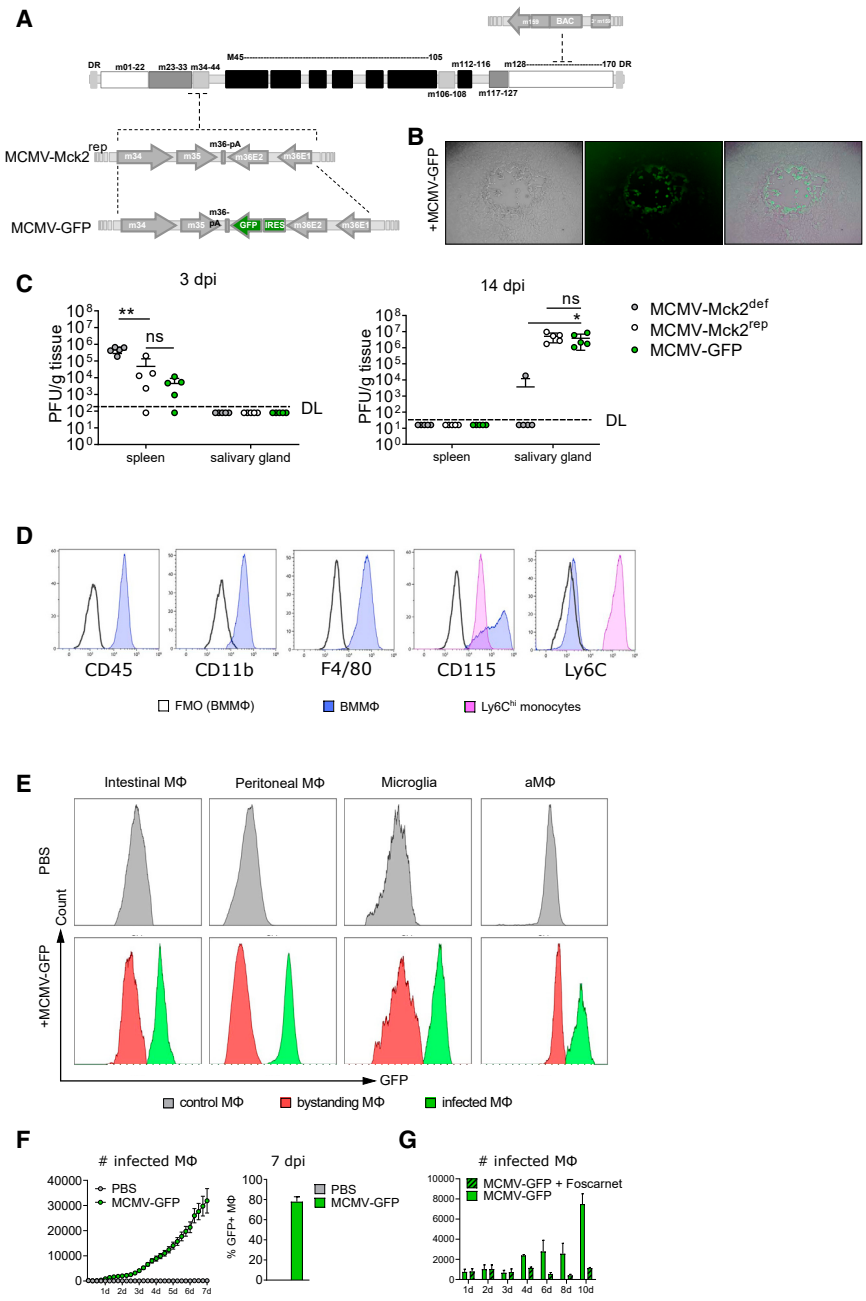

Figure S1. CMV-infected macrophages are phenotypically distinct from bystander macrophages, related to Figure 1.

A) Schematic representation of the genetic modifications introduced into the repaired bacterial artificial chromosome (BAC) based MCMV genome (*REP3.3*; Jordan et al., 2011). MCMV-GFP expresses the marker gene GFP fused to the M36 gene by insertion between the stop codon of the second exon of m36 (m36E2) gene ants its pA signal. Due to the presence of an IRES element containing an internal ribosomal entry site the GFP translation is connected to the translation of the m36 transcript. The BAC sequences - flanked by a duplication of the 3′segment of the m159 gene - are removed by homologous recombination during passages of the rescued virus on MEFs thereby repairing the m159 locus (Wagner et al., 1999).

B) Fluorescence microscopy of MCMV-GFP36 infected MEF, data is representative for at least 5 experiments.

(legend continued on next page)

C) BALB/c mice were infected intraperitoneally with $5x10^5$ PFU of either unrepaired MCMV (MCMV-$Mck2^{def}$), harboring a mutation in the Mck2 locus (Jordan et al., 2011), repaired MCMV (MCMV-$Mck2^{rep}$) or repaired MCMV expressing GFP (MCMV-GFP). PFU assays from spleen and salivary gland were performed 3dpi and 14dpi. Dashed line indicates detection limit (DL). n = 5 per group/1.

D) Flow cytometry of BMMΦ and monocytes.

E) Intestinal MΦ (colonic lamina propria), peritoneal MΦ, microglia and aMΦ were infected with MCMV-GFP and GFP expression was measured 1dpi. Histogram is representative for 3 independent experiments.

F) Wt BMMΦ were mock-infected or infected with a low dose of MCMV-GFP for 7 days. Using the IncuCyte-system (Sartorius) GFP-positive cell counts were assessed every 6 hours (left). 7 dpi GFP^+ BMMΦ were quantified via flow cytometry. n = 2 per group/1.

G) Wt BMMΦ were infected with a low dose of MCMV-GFP with and without 500μM Foscarnet-Natrium. GFP positive BMMΦ were quantified via flow cytometry. n = 5/2

Data are mean ± SEM, *p < 0.05, **p < 0.01, ***p < 0.001. One-way ANOVA followed by Tukey's multiple comparison test revealed statistical significance.

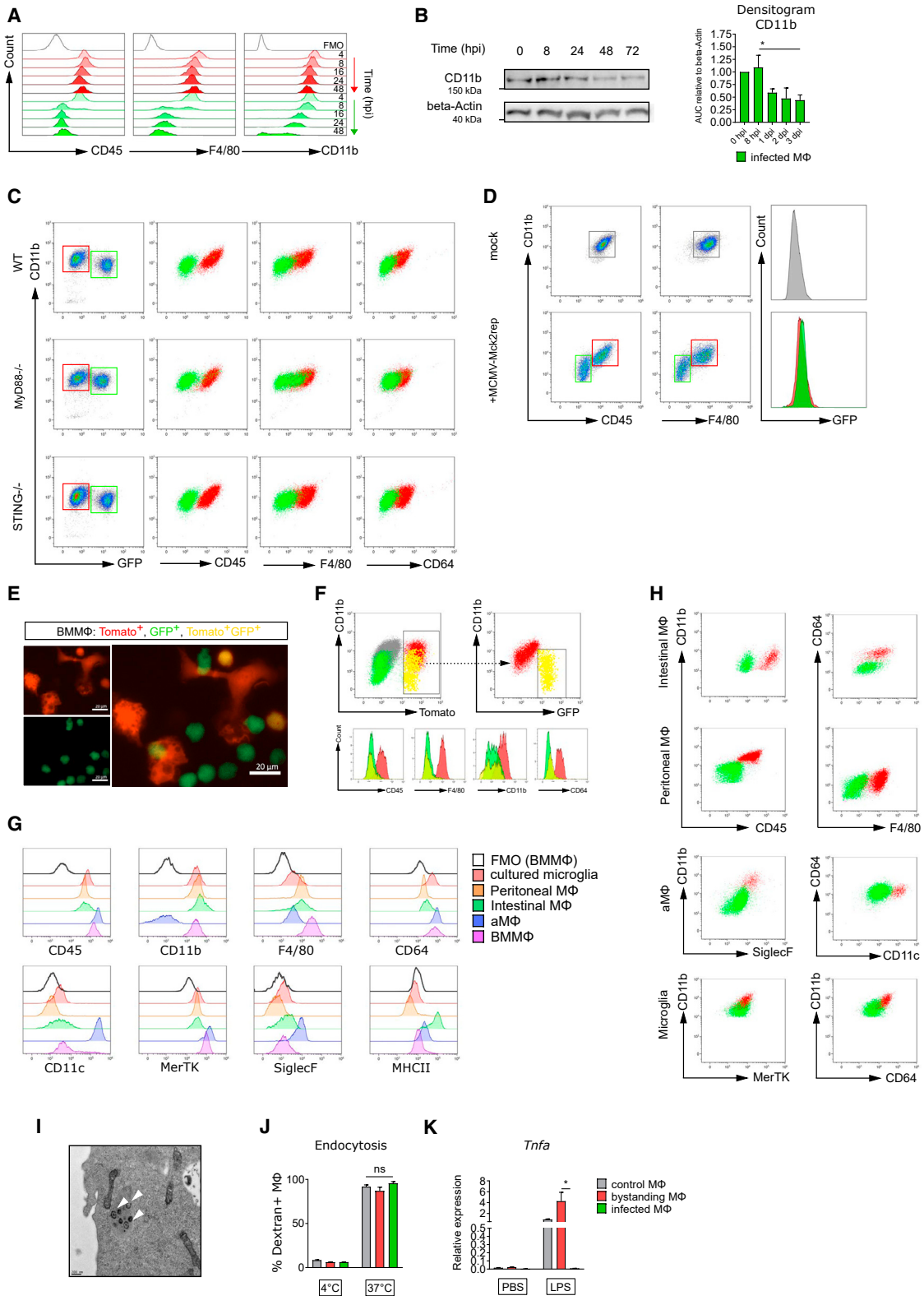

Figure S2. CMV infection changes macrophage phenotype and functionality, related to Figure 2

A) Expression of indicated surface markers on bystanding (red, upper panel) and infected BMMΦ (green, lower panel) obtained via flow cytometry at 4, 8, 16, 24, 48 hpi (indicated by increasing color intensity). Unfilled histogram (top panel) shows expression of FMO control. n = 2/2.

(legend continued on next page)

B) Expression of CD11b in whole cell lysates from infected BMMΦ at indicated time points detected by western blot. The area under the curve (AUC) was normalized to beta-actin. n = 3/3. Paired t test.
C) Flow cytometry plot of BMMΦ from wt, *Myd88*$^{-/-}$ and *Tmem173*$^{-/-}$ (STING$^{-/-}$) mice infected with MCMV-GFP. Bystanding BMMΦ (red) showed steady surface marker expression, while infected MΦ (green) downregulated CD11b, CD45, F4/80 and CD64 at 1dpi. n = 8/8 (wt), 3/1 (*Tmem173*$^{-/-}$) and 3/2 (*Myd88*$^{-/-}$).
D) Flow cytometry plot of MΦ infected with MCMV-Mck2^{rep}. Bona fide infected BMMΦ (green) were identifiable by surface marker downregulation compared to bystanding BMMΦ (red). Mock infected BMMΦ (gray) serve as control for protein expression. Representative for n = 3/1.
E) and F) After induction of recombination with hydroxytamoxifen, BMMΦ from *Cx$_3$cr1*^{creER} ROSA26-Tomato^{flox} mice were infected with MCMV-GFP and analyzed 2 dpi by fluorescence microscopy (E) and flow cytometry (F). BMMΦ are GFP- Tomato- (not recombined, not infected) GFP+, (not recombined, infected), Tomato+ (recombined, not infected) and GFP+ Tomato+ (recombined, infected). Representative for n = 3/1.
G) Surface marker expression analysis of tissue MΦ types by flow cytometry.
H) Flow cytometry plots of intestinal MΦ, peritoneal MΦ, microglia and aMΦ infected with MCMV-GFP 1 dpi *ex vivo*. Plots show surface marker downregulation of GFP-positive infected MΦ (green) compared to GFP-negative bystanding MΦ (red). Dot plots are representative for 3 independent experiments.
I) Representative TEM image of viral particles in infected BMMΦ (white arrow heads).
J) BMMΦ subsets were incubated with Dextran-AF647 (10kDa) for 1 hour at 4°C or 37°C to assess endocytosis. Percentage of AF647^{+} MΦ were analyzed via flow cytometry. n = 3/3. Two-way ANOVA followed by Tukey's multiple comparison.
K) Sorted control, bystanding and infected BMMΦ were stimulated with LPS (50ng/ml) for 4 hours and *Tnf* expression levels were normalized to *Gapdh*. Two-way ANOVA followed by Tukey's multiple comparison test.
Data are mean ± SEM, *p < 0.05, **p < 0.01, ***p < 0.001.

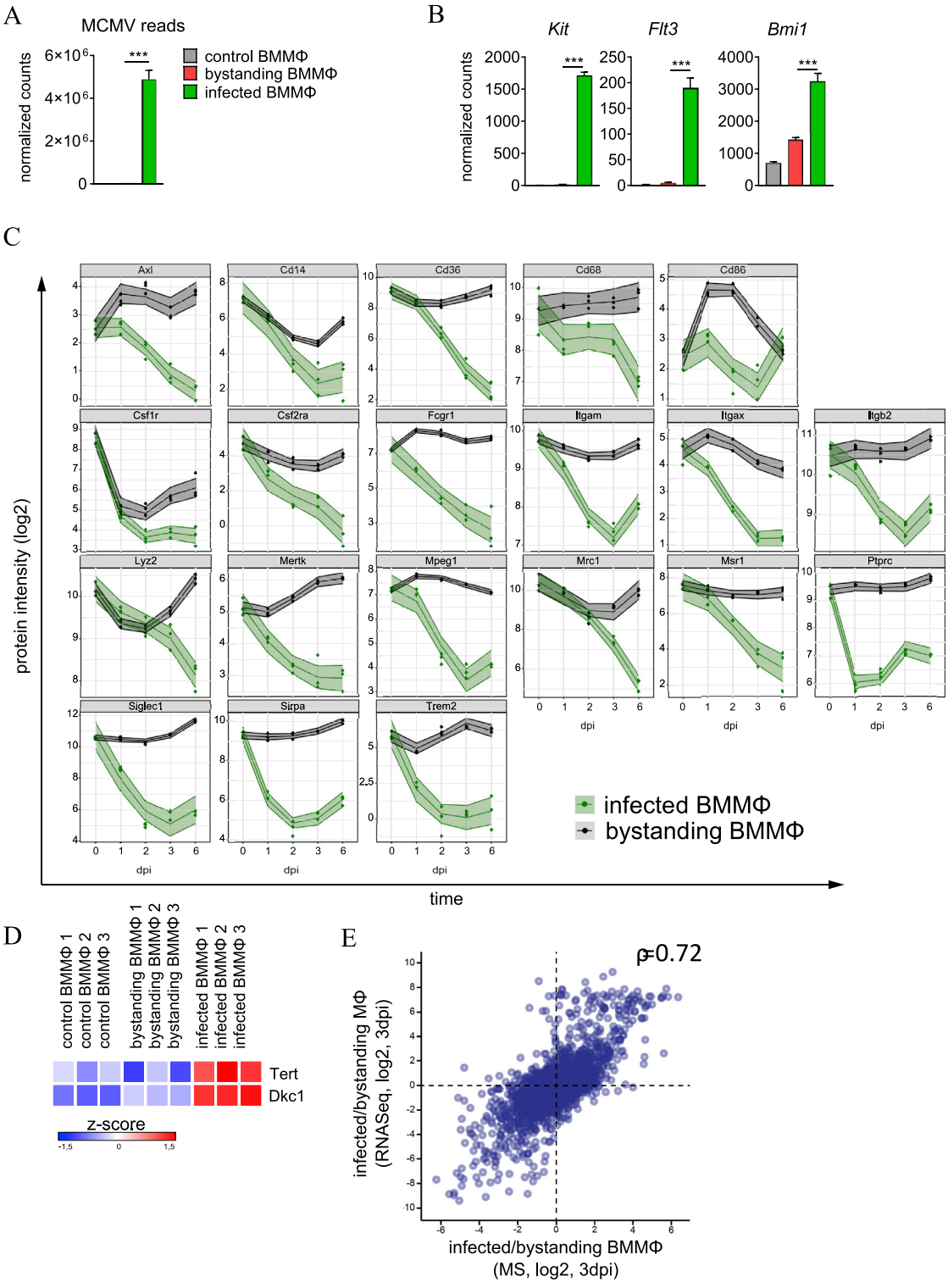

Figure S3. CMV elicits stem cell-like features in macrophages, related to Figure 3

A) Quantification of viral reads detected by RNASeq 3 dpi. Data represent 3 mice per BMMΦ subset.

B) Normalized read counts of genes, typically expressed in hematopoietic stem cells, at 3 dpi.

(legend continued on next page)

C) Log_2 intensity of MΦ marker proteins. "0 dpi" shows protein abundance level in control BMMΦ. Protein expression kinetics of bystanding and infected BMMΦ are depicted for 1, 2, 3, and 6 dpi. Each dot represents one mouse, central line indicates mean of biological triplicates and flanking lines indicate the 95% confidence level interval, the area within confidence interval is highlighted in color for bystanding (black) and infected (green) MΦ.
D) Heatmap of telomerase genes in BMMΦ subsets. Genes are represented in triplicates per subset.
E) Correlation between proteomics and transcriptomics fold changes for infected BMMΦ over control BMMΦ at 3 dpi.
Data are mean ± SEM, *$p < 0.05$, **$p < 0.01$, ***$p < 0.001$. One-way ANOVA followed by Tukey's multiple comparison test revealed statistical significance.

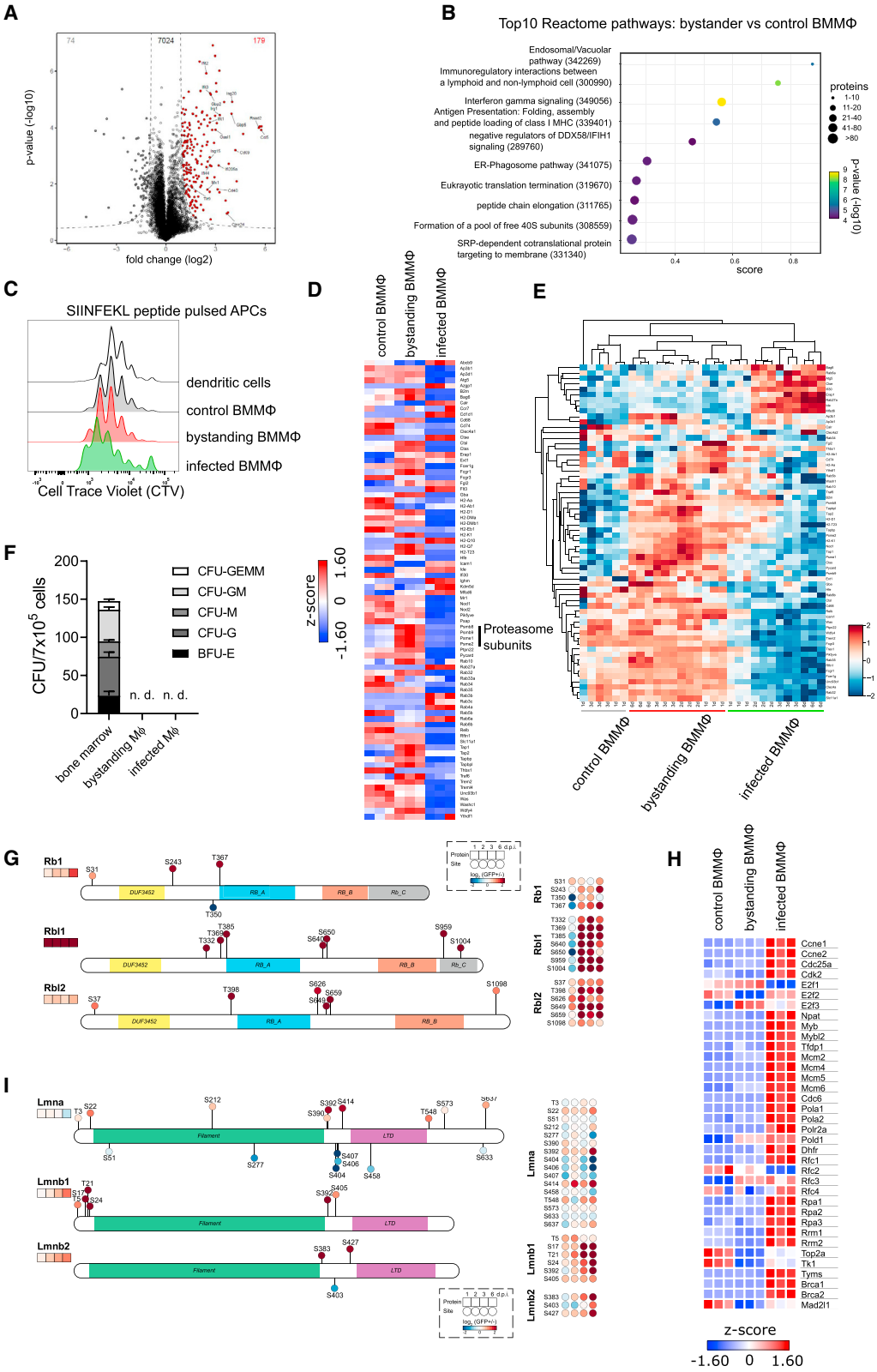

(legend on next page)

Figure S4. CMV-infected macrophages lose antigen-presenting capacity and provide their cell cycle machinery for viral replication, related to Figure 4

A) Volcano plot of significantly regulated proteins (t test, 5% FDR dotted line) of control (gray) versus bystanding (red) BMMΦ at 1 dpi.
B) Top10 signaling pathways (Reactome) enriched (1D enrichment with Fisher exact test, 1% FDR) in bystanding versus control BMMΦ at 1 dpi.
C) CTV-proliferation profiles of OTI T cells 3 days after co-culture with SIINFEKL-peptide pulsed dendritic cells and BMMΦ subsets.
D) E) Heatmaps of transcripts (D) or proteins (E) associated with antigen processing and presentation (GO:0019882).
F) CFU assay of nucleated bone marrow cells and sorted bystander and infected MΦ. Cells were cultured in MethoCult for 7 days. N. d. = not detected, CFU (colony forming unit)-GEMM (granulocyte, erythroid, macrophage, megakaryocyte), - GM (granulocyte, macrophage), - M (macrophage), - G (granulocyte), BFU-E (burst forming unit-erythroid). Data represent 4 mice in 2 independent experiments.
G) Schematic representation of RB1 and RBL1/2 and their phosphorylation sites. Known domains and motifs are indicated. Protein expression in infected MΦ relative to bystanding MΦ is time-resolved in the left panel (squares), phosphorylation sites and their relative abundance in the right panel (circles). "Lollipops" heights illustrate the overall maximum fold change between infected and bystanding MΦ.
H) Heatmap of transcription factor E2F target genes obtained from RNA-seq.
I) Schematic representation of LMNA, LMNB1/2 and their phosphorylation sites. Known domains and motifs are indicated. Protein expression in infected MΦ relative to bystanding MΦ is time-resolved in the left panel (squares), phosphorylation sites and their relative abundance in the right panel (circles). "Lollipops" heights illustrate the overall maximum fold change between infected and bystanding MΦ.

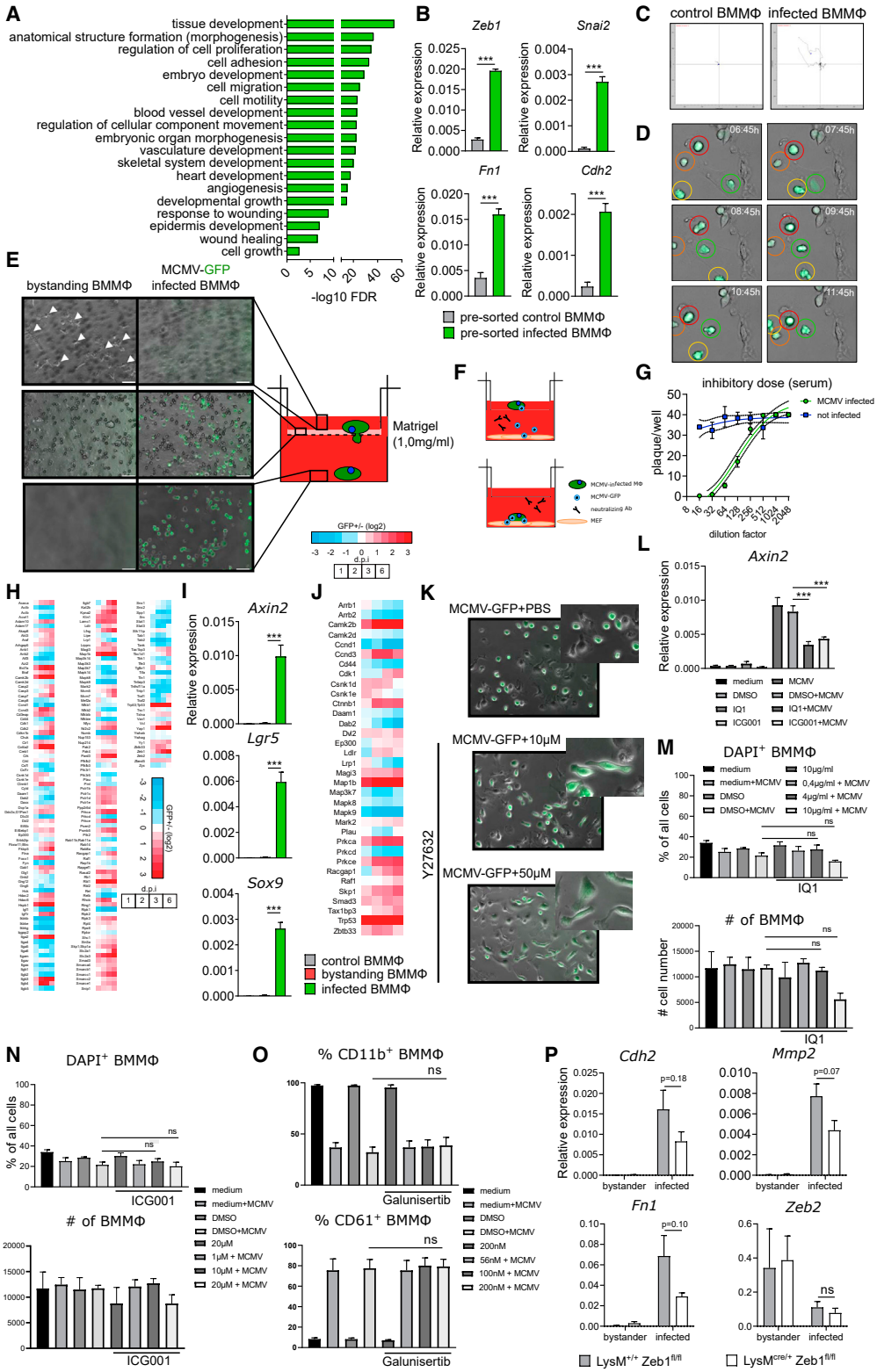

Figure S5. Induction of Wnt pathway causes transformation of infected macrophages with increased mobility and invasiveness, related to Figure 5

A) GO terms overrepresented in cells undergoing EMT (Gröger et al., 2012) were compared to enriched GO terms in infected BMMΦ compared to bystanding BMMΦ.

(legend continued on next page)

B) QRT-PCR of pre-sorted BMMΦ after subsequent mock or MCMV-GFP infection, 3 dpi. n = 4/2.
C) Representative cell tracking of control BMMΦ and infected BMMΦ.
D) Snap shot images from time lapse microscopy of MCMV-GFP infected cells. Individual cells are highlighted with colored circles in each image. The cell highlighted with a green circle closely interacts with an uninfected bystanding cell.
E) Scheme and representative fluorescence microscopy images of invasion assay. Top panel shows bystanding (left) and no infected MΦ (right) on top of matrigel layer. Middel panel shows only infected MΦs invaded into the matrigel layer to reach the insert pores. Bottom panel shows infected (GFP^+) MΦs at the bottom of the cell culture plate.
F) Scheme of experiment to determine mode of viral spread *in vitro*.
G) Titration of pooled sera of infected (42-72 dpi) and uninfected mice via plaque-reduction-assay to assess the neutralizing capacity of cell-free MCMV infection on MEF.
H) Heatmap of proteins associated with EMT (as in Figure 5G - right) significantly regulated (ANOVA, Benjamini-Hochberg Correction 0.01) in infected MΦ at 1, 2, 3 and 6 dpi.
I) QRT-PCR of Wnt target gene *Axin2*, *Lgr5* and *Sox9* relative to *Gapdh*.
J) Heatmap of proteins associated with Wnt pathway significantly regulated (ANOVA, Benjamini-Hochberg Correction 0.01) in infected MΦ at 1, 2, 3 and 6 dpi.
K) Representative fluorescent microscopy pictures of MΦ treated with vehicle (top) or different doses of ROCK inhibitor Y27632 (middle, bottom) and infected with MCMV-GFP.
L) QRT-PCR of Wnt target gene *Axin2* for indicated conditions. IQ1 and ICG001 were administered in 4μg/ml or 10μM, respectively. n = 7/3.
M) N) Percentage of $DAPI^+$ dead cells (top) and absolute cell counts (bottom) in Wnt inhibitor experiments assessed via flow cytometry. n = 4-5/3.
O) Quantification of $CD11b^+$ (top) and $CD61^+$ (bottom) MΦ cultured in medium, vehicle (DMSO) or Galunisertib with and without MCMV-GFP infection, measured via flow cytometry 2 dpi. n = 5/3.
P) QRT-PCR of *Mmp2*, *Cdh2*, *Fn1* and *Zeb2* in bystanding and infected MΦ of $LysM^{+/+}$:$Zeb1^{fl/fl}$ or $LysM^{cre/+}$:$Zeb1^{fl/fl}$. n = 4/2. Unpaired t test was used to test for statistical significance.
Data are mean ± SEM, *p < 0.05, **p < 0.01, ***p < 0.001. One-way ANOVA followed by Tukey's multiple comparison test revealed statistical significance, if not stated otherwise.

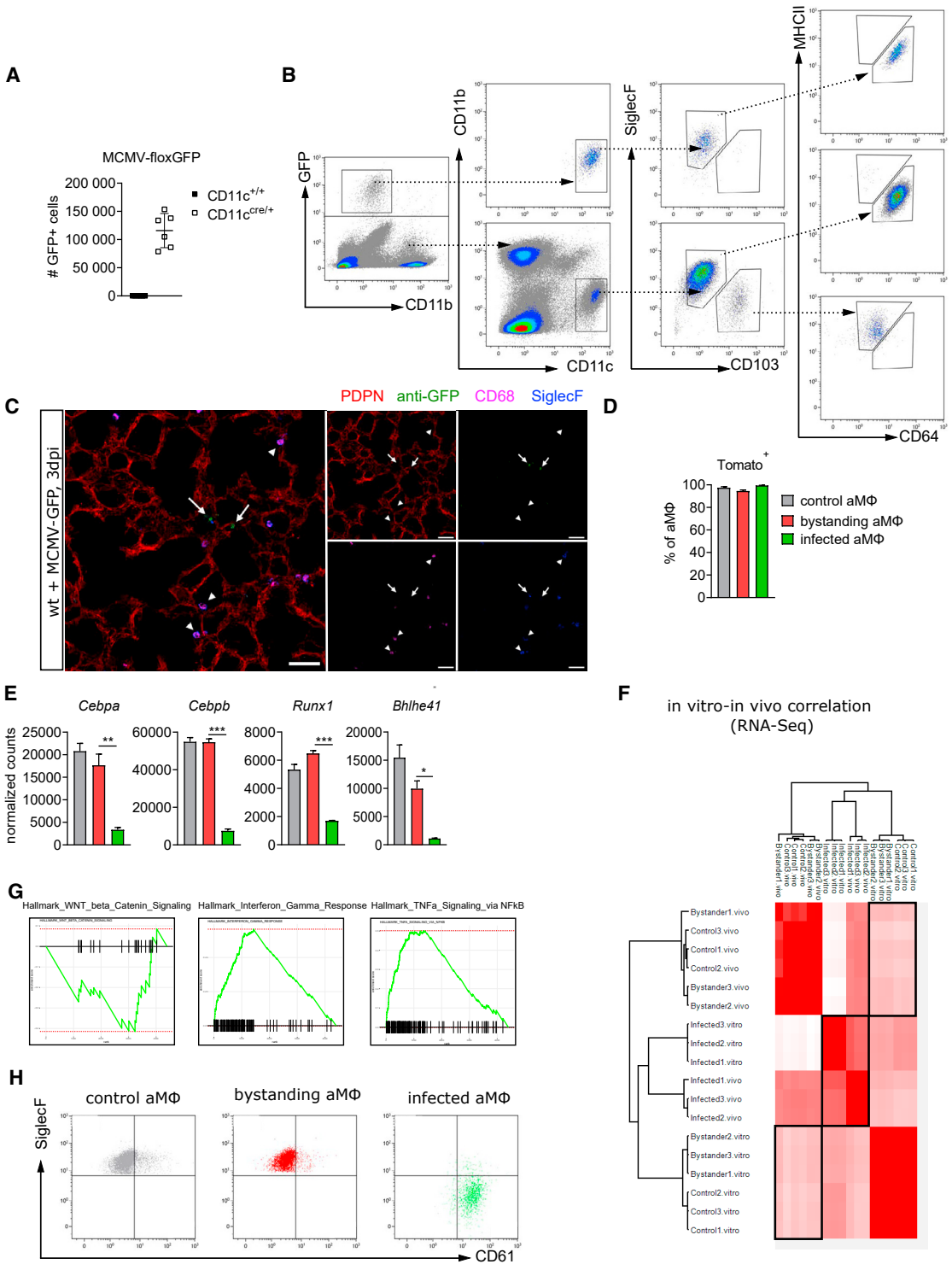

Figure S6. Infected alveolar macrophages are reprogrammed *in vivo*, related to Figure 6

A) Validation of MCMV-floxGFP. Absolute number of GFP$^+$ infected cells 3 days after infected of *Itgax*$^{+/+}$ and *Itgax*$^{cre/+}$ mice with MCMV-floxGFP, quantified via flow cytometry. N = 6/2.

B) Representative gating of bystanding aMΦ, CD103$^+$ DC and infected cells 12 hpi of *Itgax*$^{cre/+}$ mice with MCMV-floxGFP.

C) Immunofluorescence histology of bystanding (arrow head) and infected (arrow) AM in the lungs of *Itgax*$^{cre/+}$ infected with MCMV-floxGFP, 3dpi. Merged image contains Podoplanin (PDPN, red), anti-GFP (green), SiglecF (blue), CD68 (pink). Scale bars: 50 μm. Data is representative for 4 mice.

(legend continued on next page)

D) Quantification of Tomato$^+$ control, bystanding and infected aMΦ 3dpi. n = 6/3 (control), n = 11/4.
E) Normalized counts of transcription factors determining MΦ differentiation (*Cebpa*, *Cebpb*, *Runx1*) and maintaining MΦ tissue specificity (*Bhlhe41*). One-way ANOVA followed by Tukey's multiple comparison test.
F) Correlation of RNA-seq reads from *in vitro* and *in vivo* obtained data. Only genes, which were present in every of each condition were considered for analysis.
G) Gene set enrichment analysis comparing infected and bystanding aMΦ indicates activation of Wnt-pathway in infected aMΦ (left) and Interferon gamma response, NFκB signaling in bystanding aMΦ (middle, right).
H) Representative flow cytometry plot of CD61 surface expression on control, bystanding (SiglecF$^+$ CD61$^-$) and infected (SiglecF$^-$ CD61$^+$) aMΦ, 3 dpi.
Data are mean ± SEM, *p < 0.05, **p < 0.01, ***p < 0.001.

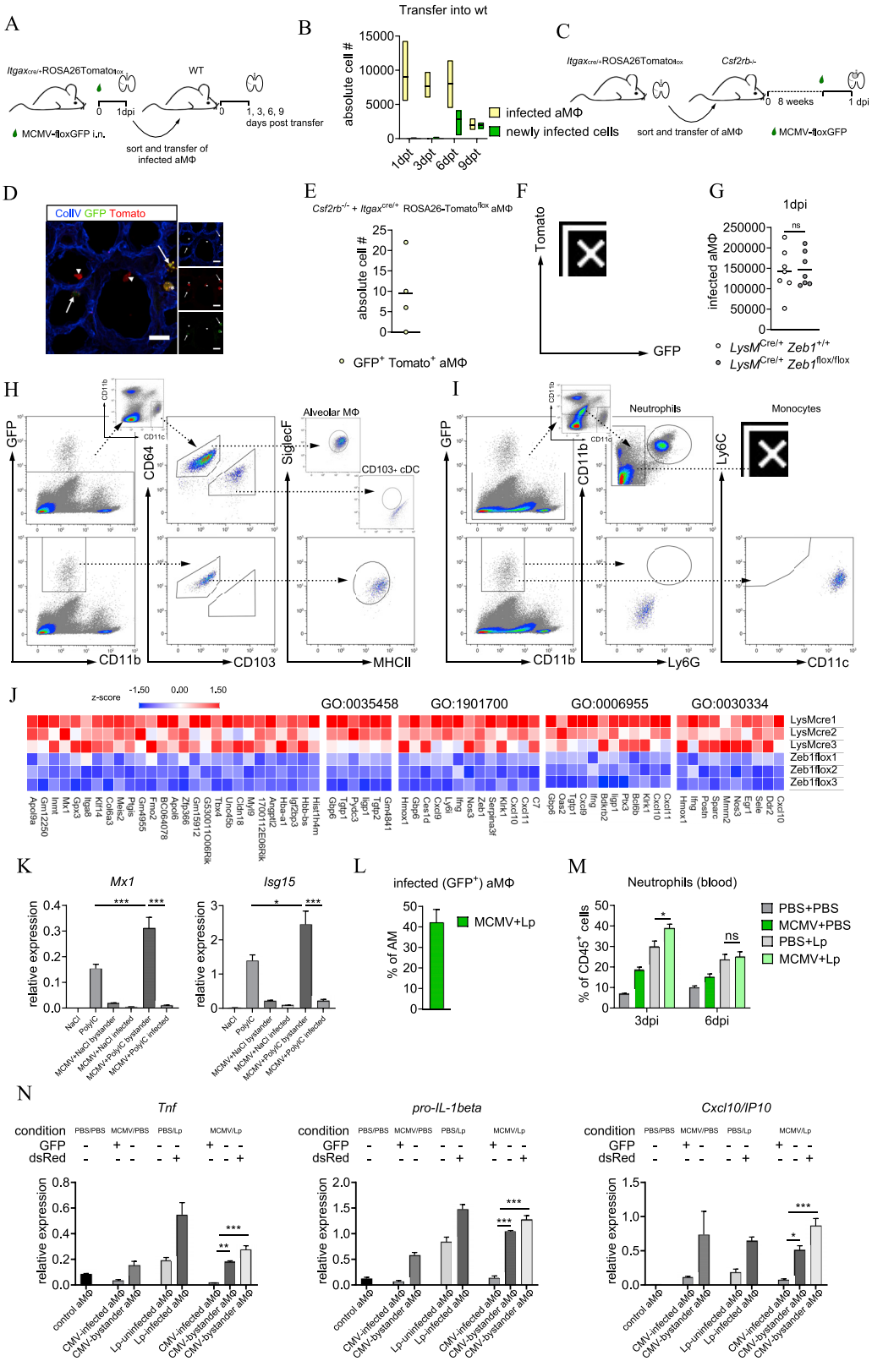

(legend on next page)

Figure S7. Infection of alveolar macrophages impairs their function and renders them susceptible to secondary infection, related to Figure 7

A) Scheme of infected aMΦ (Tomato$^+$ GFP$^+$) transfer into wild-type mice. *Itgax*$^{cre/+}$ ROSA26-Tomato^{flox} mice were infected with MCMV-floxGFP i.n. and aMΦ subsets were sorted 1 dpi. Immediately after sorting cells were transferred into wild-type mice and lung homogenates were analyzed at indicated time points.

B) Number of transferred infected aMΦ at indicated days post transfer (dpt) via flow cytometry. Data are presented as floating bars (min to max; line: mean). n = 3 per time point/2-3.

C) Scheme of aMΦ transfer into *Csf2rb*$^{-/-}$ mice and subsequent infection.

D) Representative image of a bystanding aMΦ in the alveolus (arrow heads) and infected aMΦ in the alveolar space (arrows) and interstitium (asterisk). Scale bar is 20μm.

E) Absolute number of aMΦ in the mediastinal lymph node, 1dpi. n = 4/2.

F) Representative flow cytometry plot of infected aMΦ (GFP+ Tomato+, yellow) in the mediastinal lymph node, 1 dpi. Gated from all single cells.

G) Number of infected cells in *LysM*$^{cre/+}$:*Zeb1*$^{+/+}$ and *LysM*$^{cre/+}$:*Zeb1*$^{flox/flox}$ mice 1dpi with MCMV-floxGFP. n = 7/2.

H) I) Representative gating of bystanding aMΦ, CD103$^+$ DC (H), neutrophils, monocytes (I) and infected cells (H and I) 12 hpi of *LysM*$^{cre/+}$ mice with MCMV-floxGFP. n = 4/2.

J) Heatmap of upregulated ($p \leq 0.05$, $\log_2$fc > 1) genes in *LysM*$^{cre/+}$ mice compared to *LysM*$^{cre/+}$:*Zeb1*$^{flox/flox}$ and associated GO terms when indicated.

K) QRT-PCR of *Mx1* and *Isg15* of sorted aMΦ after (re-) stimulation with poly(I:C). n = 3/2.

L) Proportion of MCMV-infected aMΦ 3 days after Lp infection.

M) Relative neutrophil numbers in the blood determined via flow cytometry. n = 5/3 (without Lp infection) or n = 9/3 (with Lp infection).

N) QRT-PCR of cytokines and chemokines of sorted aMΦ subsets16hpi with *Lp*. n = 3/1.

Data are mean ± SEM, *p < 0.05, **p < 0.01, ***p < 0.001. One-way ANOVA followed by Tukey's multiple comparison test, if not stated otherwise.